Politecnico di Milano

Scuola di Ingegneria Industriale e dell'Informazione

Tesi di Laurea Magistrale in Ingegneria Biomedica

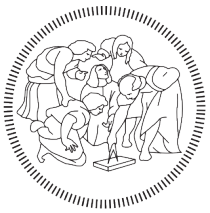

POLITECNICO
MILANO 1863

The Role of Ocular Biomechanics and Hemodynamics in Determining Intraocular Pressure Dynamics: a Mathematical Approach

---

Relatore: Prof.ssa Maria Laura COSTANTINO

Correlatore: Prof.ssa Giovanna GUIDOBONI

Tesi di Laurea di:
Francesca STEFANONI,
matricola 837889

Anno Accademico 2016-2017

ACKNOWLEDGEMENTS

The first part of this thesis has been carried out at the Institut de Recherche Mathématique Avancée, Université de Strasbourg (CNRS, Strasbourg, France), where I spent four months working as research assistant. My research visit in Strasbourg has been supported by funding from the University of Strasbourg.

I would first like to thank my thesis advisor Prof. Maria Laura Costantino (Politecnico di Milano, Italy) who gave me the opportunity to develop my thesis abroad, experiencing this engaging international team, and trusted me from the beginning.

I wish to thank my co-advisor Prof. Giovanna Guidoboni (University of Missouri, MO, USA) who suggested me this project without ever ceasing to support my proposals.
Commitment and passion you put in research as in life inspired me more and more throughout this research. You are a shining example that "If you want something, reach out and grab it" is always possible with passion, organization and dedication.

I also want to thank Prof. Christophe Prud'Homme and Prof. Marcela Szopos (Université de Strasbourg, France) for their kind hospitality in the Department in Strasbourg and their precious advice, especially concerning the computational part of this project.

Prof. Alon Harris (Eugene and Marilyn Glick Eye Institute and Indiana University School of Medicine, Indianapolis, USA) and Dr. Dario Messenio (Eye Clinic, Department of Clinical Science, ASST Fatebenefratelli Sacco and University of Milan, Italy) provided many useful clinical suggestions for the development of the model.

Abstract

Intraocular pressure (IOP) is the pressure created by the fluids within the eye. Elevated IOP, a condition referred to as ocular hypertension, is associated with many diseases and is an acknowledged risk factor for vision loss. Thus, it is of great clinical interest to identify the factors influencing it. IOP assessment is a simple, quick and non invasive test that can be performed in any ophthalmology clinic. Interestingly, pressure values inside the eye exhibit a static component, mainly due to aqueous humor inflow and outflow balance, and a dynamic component, mainly due to blood flow oscillations. To date, most of the theoretical studies have focused on the static component.

In the present project we aim at investigating and quantifying the influence of biomechanical and hemodynamical properties of ocular tissues and fluids on both IOP components by means of mathematical modeling.

We propose three subsequent models that can be thought of as successive steps towards the modeling of whole eye dynamics. Each model is designed as an electrical analogue of the physiology of the eye, including details regarding structural mechanics and fluid dynamics. Calibration and validation are performed using published data. Models are implemented using the open access software OpenModelica in order to facilitate further extensions and connections with other models already available for different parts of the eye.

To quantify the effect of variations in biomechanical and hemodynamical

factors on the static and dynamic components of IOP, we perform sensitivity analysis. Moreover, we assess the extent to which different factors influence IOP distribution in ocular hypertensive eyes and we simulate the effect of IOP-lowering medications in both ocular normotensive and ocular hypertensive subjects to evaluate their efficacy.
Lastly, we present a sketch of a mathematical model including a more detailed analysis of the mechanical properties of ocular internal structures, namely cornea, sclera and vitreous humor, which contribute to IOP dynamics. This last model provides an insight for future developments of this study.

This work actually provides the very first attempt to consistently combine the static and dynamic components contributing to the pressure distribution inside the eye. The models will help elucidate the relationship between IOP dynamics and relevant factors that may vary among patients or in the same patient over time. The outcomes of this research will be particularly relevant for glaucoma research, since, to date, elevated IOP is the only treatable glaucoma risk factor despite the fact that up to 25% of glaucoma patients progress to blindness even though IOP is within normal levels and a high percentage of individuals with elevated IOP never develops glaucoma. In a long term perspective, the software developed will be integrated in a larger virtual simulator for ocular biophysics, developed within the context of an international collaboration between University of Missouri (MO, USA), Indiana University (IN, USA), Université de Strasbourg (France) and Politecnico di Milano (Italy). It may lead to a new instrument for clinical use that could provide physicians with an integrated view of the patient's status to monitor, prevent and treat diseases in a patient-specific manner.

Keywords — intraocular pressure, ocular hypertension, ocular biomechanics, ocular hemodynamics, eye, acqueous humor, choroidal blood

flow, ocular deformability, vitreous humor, cornea, sclera, glaucoma, mathematical model, electrical analogy, IOP-lowering medications, sensitivity analysis, intraocular pressure assessment, OpenModelica

Sommario

La pressione intraoculare è creata dai liquidi all'interno dell'occhio. Un suo valore elevato, condizione conosciuta come ipertensione oculare, è associato a molte patologie ed è un noto fattore di rischio per la perdita della vista. Pertanto, è di grande interesse clinico identificare i fattori che la influenzano. La valutazione della pressione intraoculare avviene per mezzo di un test semplice, rapido e non invasivo che può essere eseguito in qualsiasi ambulatorio oftalmologico. È interessante notare che i valori di pressione all'interno dell'occhio mostrano una componente statica, dovuta principalmente all'equilibrio tra umore acqueo entrante e uscente dall'occhio, e una componente dinamica, dovuta principalmente alle oscillazioni del flusso sanguigno. Finora, la maggior parte degli studi teorici si è concentrata sulla componente statica.

Lo scopo di questa tesi è di studiare e quantificare l'influenza delle proprietà biomeccaniche ed emodinamiche dei tessuti e dei fluidi oculari su entrambe le componenti della IOP, mediante modellizzazione matematica dei fenomeni.

Si propongono tre modelli susseguenti che possono essere pensati come passi successivi verso la modellizzazione della completa dinamica dell'occhio. Ogni modello è progettato come un analogo elettrico della fisiologia oculare, e include dettagli riguardanti la meccanica delle strutture e la dinamica dei fluidi. La calibrazione e la validazione sono effettuate utilizzando dati presenti in letteratura. I modelli sono imple-

mentati usando il software OpenModelica per agevolare ulteriori estensioni e connessioni con altri modelli già disponibili per diversi aspetti dell'occhio.
Per quantificare l'effetto di variazioni nei parametri biomeccanici ed emodinamici sulle componenti statica e dinamica della pressione intraoculare, viene eseguita un'analisi di sensitività. Inoltre, si valuta la misura in cui i diversi fattori influenzano la distribuzione della pressione oculare in occhi ipertensivi oculari e si simula l'effetto di farmaci che agiscono sull'abbassamento della pressione intraoculare sia su suggetti normotensivi che su soggetti ipertensivi, allo scopo di valutarne l'efficacia.
Infine, viene presentato un primo tentativo di includere nel modello un'analisi più dettagliata delle proprietà meccaniche delle strutture dell'occhio, ossia di cornea, sclera e umore vitreo, che contribuiscono alla dinamica della pressione oculare. Questo ultimo modello fornisce uno spunto per sviluppi futuri di questo studio.

Questo progetto fornisce il primo tentativo di combinare in modo coerente le componenti statica e dinamica che contribuiscono a determinare la distribuzione della pressione intraoculare. I modelli presentati potranno aiutare a chiarire la relazione tra la dinamica della pressione dell'occhio e fattori rilevanti che possono variare tra pazienti o nello stesso paziente nel tempo. I risultati di questa ricerca saranno particolarmente rilevanti per la ricerca sul glaucoma. Ad oggi, infatti, l'elevata pressione intraoculare è l'unico fattore di rischio curabile per il glaucoma benché più del 25% dei pazienti affetti da glaucoma progredisca nella cecità anche se la pressione intraoculare rientra nei livelli fisiologici e un'alta percentuale di individui con pressione oculare elevata non sviluppi mai il glaucoma. In una prospettiva di lungo termine, il software sviluppato sarà integrato in un più grande simulatore virtuale della biofisica oculare, realizzato nel contesto di una collaborazione internazionale tra University of Missouri (MO, USA), Indiana University

(IN, USA), Université de Strasbourg (France) e Politecnico di Milano (Italia). Il software potrà costituire un nuovo strumento per uso clinico con lo scopo di fornire ai medici una visione integrata dello stato del paziente per monitorare, prevenire e curare le malattie in modo paziente-specifico.

Parole chiave — pressione intraoculare, ipertensione oculare, biomeccanica dell'occhio, emodinamica dell'occhio, occhio, umore acqueo, coroide, deformabilità oculare, umore vitreo, cornea, sclera, glaucoma, modello matematico, analogo elettrico, analisi di sensitività, misura della pressione intraoculare, OpenModelica

Contents

List of Tables

List of Figures

Chapter 1

Introduction

The human brain is the most complex arrangement of matter in the known universe. Through our five senses it processes and re-elaborates vast amounts of information that allows us to see, hear, taste, touch and balance. It commands our muscles, it learns, remembers, hungers, loves and hates. Understanding how the brain works is a major research challenge, and thousands of scientists are studying it in the expectation that through greater understanding we can eventually overcome many diseases and injuries.

Moreover, the only part of the brain that can be seen directly is the eye, and in fact the eye has been often referred to as *"the window to the soul"*.
Over the years, scientists have struggled with this concept, searching for scientific evidence to determine whether eye research could be useful for investigating the brain and diagnosis of its diseases [58].

Figure 1.1: *The eye is a window to the brain*

The eye is a complex physiological system controlled by mechanical, biochemical, and neurological factors, that, under normal conditions, ensure the stability and regulation of intraocular pressure (IOP). Stability

and regulation are essential for the maintenance of the visual function of the eye and for the nutrition of its tissues.

Anatomically and developmentally, the retina is known as an extension of the central nervous system (CNS). Several well-defined neurodegenerative conditions that affect brain and spinal cord have manifestations in the eye, and ocular symptoms often precede conventional diagnosis of such CNS disorders. Furthermore, various eye-specific pathologies share characteristics of other CNS pathologies [58].

In many neurological diseases, such as multiple sclerosis or stroke, we can see changes in the optic nerve that provide a direct diagnosis. And if pressure in the brain increases, possibly due to a brain tumor or injury, we can see this as a swelling of the optic nerve. Optic nerve, containing nerves that carry visual messages from the retina to the brain, is visible in the back of the eye by using an ophthalmoscope and shining a bright light into the eye. Together with optic nerve, this examination shows the innermost layer of the eye, namely the retina. So changes in the back of the eye can be used in the diagnosis of high blood pressure, diabetes, glaucoma, age-related macular degeneration or genetic diseases, such as retinal dystrophies.

The main limitation in accessing the eye is that, to date, all the techniques used in clinics to assess IOP actually measure the pressure difference across the cornea, also known as trans-corneal pressure difference (TCPD). But since the pressure distribution inside the eye is not yet fully understood, the relationship between TCPD and IOP remains elusive. For this reason, it is of great clinical interest to clarify the relationship between this internal pressure and the measurable pressure across the cornea. Even though it is well known that many factors influence this relationship, including geometrical and material properties characterizing ocular tissues and fluids, to date, there is a lack of quan-

titative understanding of how and to what extent these factors influence the IOP assessment in a specific patient.

This thesis is a step towards achieving this purpose, and is motivated by the fact that:

(i) ***elevated IOP***, a condition referred to as *ocular hypertension*, ***is an acknowledged risk factor for vision loss***, and in particular a risk factor for glaucoma,

(ii) ***IOP is the only treatable risk factor for glaucoma***, and

(iii) ***how ocular biomechanical and hemodynamical properties combine*** in the eye to give rise to the ***dynamics of IOP*** is still an open question in ophthalmology.

The purpose of this work is to present a **quantitative formulation of the dynamics of IOP** as functions of the interrelation of (⋄) **mechanical properties of the eye** and (⋄) **fluid dynamics of blood flowing into the eye**.
In particular, we highlight and quantify the effect of variations in ocular tissues and fluids properties on the static and dynamic components of IOP, namely the steady-state and the time dependent characteristics of IOP respectively. The visual, neurological, and muscular functions of the eye are not taken into account in this work.

The equilibrium state of the eye, in which IOP is maintained at a nearly constant level of 15-20 mmHg above ambient pressure —one of the highest of any organ of the body—, is due to a delicate balance of fluid flow, the so-called *aqueous humor* (AH), into and out of the eye. Under pathological conditions, the outflow resistance may increase, leading to an accumulation of fluid inside the eye, with a concomitant increase in pressure that can cause a disease.

All eyes exhibit similar general dynamic properties, even though different structures inside the eye possessing various patient-specific characteristics make it challenging to define an "average eye". Nonetheless, the eye can be modeled via mathematical analysis, and in fact this work is part of a larger interdisciplinary project with the aim to design and build a software for clinical use that represents a 3D eye. Yet, in order to formulate mathematical models of the eye, assumptions must be made, experimental averages obtained, and relationships postulated.

A great body of literature exists concerning various biomechanical and hemodynamical features of the eye, but the results are not well correlated. Most of the research has necessarily been conducted on animals, usually monkeys, cats and rabbits, whose eyes do not have precisely the same anatomical structure of the human eye. Research on humans is usually limited to eyes before and after enucleation for pathological reasons, none of which can be considered "physiological".
Moreover, to date, mathematical models that include both the time-dependence of ocular fluid and blood flow together with the deformability properties of ocular structures, whose interactions give rise to the dynamics of IOP, do not exist or they are not easily reproducible or usable. As a main example, in [53] Kiel et al investigated into the relationship between ciliary blood flow and aqueous humor production, identifying a dynamic relationship. In the same work he also presented a theoretical model of ocular hydrodynamics integrating Moses' earlier work [47] with his own additional findings and taking inspiration from Brubaker's analog model of aqueous humor dynamics [10]. The resulting model was a computer based mathematical model developed in STELLA, a graphical programming language well suited for modeling hydrodynamic processes. The model, as can be seen in Figure 1.2, is quite difficult to interpret or integrate with other models of the eye.

In the present project, we make use of geometrical and material prop-

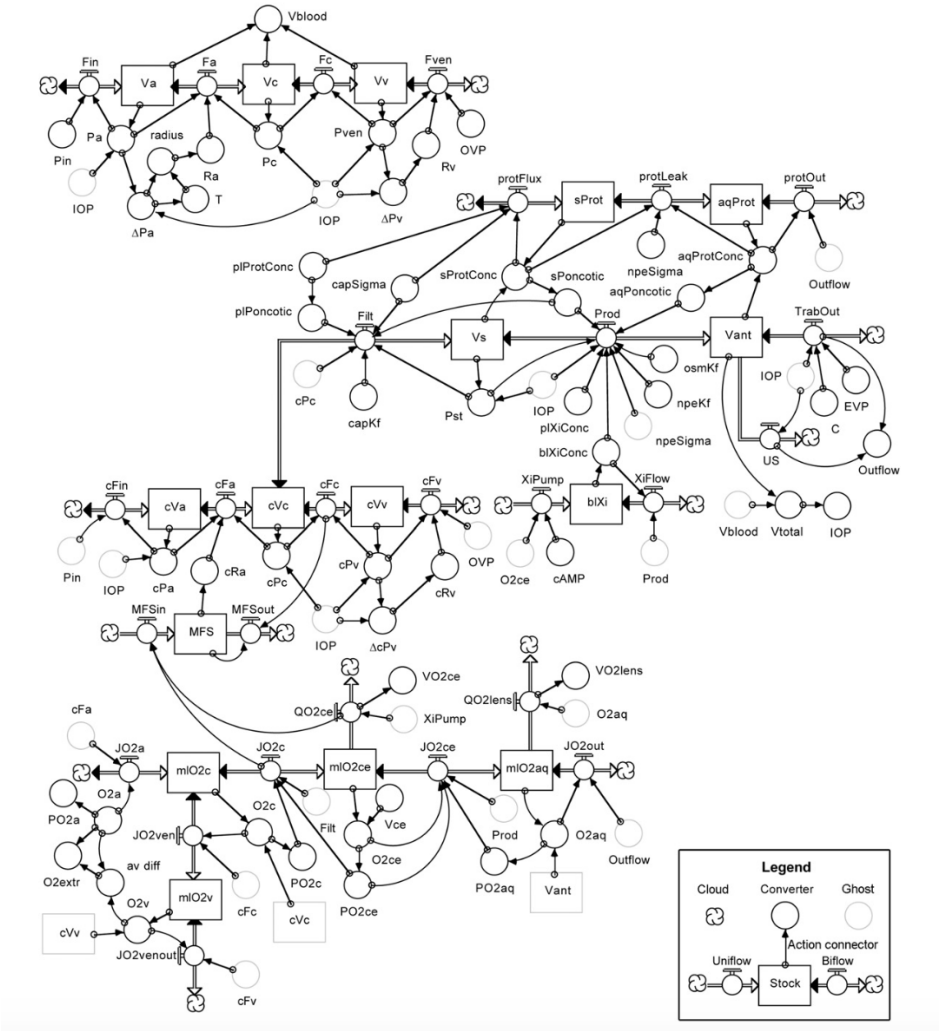

Figure 1.2: *Flow diagram of the model of ocular hydrodynamics written in STELLA in a work of Kiel et al in 2011 [53]. Graphic objects: "Stocks" (or reservoirs), rectangular box that can gain or lose material; Flow regulators ("Uniflow" and "Biflow"), spigot on a double-lined arrow connecting stocks or clouds (special stocks that provide continuous sources or sinks for the flowing material); "Converters", circle that can contain an equation or a constant; "Action Connectors", single-lined arrows that pass information between objects.*

erties assessed on humans, when available. Also, while quantifying the influence of parameter variations on the internal pressure, we consider both the static and dynamic components of IOP.

1.1 Anatomy of the eye

The material presented in this section is a summary of what contained in Chapter II of Ansari et al [48] and in Chapter II of Kiel's book [40].

The eye is a nearly spherical fluid-filled elastic shell with an anterior (corneal) bulge. The eyeball itself occupies only about 20% of the orbital volume, with the remaining space filled with muscles and ligaments, blood vessels, nerves, and adipose tissue. In the human eye, the outer diameter of the eye ball is about 24 mm, giving an external volume of about 7000 μl. The thickness of the eye covering —the cornea at the front and the sclera behind— varies between 0.3 and 1.3 mm, so the eye's internal volume is approximately 6000 μl.

Eye compartments include corneo-scleral top layer, lens, vascular bed, vitreous humor, iris, choroid, retina and anterior and posterior chambers filled with aqueous humor (AH). Light enters the transparent cornea (index of refraction IR=1.376), traverses the anterior chamber filled with AH (IR=1.336), and is focused by the lens (IR=1.42), under the control of the ciliary muscles, to form an image upon the retina. The retina is linked via the optic nerve to the brain, where the image is interpreted.

A schematic section of the human eye is depicted in Figure 1.3, and details of ocular structures are described below.

Cornea. Outer, transparent structure at the front of the eye that covers iris, pupil and anterior chamber. It is the eye's primary light-focusing structure and is made of 5 layers, 0.6-1.0 mm thick with normal radii of curvature of 7.8 mm (anterior surface) and 7.0 mm (posterior surface). Since transparency is essential to fulfill the eye's visual function, blood, which is opaque, cannot nourish the tissues of the eye lying within the light pathway or visual axis. For this reason, cornea and lens are nourished by AH.

Lens. Transparent structure suspended behind the iris that helps focus

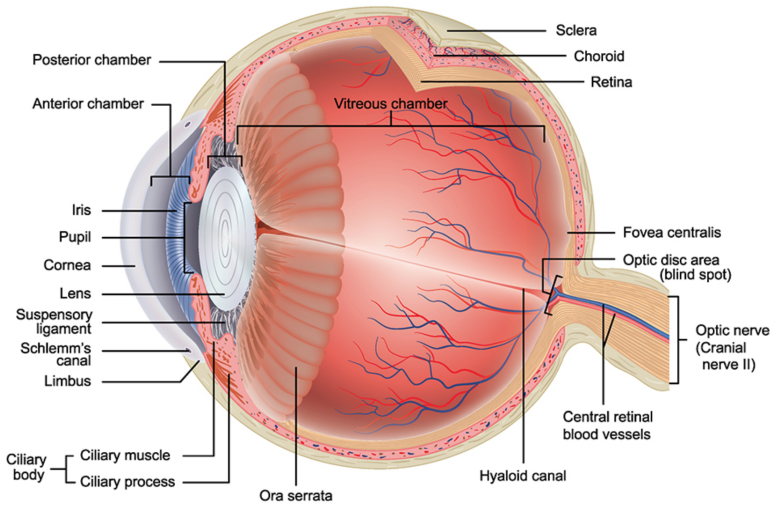

Figure 1.3: *Schematic section of the human eye [1]*

light on the retina. It primarily provides a fine-tuning adjustment to the primary focusing structure of the eye, which is the cornea.

Sclera. Fibrous outer layer of the eye shell that protects the inner layers of the eye.

Vitreous humor. Clear jelly-like substance that fills the eye from the lens to the back of the eye.

Iris. Colored ring of tissue behind the cornea that regulates the amount of light entering the eye by adjusting the size of the pupil.

Choroid. Mid layer of the eye shell, located between the sclera and the retina. It is a spongy, vascular layer that supplies blood to the outer part of the retina.

Retina. Inner layer of the eye shell that absorbs the light and sends visual stimuli to the brain. It contains the macula and the fovea that are regions responsible for visual acuity. The retinal vascular bed nourishes the retinal ganglion cells that are responsible for the transmission of visual information from the retina to the brain, via the optic nerve.

Macula. Portion of the eye at the center of the retina that processes

sharp, clear straight-ahead vision.

Fovea. Depression at the center of the macula that provides the greatest visual acuity.

Optic nerve. Bundle of nerve fibers at the back of the eye that carry visual messages from the retina to the brain.

Optic nerve head. Location where the axons of the retinal ganglion cells comes together and exit the eye to form the optic nerve, and where the major blood vessels enter to supply the retina.

Lamina cribrosa. Located in the optic nerve head (ONH), it is composed of layers of collagen fibers that insert into the sclera canal wall. The axons of the retinal ganglion cells and the central retinal artery and vein run through the lamina. It is responsible for maintaining the pressure difference between the IOP and the pressure in the optic nerve canal (retrolaminar tissue pressure).

Anterior chamber. Region of the eye between the cornea and the lens that contains aqueous humor.

Aqueous humor. Transparent fluid which is 98.1% water and contains sugar and amino acids. It is secreted by the ciliary body from the circulating blood and it fills the anterior chamber ($2.5-4\%$ of the total volume of the eye globe), while maintaining the pressure inside the eye, keeping the eye inflated and transporting nutrients to the avascular tissues of the lens and cornea.

Trabecular meshwork. Spongy tissue located near the cornea through which aqueous humor flows out of the eye.

Ciliary body. Located in the anterior part of the eye, it contains the ciliary muscle, which controls the shape of the lens, and the ciliary

epithelium, which produces the aqueous humor through its folds, called ciliary processes.

Blood flow. The arterial input to the eye is provided by several branches of the ophthalmic artery, which is derived from the internal carotid artery.

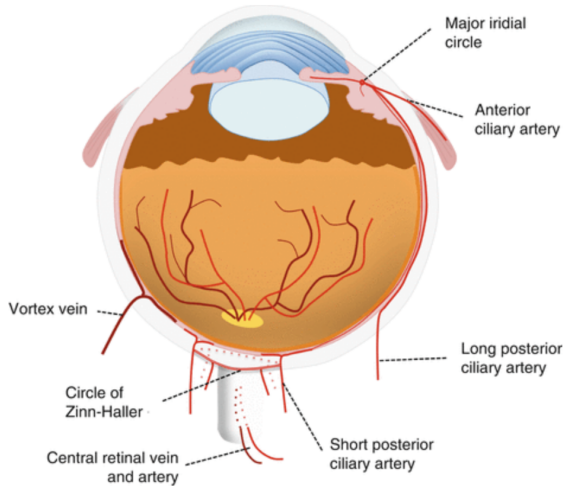

Figure 1.4: *Ocular circulation [2]*

These branches include the central retinal artery, the short and long posterior ciliary arteries, and the anterior ciliary arteries. Venous outflow from the eye is primarily via the vortex veins and the central retinal vein, which merge with the superior and inferior ophthalmic veins that drain into the cavernous sinus, the pterygoid venous plexus and the facial vein (see Figure 1.4).

The *iris* and *ciliary body* are supplied by the anterior ciliary arteries, the long posterior ciliary arteries and anatosmotic connections from the anterior choroid. Anterior ciliary arteries travel with the extraocular muscles and then they pierce the sclera near the limbus, whereas long posterior ciliary arteries pierce the sclera near the posterior pole and then travel anteriorly between the sclera and choroid. Then they both join the major arterial circle of the iris, which gives off branches to the iris and ciliary body. Most of the venous drainage from the anterior segment is directed posteriorly into the choroid and thence into the vortex veins.

The complex vascular supply of the *optic nerve* is divided into three zones. The zone of the optic nerve that precedes the lamina cribosa (pre-laminar zone) is supplied by collaterals from the choroid and retina circulations. The laminar zone is supplied by branches from the short

posterior ciliary and pial arteries. The post-laminar zone is supplied by the pial arteries. Venous drainage occurs via the central retinal vein and pial veins. The laminar zone marks the transition in optic nerve vessels from exposure to the IOP to the cerebral fluid pressure within the optic nerve sheath.

The *retina* is supplied by the central retinal artery and the short posterior ciliary arteries. The short posterior ciliary arteries pierce the sclera around the optic nerve then arborize to form the arterioles of the dense outer layer of choroidal vessels. The arterioles supply the choriocapillaris lobules that drain into venules. These venules join the larger ones of the outer conduit layer that coalesce into the 4-5 vortex veins which pierce the sclera at the equator. The central retinal artery travels in or beside the optic nerve as it pierces the sclera then branches to supply the layers of the inner retina. Retinal venules and veins coalesce into the central retinal vein, which exits the eye with the optic nerve parallel and counter-current to the central retinal artery. Maintenance of this blood supply is of prime importance, as vision is lost if the central retinal artery is occluded [46].

The effect of high, prolonged IOP may cause the lamina cribrosa depression to constrict. In this process, certain blood vessels, in particular the pial artery and vein which supply the periphery of the optic nerve, may collapse under the excessive external pressure. At higher levels of IOP, blood flow may be further impaired in the central retinal artery and vein which supply the core of the nerve bundle.
At still higher levels of IOP, these vessels become susceptible to collapse at the point where they enter the lamina cribrosa depression. Anteriorly, they are wrapped in a relatively stiff extension of the scleral envelope against which the blood vessels will be squeezed. Posterior to this transition section, however, this stiff outer sheath gives way to the more flexible dura which deforms more readily in response to the high IOP transmit-

ted through the lamina cribrosa. Deformation of the dural sheath tends to relieve partially IOP and consequently to retard, if not preclude, the collapse of these important vessels.

1.2 Glaucoma

Glaucoma is a group of diseases that can lead to damage to the eye's optic nerve and result in blindness. It tends to be inherited and may not show up until later in life due to the existence of no early symptoms or pain in most affected patients. By the time people experience problems with their vision, they usually have more than 50% of the ganglion cells damaged, thus they have lost a significant amount of their sight. Open-angle glaucoma, the most common form of glaucoma, is one of the leading causes of blindness in the United States and the number one cause of blindness among African Americans [49].

It usually happens when fluid builds up in the front part of the eye causing pressure in the eye to increase. The increased IOP can damage the optic nerve, which transmits images to the brain. If the damage continues, without treatment glaucoma can lead to total permanent vision loss within a few years.

1.2.1 Risk factors of glaucoma

Glaucoma is not defined as what its causes are, since they remain mostly unknown, but just as how it manifests. Typical behaviors of glaucomatous eyes are: a thinning of the retinal nerve fiber layer, a cupping of the optic disc, and a characteristic loss of vision starting from the periphery.

Even if elevated IOP is an acknowledged risk factor for glaucoma and furthermore is the only one that can be treated (through eye drops or surgery), yet there is significant evidence that other factors might be involved in the disease. In fact, more than 25% of glaucoma pa-

tient continue to progress in vision loss despite meeting target IOP levels [76][13][14][52][42][27], and a high percentage of individuals with elevated IOP never develops glaucoma [26][28].
Several factors have been recognized as possible concauses for glaucoma, for example vascular alterations and myopia, just to name a few. But precisely, how they combine to determine the onset of glaucoma in some people is still an open question in ophthalmology.

Risk factors of glaucoma include:

- elevated IOP, diurnal IOP fluctuations,
- increased age, myopia, sleep apnea (a sleep disorder characterized by pauses in breathing or periods of shallow breathing during sleep), diabetes, migraine, previous ocular injury, disc hemorrhage,
- family history, genetics, ethnicity (African descent),
- decreased intracranial pressure (ICP), low ocular perfusion pressure, systemic hypertension, nocturnal systemic hypotension,
- thinness of the cornea.

Elevated IOP.
The eye constantly produces aqueous humor. As new aqueous flows into the eye, the same amount should drain out. The fluid drains out through an area called the drainage angle that is a mesh-like channel. This process keeps IOP stable. If the drainage angle is not working properly (see Figure 1.5(b)), the liquid builds up so that pressure inside the eye rises causing damage to the optic nerve. The optic nerve is made of more than a million tiny nerve fibers. It is like an electric cable made up of many small wires. As these nerve fibers die, the person develops blind spots in his vision. Since most of the time the blind spots start from the periphery of the visual field, the person might not become aware of the vision loss till most of the optic nerve fibers have died. If all of the fibers

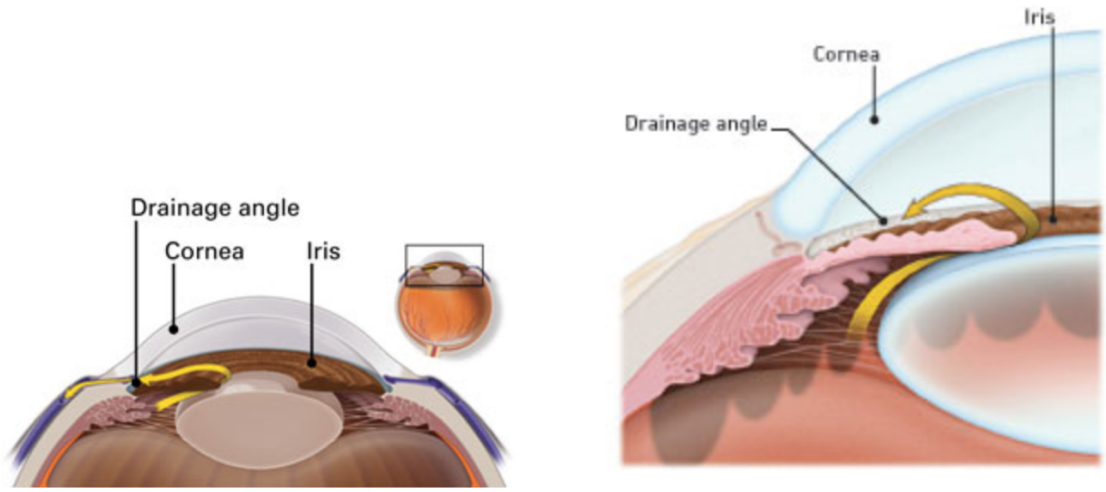

(a) *Drainage angle in a healthy eye: excess fluid leaves the eye through the meshwork, keeping pressure stable.*

(b) *Effect of a blocked drainage angle: excess fluid cannot flow out of the eye causing the fluid pressure to increase.*

Figure 1.5: *Closed-angle glaucoma [56]*

die, the patient will become permanently blind.

High myopia.

Increasing evidence indicates that high myopia is important in the pathogenesis of glaucoma, especially for primary open-angle glaucoma (POAG) [43], although increased IOP remains the major risk factor for this condition.

Diabetes.

Results of a meta-analysis investigation based on 13 epidemiological studies report the existence of a direct relationship between diabetes mellitus (DM) and POAG [80]. Proposed biological links between DM and POAG are the following. (i) The presence of long-standing hyperglycemia, along with lipid anomalies, increases the risk of neuronal injury from stress. (ii) Diabetic eyes have a reduced capacity to auto-regulate blood flow and they exhibit decreased retinal blood flow. As a result, they show relative hypoxia and overexpression of hypoxia-inducible factor-1. Importantly, levels of HIF-1α increased in ganglion cells, in the retina, and in the optic nerve head of human glaucomatous eyes in

response to elevated IOP. (iii) The remodeling of the connective tissue of the optic nerve head might reduce compliance at the trabecular meshwork and the lamina cribrosa, resulting in increased IOP and greater mechanical stress on the optic nerve head, respectively. Research has demonstrated that diabetes can exacerbate connective tissue remodeling and amplify these biomechanical changes. Genetic factors and diabetes-related autonomic dysfunction are likely to play a role of this association.

Previous ocular injury.

Less common causes include a blunt or chemical injury to the eye, severe eye infection, blocked blood vessels inside the eye, and inflammatory conditions.

Race and ethnicity.

Eleven population-based studies on populations of African origin and five on populations of European origin observed that the prevalence of POAG is significantly higher in white Australians than in the Dutch and significantly lower among black populations in South Africa, Nigeria, Tanzania and the United States than in Ghana, St. Lucia or Barbados. Notably, the prevalence was significantly lower in Afro Caribbeans living in London than in St. Lucia or Barbados [75]. These potential ethnic diversity in the prevalence of POAG might be attributed to the different methodology and definition of POAG, and to potential difference in social, behavioral and environmental factors and/or genetic predisposition. Moreover, racial differences have been associated with differences in ocular structures, ocular blood flow and systemic conditions [12].

Decreased intracranial pressure.

Cupping of the optic nerve head and the lamina cribrosa is a characteristic pathological manifestation of glaucoma. Under homeostatic conditions, the lamina cribrosa is subjected to a posteriorly directed pressure difference of roughly 4 mmHg, that arises out of the posteriorly directed IOP and the anteriorly directed ICP and creates a pressure gradient

across the lamina cribrosa, known as translaminar pressure gradient (TLPG). IOP and ICP are anatomically and physiologically interlinked pressure components and changes in one may be reflected by changes in the other within a biological range. Under pathological conditions like glaucoma, a low ICP in the presence or absence of a high IOP will cause an increasingly unbalanced posteriorly directed force on the lamina cribrosa. The thickness of the lamina cribrosa and the resulting elastic resilience of the surrounding sclera also play a significant role in maintaining the homeostatic condition around the optic nerve head [20].

1.2.2 Types of glaucoma

Primary glaucoma is glaucoma that develops due to an unknown cause. *Secondary glaucoma* develops from a known cause, usually due to a serious eye injury, cataract, tumor, or diabetes.
Although they have different causes, primary and secondary glaucoma share the same signs and symptoms. They both can takes two forms:

- *Open-angle glaucoma.* This is the most common type of glaucoma and is also called *primary glaucoma* or *chronic glaucoma.*
  It happens when the angle between the iris and cornea is wide and open but drainage canals, namely trabecular meshwork, are subjected to a slow obstruction processes. For this reason, the drain structure in the eye looks normal but fluid doesn't flow out like it should (see Figure 1.6).
  It happens gradually and causes eye pressure to rise starting to damage the optic nerve. This type of glaucoma is painless and causes no vision changes at first.
  Some people can have optic nerves that are sensitive to normal eye pressure. This means their risk of getting glaucoma is higher than normal.

- *Angle-closure glaucoma.* It is less common in the West than in Asia and is also called *closed-angle glaucoma* or *narrow-angle glaucoma.*
  It happens when the angle between the iris and cornea is closed or narrow so that the iris can end up blocking the drainage angle and flow from the posterior to the anterior chambers is obstructed (see Figure 1.7).
  When the drainage angle gets completely blocked, eye pressure rises very quickly. This is called an acute attack since it has symptoms and damage that are usually very noticeable and demands immediate medical attention.It is also linked to long-sightedness and cataracts, a clouding of the lens inside the eye. Many people with this kind of angle-closure glaucoma develop it slowly and in this case the disease is called chronic angle-closure glaucoma. There are no symptoms at first, so the patient don't know he has it until the damage is severe or he has an attack.
  Angle-closure glaucoma can cause blindness if not treated right away.

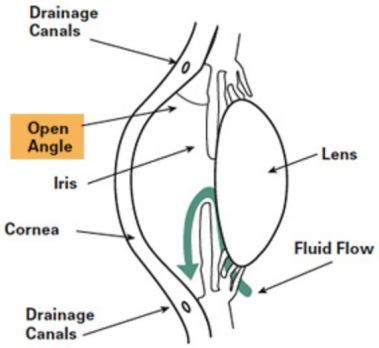

Figure 1.6: *Open-angle glaucoma [26]*

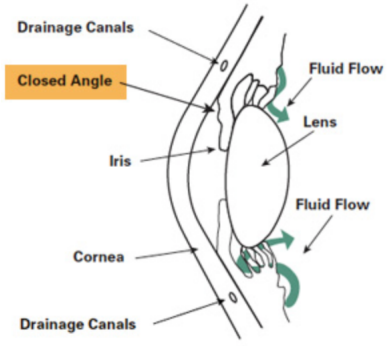

Figure 1.7: *Angle-closure glaucoma [26]*

Visual loss resulting from glaucoma cannot be restored, and present therapy is directed towards maintaining IOP at a level which does not cause further damage to the optic nerve.

1.3 Techniques for non-invasive ocular measurements

Clinical assessment of open angle glaucoma is usually performed through standard measurements of visual acuity, visual field, IOP, optic nerve head morphology, central corneal thickness and axial length [12]. In particular:

- visual acuity can be measured via the *Early Treatment Diabetic Retinopathy Study vision chart*,
- visual field can be measured using *Standard Automated Perimetry* (SAP) [35][29],
- the *average value of IOP* over a cardiac cycle can be measured via *Goldmann applanation tonometry*, while *IOP oscillations* over a cardiac cycle can be measured via *PASCAL Dynamic Contour Tonometer* [17],
- the morphology of the optic nerve head is usually estimated by analyzing images obtained with a *Fundus Camera*,
- central corneal thickness can be measured with an *ultrasonic corneal pachymeter*, and
- axial length can be measured via *optical biometry*.

In addition to these basic assessments, specific ocular structural and vascular parameters can be clinically measured via advanced imaging technologies, including:

- *Color Doppler Imaging* (CDI), that is used to measure blood flow velocity in the main arteries supplying the eye,
- *Fourier-domain Optical Coherence Tomography* (FD-OCT), that can be used to measure retinal nerve fiber layer thickness and structure

of the optic nerve head. If equipped with Doppler functionality, it captures high-resolution Doppler information from retinal vessels in three dimensions within a fraction of the cardiac cycle [78] and can be used to build patient-specific representations of ocular geometry,

- *Heidelberg Retinal Tomography*, that can be used as a secondary structural modality to OCT,

- *Retinal Oxymetry*, that measures oxygen saturation in arteries and veins in addition to diameters of these vessels,

- *Confocal Scanning Laser Doppler Flowmetry* (CSLDF), that measures the capillary blood flow of the retina and optic nerve head providing a two-dimensional map of ocular perfusion in these areas (main limitation is that velocity and volume are measured in arbitrary units),

- *confocal Scanning Laser Ophthalmoscope*, (cSLO) an instrument that can be used for several retinal imaging modalities including fluorescein angiography, indocyanine green (ICG) angiography and fundus autofluorescence [6],

- *Laser Speckle Flowgraphy* (LSFG), that allows for the quantitative estimation of blood flow in the optic nerve head, choroid, retina and iris in vivo [50], and

- *Retinal Vessel Analyzer* (RVA), a measuring device for online measurement of the diameter of retinal vessels in relation to time and locations along the vessel [72].

1.3.1 IOP assessment

As introduced in the Abstract of this thesis, IOP assessment is a simple, quick and non invasive test that any ophthalmology clinic can perform. In particular, both the static and the dynamic components of IOP can

be measured. Tonometers, namely instruments for measuring pressure in the eyeball, divide into two groups: indentation and applanation types.

The principle of ***indentation tonometry*** is that a force or a weight will indent or sink into a soft eye further than into a hard eye. The accuracy depends on the assumption that all eyes respond the same way to the external force of indentation, which is not the case. Variables that can introduce potential error are: low scleral rigidity —that can be caused by glaucoma or vitreoretinal surgery—, blood volume alteration, and thicker cornea that leads to a falsely high IOP reading.

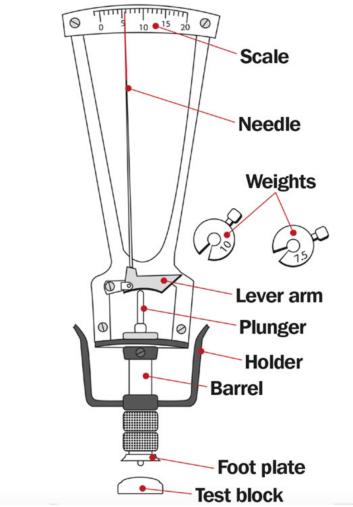

Figure 1.8: *Schiotz indentation tonometer [37]*

Schiotz tonometer works on the basic concept of indentation tonometry. The body of the tonometer consists of a curved footplate which is placed on the anesthetized cornea in a position that allows free vertical movement of the plunger. The plunger moves freely, except for the effect of friction, within a shaft in the footplate and the degree to which it indents the cornea gives an estimate of the IOP. A scale at the top of the plunger gives a reading depending on how much the plunger sinks into the cornea, and a conversion table converts the scale reading into IOP measured in mmHg (see Figure 1.8). Although not considered a standard instrument in glaucoma care, it is still in use because it is reasonably reliable, easy to use, has no electronic component, is inexpensive to use and maintain, and its calibration is simple [61].

Applanation tonometry is based on the Imbert-Fick principle, which states that the pressure inside an ideal dry, thin-walled sphere equals the force necessary to flatten its surface divided by the area of flattening. With this technique, the cornea is flattened and IOP is de-

termined by varying the applanating force or the area flattened.
Four shortcomings may contaminate this theory application: (i) in flattening a corneal segment from a spherical surface to a plane, the volume of aqueous humor under the peak of the cornea is displaced. This displaced volume stretches the eye with consequent increase of IOP. (ii) Tear fluid fills the angle between cornea and plane contact surface, and this surface of liquid may be mistaken for part of the corneal flattened area, implying a overestimation corneal contact area and hence a lower IOP. (iii) Surface tension of tear fluid adds a force to the applied force, so that the total force actually flattening the cornea is greater than the measured one, and resultant IOP is underestimated. (iv) Cornea resists bending, thus a force is required to distort the cornea to the flat shape. Therefore the measured force that is applied to achieve a given area of plane contact will be greater by the added spring force than the real force required to counterbalance IOP over that area, with a consequent overestimation of IOP.

In *Goldmann applanation tonometer* these difficulties are faced by: (i) keeping the contact area small, namely 3.06 mm of diameter (set by a bi-prismatic device), so that resultant displaced volume is small and the increase caused in IOP is only about 3% greater than real IOP, (ii) distinguishing tear surface from flattened cornea by staining the tears with fluorescein, and (iii)-(iv) choosing the contact area so that the two forces added by surface tension of tear fluid and by the resistance of cornea to bending balance each other. Thus the force is adjusted until the flattened area meets the criterion. in the end, force in grams ridden by the tonometer equals IOP in millimiters of mercury

Figure 1.9: *Goldmann applanation tonometer [44].*

when multiplied by 10 (see Figure 1.9).
The Goldmann applanation tonometer, long considered the gold standard for IOP measurement, is likely to underestimate IOP in eyes with thin corneas and to overestimate IOP in eyes with thick, more rigid corneas, due to the before-mentioned limitation (iv) [30][16][79]. This may be the explanation of a result of the Ocular Hypertension Treatment Study and other studies, according to which thin corneas are a risk factor for the transformation from ocular hypertension to open-angle glaucoma as well as for the progression of normal-tension glaucoma [9][25][65][45]. Moreover, myopic patients are considered to be at a greater risk of developing glaucoma, thus they require a particularly careful screening. Many of these individuals undergo the surgical modification of their corneas and, unfortunately, these procedures render accurate IOP measurement by standard methods, namely applanation tonometry, difficult or impossible [64].

The majority of tonometer designs proposed to date are based on the principle that a force is applied to the cornea to achieve a defined amount of distortion (indentation or applanation) of the cornea. The device measures the required force and infers the patient's IOP. The relationship between force and distortion depends on the patient's IOP and on the mechanical properties of the cornea also. As a result, a force measurement can yield accurate IOP readings only if the mechanical properties of all eyes are always the same. This is quite obviously not a valid assumption. In fact, as noted by Goldmann himself in his original description of his applanation tonometer, corneal thickness may vary between 400 and 650 μm among individuals. Furthermore, corneal shape (radius and astigmatism), elasticity, and rigidity differ widely among patients.

The ***dynamic contour tonometer*** (DCT) uses the principle of contour matching instead of applanation. The tip has a concave sur-

face which touches but allows the cornea to assume a shape (close to its steady-state shape) in which no tangential and bending forces are acting within the area of the cornea touching the tip. If the apex of the cornea is tension-free, the pressure acting on both of its sides (inside and outside) must be exactly equal. The pressure sensor placed on the outside of the cornea thus measures a pressure —the one at the corneal apex— that is equal to IOP. Detailed mechanical analysis [44] demonstrated that this pressure measurement is not affected neither by variations in corneal properties over a wide range of values nor by the amount of appositional force applied to hold the tip in place. Because the tip shape is designed for the shape of a normal cornea, it is yet more influenced by corneal curvature. PASCAL Dynamic Contour Tonometer is a commercially available, slit lamp-mounted device that embodies the described principle. It utilizes a piezoelectric sensor embedded in the tip of the tonometer to measure the *dynamic pulsatile fluctuations in IOP*. It can be used also to measure the ocular *pulse amplitude*.

An analysis done by Stamper in [64] showed that for IOP values ranging from 5 to 60 mmHg, DCT provides the most accurate IOP readings (within $< \pm$ 0.7 mmHg), wheres the results with Goldmann applanation tonometry were consistently below true IOP by an average of -4 mmHg [64]. Moreover, data from Goldmann applanation tonometry exhibited a significant correlation with corneal thickness, and instead the DCT data showed no correlation with corneal thickness, a finding that suggests that this tonometer alone functions independently of corneal thickness.

1.4 The role of mathematical modeling in ophthalmology

The need of qualitatively and quantitatively understanding the dynamics of complex biological systems has motivated the development of mathematical models. Mathematical modeling consists of translating "real-world problems" into mathematical equations whose solutions simulate the behavior of a physical system. These models are able to characterize the dynamic properties of underlying biological systems and to describe how they respond to therapeutic interventions. Statistical analysis of experimental and clinical data is one of the most common uses of mathematics in medicine, and a number of statistical approaches can be used to analyze results of the models. One of them is sensitivity analysis, which is employed to evaluate to what extent changes in a model input parameter or a set of model input parameters will affect the model output.

While mathematics via statistical methods can be used to analyze trends observed in data obtained in laboratories and clinics, mathematics via physically-based modeling can also be used as a "virtual laboratory" to produce "virtual data" or to study the mechanistic relationships of a system's components that combine to yield the observed trends.

In the context of IOP dynamics and risk of glaucoma, a virtual laboratory based on mathematical models can be used to simulate the relationship between ocular mechanics and hemodynamics, which is not easy to assess in vivo. In particular, mathematical models can assess the role of hemodynamical and ocular tissues mechanics in influencing IOP by:

1. describing the IOP response to variations in arterial pressure —variations in ciliary blood pressure in our model—, aqueous humor dynamics, ocular blood flow —variations in choroidal blood flow in our model—, ocular rigidity and, in particular, scleral, corneal and

vitreous deformability;

2. providing quantitative estimates of IOP variations induced by these hemodynamical and mechanical alterations.

By addressing these two points, mathematical models can provide a framework from which new therapeutic concepts for glaucoma, based on the interrelation between biomechanics and ocular hemodynamics, could be tested and tuned at low cost and in a relatively short period of time.

In this thesis, we use both the above-mentioned mathematical tools: we firstly develop a *mathematical model* that describes the interaction between hemodynamics and mechanics of ocular fluids and tissues, then we perform *sensitivity analysis* on the model to quantify the influence of parameter variations on the output of the model, that is IOP dynamics.

1.5 Outline of the thesis

This thesis is organised as follows.
In Chapter 2 we give a description of the physiology of IOP presenting two historical models.
Section 3.1 concerns the basics of our modeling, that is the electrical-hydraulic analogy which we made use of for designing the electric analogue of the physiology of IOP.
Three subsequent models are presented in Chapter 3. They can be thought of as successive steps towards the modeling of the whole eye dynamics. Results of these models are reviewed in Chapter 4, where we describe the outcomes of sensitivity analysis —both deterministic and stochastic— performed on the models.

In Chapter 5 we present an interesting clinical application of our models. We simulate the effect of IOP-lowering medications in different conditions of clinical interest (ocular normotensive healthy subjects and ocular hypertensive subjects) and quantified the influence of different parameters of the model on IOP dynamics.
In Chapter 6 we review the more detailed model on which we are still working on and that will provide an insight for future developments.

Chapter 2

Modeling IOP physiology: a historical perspective

In this section we will outline the main components of the physiology of intraocular pressure. The material that will be described here is a summary of what presented in Chapter III of Kiel's book [39].
Under healthy physiological conditions, IOP in humans is around 15 mmHg and relatively stable due to the existence of a homeostatic feedback loop. Efferent limbs of this feedback loop are known thanks to the multiple pharmacological targets available to manipulate IOP, whereas the afferent one is not yet evident. IOP presents small variations caused by cardiac and respiratory oscillations —in the range of 1-2 mmHg and in phase with cardiac cycle— and larger variations due to diurnal and circadian changes. Thus, a complete modeling of the physiology of IOP should take into account both these time scales of fluctuations (see Figure 2.1).

Main functions of the pressure inside the eye are the maintenance of ocular shape and optical properties, even if studies showed only a slight correlation between pressure and refraction [77]. Moreover, IOP is a consequence of the regulation of aqueous production that is needed to provide adequate nourishment of the avascular cornea and lens.
In the following we review two historical models that describe IOP phys-

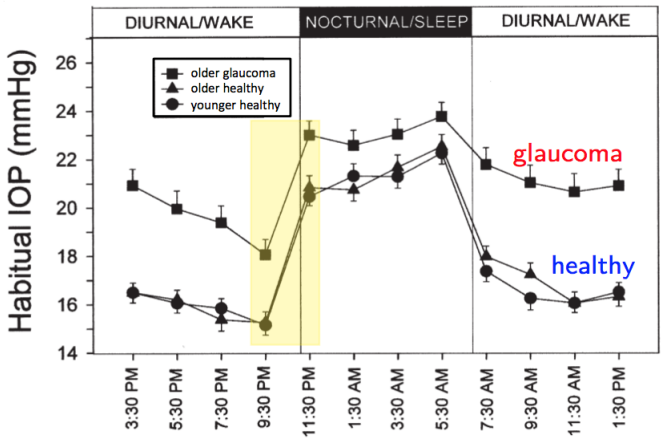

Figure 2.1: *IOP day-night changes in healthy and glaucomatous eyes [73]*

iology.

(i) The **pressure-volume model**, which rests on the exponential relationship that links IOP and total ocular volume as a function of the elastic properties (γ is the elastance, or "rigidity") of the ocular walls:

$$IOP = f(V_{tot}, \gamma). \tag{2.1}$$

(ii) The **hydraulic model**, which describes IOP as a function of aqueous flow F and outflow resistance R ($R = 1/C$, where C is outflow conductance):

$$IOP = F/C + EVP. \tag{2.2}$$

EVP is the episcleral venous pressure.

2.1 Pressure-volume model

The relationship between IOP and V_{tot} (see Figure 2.2) is exponential and depends on the ocular rigidity coefficient. Indeed, the structural characteristic of the ocular coats dictate a particular P-V relation that defines the change in volume due to changes in IOP. Ocular volume is primarily influenced by vitreous, lens, aqueous and blood, the first two

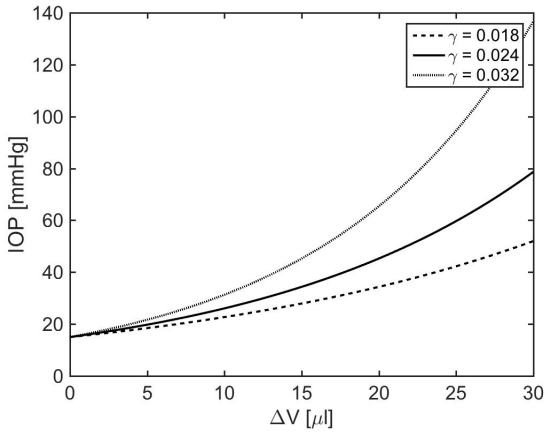

Figure 2.2: *Ocular P-V relationship plotted with different values of ocular wall rigidity*

determinants being relatively stable over time. Thus, variations in IOP are mainly due to *variations of aqueous volume* (posterior and anterior chamber, light blue portion in Figure 2.3) *and blood volume* (ciliary and choroidal circulation, red vessels in figure).

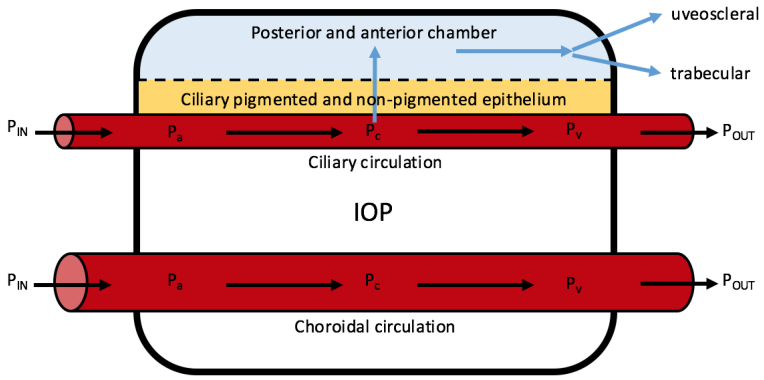

Figure 2.3: *Factors contributing to IOP: aqueous humor (light blue arrows) and blood (black arrows) volumes. P_{IN}: extraocular arterial pressure, P_a: intraocular arterial pressure, P_c: intraocular capillary pressure, P_v: intraocular venous pressure, P_{OUT}: extraocular venous pressure.*

- **Changes in aqueous volume** result from imbalances in aqueous production and outflow. Aqueous is produced in the ciliary body through *ultrafiltration* from the ciliary circulation into the stroma and pigmented epithelium and *active secretion* by the non-pigmented epithelium.

Aqueous outflow occurs via the *trabecular* and the *uveoscleral pathways*.

- **Changes in ocular blood volume** result from imbalances in blood inflow and outflow. Ocular blood volume is mainly contained in the *choroid* which is supplied by the short posterior ciliary arteries and drained by the vortex veins at the equator. Choroidal blood volume accounts for most of the changes in eye blood volume.

This model highlights the role of the structural properties of ocular coats in dictating the amount of changes in volume as a function of changes in IOP, but it fails to identify where and how these changes in volume occur.

2.2 Hydraulic model

The energy source for IOP is the metabolic apparatus that drives the ionic fluxes responsible for aqueous production. Aqueous humor is formed in the ciliary epithelium, then it passes from the posterior chamber through the space between iris and lens and through the pupil into the anterior chamber and leaves the eye via trabecular pathway, Schlemm's canal and episcleral veins. A small portion of the aqueous flows into the vitreous to be absorbed in the posterior part of the eye, and apparently some of the aqueous is reabsorbed at the ciliary body [47]. Aqueous accumulates in the eye because of the compact structure of the trabecular meshwork and the positive hydrostatic pressure beyond it that impede the leak of aqueous humor from the eye. This increase in volume causes IOP to augment until it provokes the egress of aqueous. When the rate of outflow equals the rate of inflow, IOP is at steady-state.

- **Aqueous production** takes place in the ciliary processes by the transfer of fluid and solute across the blood-aqueous barrier. This

process involves three steps (circled in blue in Figure 2.4):

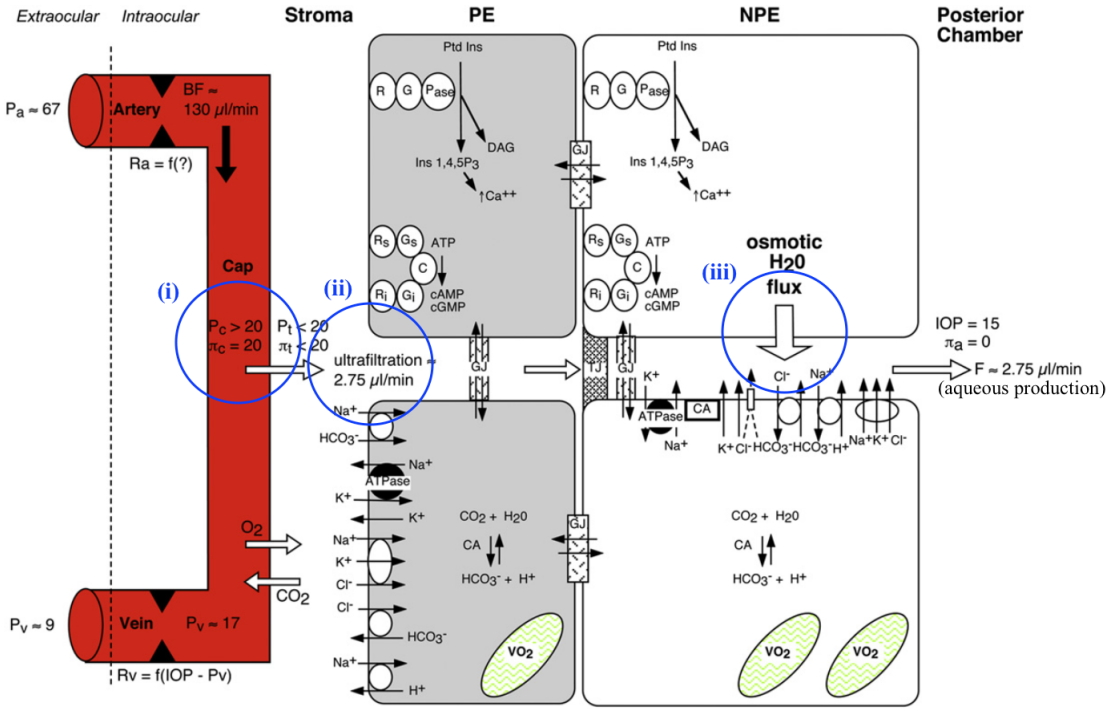

Figure 2.4: *Overview of the mechanisms that determine aqueous humor formation.*
(i) ciliary circulation, (ii) ultrafiltration, (iii) active ionic secretion. Kiel et al 1998 [39]

(i) convective delivery of water, ions, proteins and metabolic substances via the ***ciliary circulation***.

This vasculature divides into three zones [55]: the *first zone* is at the anterior base of the processes and consists of arterioles and capillaries that drain into a venular system separate from the other zones. This zone forms the boundary between the non-fenestrated capillaries of the iris and the fenestrated capillaries of the ciliary processes. The fenestrations permit passage of protein into the stroma that establishes an oncotic pressure important in aqueous humor production; the *second zone* extends more anteriorly into the processes and drains into marginal venules flowing into an efferent venous segment that travels posteriorly into the ciliary veins, namely vortex veins; the *third zone* supplies the posterior

portion of the processes.

Studies conducted on rabbits [53] showed that aqueous humor production is independent of ciliary blood flow above a critical level of ciliary perfusion, and blood flow dependent below that critical level of perfusion. This critical level occurs at around 40 P.U. (perfusion units), that is roughly 74% of ciliay blood flow baseline value and corresponds to a mean arterial pressure (MAP) of 40 mmHg. Under this value of MAP, aqueous humor flow decreases as a seemingly linear function of ciliary blood flow.

(ii) ***ultrafiltration*** of water and ions and ***diffusion*** of larger molecules from the permeable capillaries into the stroma.
The former is driven by oncotic pressure (π_c, π_t) and hydrostatic pressure (P_c, P_t) and the latter by concentration gradients.

(iii) ***active ionic secretion*** of Na^+ and other ions into the basolateral space between the non-pigmented epithelial cells (NPE) that establishes the osmotic gradient responsible for fluid movement across the barrier.
Major features of the blood-aqueous permeability barrier are:

- the tight junctions (TJ in Figure 2.4) at the apical surface of adjacent NPE cells that constitute the main barrier,
- the absence of fenestrations and the low permeability of the iris capillaries,
- the pigmented epithelial cells (PE) basement membrane and the gap junctions (GJ in figure) between PE cells that do not impede the movement of proteins.

The resultant barrier has a low hydraulic conductivity that fluid has to overcome by means of the osmotic gradient to reach the posterior chamber. This results in fluid flux from the NPE cells and across the TJ so that the fluid leaving the channels and entering

the posterior chamber is either iso-osmotic or slightly hyperosmotic relative to plasma.

- **Aqueous outflow** takes place via two pathways (see Figure 2.5):

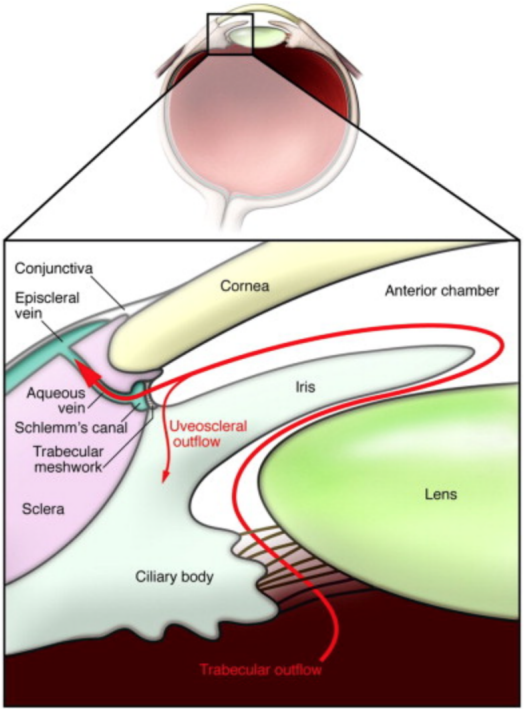

Figure 2.5: *Anterior chamber structures involved in aqueous humor outflow [74]*

(i) the pressure-dependent ***trabecular pathway*** —that constitutes 70% of the total outflow.

The trabecular meshwork is a series of overlapping sheets of connettive tissue covered with a monolayer of endothelial cells and equipped with pores of various sizes. The innermost sheets closest to the anterior chamber comprise the uveal meshwork, while the outer sheets form the corneoscleral meshwork. These layers offer little resistance to aqueous movement and help maintain the patency of the trabecular pathway thanks to their filtering and phagocytic activity.

Aqueous moves from the corneoscleral layer into the *Schlemm's*

canal via the pressure-dependent formation of giant vacuoles and pores in the endothelium of Schlemm's canal, and to a lesser extent via the tight junctions between endothelial cells. Moving from the uveal meshwork to the Schlemm's canal, the matrix becomes progressively more dense and resistant to the movement of aqueous. The majority of the resistance to aqueous flow in the trabecular pathway, namely $\simeq 90\%$, occurs between the corneoscleral layer and the Schlemm's canal. Conversely, Schlemm's canal and the collecting channels up to the *episcleral veins* contribute little to the total trabecular resistance.

Trabecular resistance varies with the contractile state of the ciliary muscle due to the existence of tendon attachments within the meshwork: increased muscle tension pull on the inner trabecular lamellae causing them to separate and allowing easier fluid movement, in the same way as traction on the tissue between corneoscleral layer and Schlemm's canal opens partially collapsed region of the canal promoting fluid passage.

(ii) the non-pressure-dependent ***uveoscleral pathway***.

The uveoscleral meshwork carries fluid from the anterior chamber through the ciliary muscle to the supraciliary and suprachoroidal spaces. Then aqueous humor exits the eye by percolating through sclera directly or at vascular sites. In this pathway, flow is reduced by ciliary muscle contraction.

Under normal conditions uveoscleral flow is extimated to be 0.8 $\mu l/min$ in healthy young eyes, while lower values are found in older and diseased eyes [51]. The uveoscleral outflow behaves like a constant-rate pump, although there is no evidence of any metabolic mechanism involved [47]. The lack of effect of IOP on the uveoscleral flow rate possibly is due to the compression of the soft uveal tissue against the sclera, thus controlling the egress of

flow in proportion to IOP.

Limitation of this model are the difficulty in measuring the different variables with non-invasive techniques and the correlation that exists between these variables that requires a non-linear model for IOP. Also, aqueous humor sets the steady-state IOP but it is not solely responsible for generating IOP, thus a model that considers only aqueous dynamics appears to be too restrictive. These reasons make it necessary to develop a model that considers not only the steady-state component but also factors that contribute to the dynamic part of IOP and their influence while varying one independently from the others or together.

2.3 Aqueous dynamics and IOP

2.3.1 Driving forces of aqueous flow

Three mechanisms are important in determining aqueous humor flow in the eye [47]:

(a) **hydraulic pressure head**. It is the difference in upstream pressure and downstream pressure. The rate of flow pushed by the pressure difference ΔP is given by

$$F = \Delta P\, C, \tag{2.3}$$

where C is measured in $\mu l/min/mmHg$ and is called *facility*. C is proportional to the radius of the tube and inversely proportional to its length and fluid viscosity. It is analogous to the electrical conductance and the inverse of the resistance.

b) **osmotic pressure difference**. It is caused by an unequal distribution of dissolved substances on the two sides of a barrier through which solvent, but not solute, may pass. Solvent moves across the

barrier from the region of higher solvent concentration to the region of lower solvent concentration. Osmotic pressure is measured by hydrostatic pressure, since it is considered as the force per unit area that must be exerted on the region of low solvent concentration to stop net movement of solvent.

Therefore the total pressure head through a semipermeable barrier is given by the contribute of hydrostatic and osmotic pressure differences and the resultant rate of flow is

$$F = [(P_{1,hydro} - P_{1,osm}) - (P_{2,hydro} - P_{2,osm})]\, C. \tag{2.4}$$

Flow caused by hydrostatic pressure against an osmotic pressure gradient is called *ultrafiltration*.

(c) **metabolic pump**. It transports various substances against a concentration gradient. Two examples are the ascorbate pump and the bicarbonate-water pump. The former uses the energy supplied by the sodium-potassium adenosine triphosphatase (ATPase) that supplies the energy for the transport of ascorbate from the ciliary epithelium into the posterior chamber. The latter uses carbonic anhydrase that transports bicarbonate. The carbonic anhydrase inhibitor acetazolamide decreases aqueous secretion and so IOP.

2.3.2 Relationship with IOP

As Moses showed in his hypothetical graph (see Figure 2.6) [46], steady-state IOP occurs when aqueous production equals aqueous outflow. Total outflow is computed as trabecular outflow plus a fixed uveoscleral flow of $0.3\,\mu l/min$ and it ceases when IOP equals episcleral venous pressure —assumed to be $9\,mmHg$. Aqueous humor inflow has small negative slope until IOP exceeds 50 mmHg, whereupon the slopes become more negative and the inflow equals zero when IOP equals the assumed ciliary

arterial pressure of $70\,mmHg$.

In a healthy eye with normal aqueous production, namely $2.75\,\mu l/min$,

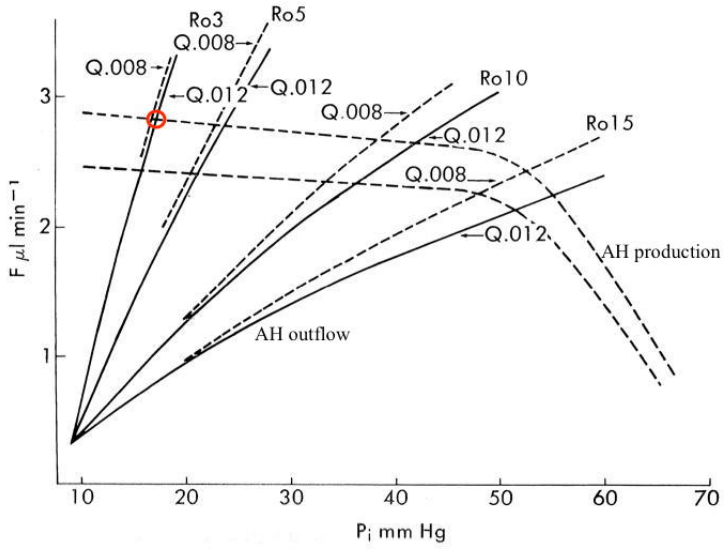

Figure 2.6: *Effect of IOP (Pi) on aqueous humor inflow and outflow. The slopes of the curves for total outflow vary with outflow resistance Ro as modified by the obstruction coefficient Q [46].*

and outflow facility, namely $0.3\,\mu l/min/mmHg$ —reciprocal of outflow resistance Ro in Figure 2.6—, aqueous production and outflow curves intersect at an IOP of $15\,mmHg$ (red circle in figure).

As often occurs in primary open angle glaucoma, outflow facility decreases without a change in the factor driving aqueous production so that necessarily IOP increases. Inhibiting aqueous production with a beta blocker to face ocular hypertension leads IOP to get back to its physiological value.

The effect of IOP increase with a decrease outflow facility while aqueous production remains constant is shown in Figure 2.7. The relationship is non-linear and the curves theoretically converge to a common IOP as the outflow facility goes to zero. It occurs because ciliary blood flow ceases when IOP reaches systolic blood pressure in the ciliary artery, namely $67\,mmHg$.

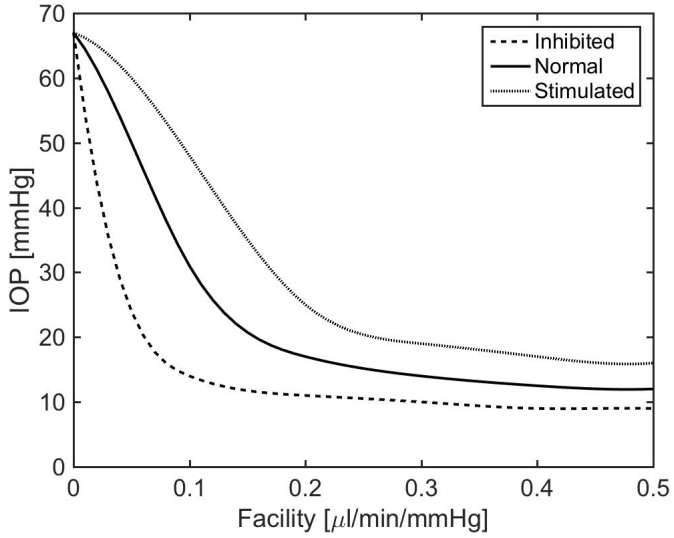

Figure 2.7: *Effect of outflow facility on IOP at three levels of ciliary secretory activity*

2.4 Effect of episcleral venous pressure on IOP

When episcleral venous pressure increases, the rise in IOP is immediate. This rapid increase in pressure cannot be the result of the decrease in pressure head for aqueous trabecular outflow, namely $IOP - EVP$, because aqueous flow is only $3\,\mu l/min$ or less. Instead this effect of IOP is due to the engorgement of intraocular blood vessels that occurs mainly in the choroid and ciliary body. The steady state is not reestablished until the vascular engorgement has been abolished and extra intraocular blood has been replaced by aqueous, a process that takes approximately 15 minutes or more [47]. Although suppression of aqueous formation with rise of IOP is minimal in the uninflamed eye [11], in the presence of the inflamed and leaky blood vessels it can be of considerable magnitude [5].

2.5 IOP and glaucoma

What is know by all the ophthalmologists is that if IOP is "high enough" for a "long enough" time, the subject will lose visual field in a characteristic pattern. As we previously described in Section 1.2, total angle closure by iris apposition to the trabecular mesh, with total block of aqueous outflow, will raise pressure in the eye. IOP may raise to 55 or 60 mmHg within hours, and total field loss may occur in a few days. However, partial angle closure, primary open-angle glaucoma, or other forms of partial outflow obstruction may cause IOP to rise into the 30 to 40 mmHg range and either cause field loss over a period of months or occasionally it may be tolerated indefinitely without field loss. In the range 20 to 30 mmHg IOP is tolerated more frequently for long periods, yet field loss at these pressure is common.
The interesting aspect is that even an eye with pressure below 20 mmHg may develop typical glaucomatous field loss.

These combinations of IOP and visual field state have led to terms as "*ocular hypertension*" —potentially damaging IOP with no detectable field loss— and "*low tension glaucoma*" —normal IOP with glaucoma-type field loss— and they induce to think of other determinants of glaucoma in addition to a high IOP. For this purpose a mathematical model that describes the ocular biomechanical and hemodynamical interaction in determining IOP could be useful to uncover relevant patient-specific parameters that mostly influence one's IOP and that, all combined, could eventually determine the onset of glaucoma in a specific patient.

Chapter 3

Modeling IOP physiology: new contributions

In this section we will present three subsequent models that we developed to investigate the relationship between ***ocular hemodynamics, biomechanics*** and ***IOP dynamics***.

Models are designed as electrical analogues of the physiology of the eye, including details regarding structural mechanics and fluid dynamics. As introduced in Chapter 1, pressure values inside the eye exhibit a *static component*, mainly due to the balance of aqueous humor inflow and outflow, and a *dynamic component*, mainly due to blood flow oscillations. We consider both the static, namely the steady-state characteristics of IOP, and the dynamic, namely the time dependent characteristics of IOP, components and, in particular, we investigate and quantify the influence of tissues (vitreous humor, cornea and sclera) deformability and blood flow pulsatility on the dynamic measurements of IOP.

Model calibration and validation are performed using published data. All the models have been implemented using the open access software OpenModelica in order to facilitate further model extensions and connections with other models already available for different parts of the eye.

3.1 Electrical analogy to fluid flow

Our modeling approach is based on the electrical analogy to fluid flow, according to which the analysis of an electric circuit can be compared to the one of a hydraulic circuit. In particular:

- **electrical current** $I = dQ/dt$ flowing in the circuit, generated by the movement of electrons (electric charge Q) is the analogue of **flux** (volumetric flow rate) $J = dV/dt$ of a fluid flowing through hydraulic pipes,
- **potential difference** $\Delta v = W/Q$, that moves electrical charges (W stands for work), is the analogue of **pressure difference** $\Delta P = U/V$, namely a difference of pressure level between two nodes of the hydraulic circuit, that generates a current of the liquid (U stands for energy),
- **voltage source**, that keeps a constant potential difference at its terminals which allows to maintain a flow of current in the circuit, is the analogue of **hydraulic pump**, that gives the necessary energy to the fluid to flow from the lower compartment to the higher, maintaining constant the difference in height,
- **electrical resistance** $R = \Delta v/I$, the "barrier" that current meets flowing through the circuit, is the analogue of **hydraulic resistance** $R = \Delta P/J$,
- **electrical conductance** G, that linearly relates potential and current, namely $I = Gv$, is the analogue of **hydraulic facility** (also known as hydraulic conductance) L, that linearly relates pressure and flux, namely $J = LP$,
- **electrical capacitance** C, that relates changes in potential with a

generated current, namely $I = \frac{d}{dt}(C\Delta v)$, is the analogue of **hydraulic capacitance**, that accounts for volume storage due to structural deformability, namely $\frac{dV}{dt} = \frac{d}{dt}(CdP)$.

3.2 Basic modeling assumptions

The main assumption of our model is that the total volume of the eye is given by the sum of three contributions:

$$V_{tot} = V_{AH} + V_{blood} + V_{struct}, \tag{3.1}$$

where:

1. V_{AH} is the volume of aqueous humor in the eye, considered to be equal to the volume of anterior chamber (V_{ant}). This approximation doesn't account for the small portion of aqueous humor that flows into the vitreous to be absorbed in the posterior part of the eye. However, this assumption is justified by the fact that, as shown by Moses [47], most of the aqueous humor flows into the anterior chamber after being formed at the ciliary processes.

2. V_{blood} is the volume of blood in the eye, including the blood flowing in the ciliary body, retina and choroid. However, since $V_{cil} = 0.01\,ml << V_{ch} = 0.2\,ml$ [53] and $V_{ret} < 3.8\%\,V_{ch}$ [59], we will assume that $V_{blood} \simeq V_{ch}$. And besides, as specified in Section 2.2, aqueous humor production proves to be independent of ciliary blood flow above a critical level of ciliary perfusion, that corresponds to a MAP of 40 mmHg. Since in our models we do not account for MAP variations outside the range 93 ± 7.6 mmHg, we can state that in this context our assumption is reasonable.

3. V_{struct} is the remaining volume of the eye, accounting for the vitreous

humor and other structures including lens and iris, as suggested by Kiel et al [53].

3.3 Static Model

3.3.1 Methods

The basic assumptions of this first step into the modeling of IOP physiology are:

1. the model is stationary, as time variations are not considered;
2. pressure is assumed to be uniform inside the eye (and named IOP); and
3. V_{ch} and V_{struct} are given constants.

For this reason, the only effect on the static component of IOP is given by **aqueous humor flow balance**:

$$0 = \frac{dV_{tot}}{dt} = \frac{dV_{ant}}{dt} = J_{in} - J_{out}, \tag{3.2}$$

where J_{in} represents the AH flowing into the eye and J_{out} represents the AH flowing out of the eye (see Figure 3.3).
The model of this section is presented in the article by Szopos et al [31] and we translate it into an OpenModelica circuit.
The purposes are to (*1.*) describe the steady-state value of IOP and (*2.*) quantify the influence of parameters' variations on the static component of IOP.

The ***steady-state value of IOP*** is computed as the solution of the equation that describes the balance between AH production and AH

drainage:

$$J_{in} = J_{out}. \tag{3.3}$$

AH production: AH is produced by the epithelium of the ciliary body via the combination of a passive mechanism, the *ultrafiltration*, and an active mechanism, the *ionic secretion*, as described in Chapter 1.
Therefore, the total flow of AH entering the eye is given by

$$J_{in} = J_{uf} + J_{secr}. \tag{3.4}$$

Both the ultrafiltration and the ionic secretion are modulated by the hydraulic conductance, also known as filtration coefficient, L (flow rate per units of pressure) and follow the Starling equation for fluid flux. Precisely:

- The *ultrafiltration* is driven by hydrostatic pressures difference ($cBP - IOP$) and oncotic pressure difference ($\Delta\pi_p$) between blood and AH (the latter modulated by a protein reflection coefficient named σ_p):

$$J_{uf} = L[(cBP - IOP) - \sigma_p \Delta\pi_p]. \tag{3.5}$$

- The *ionic secretion* is driven by osmotic pressure difference ($\Delta\pi_s$) between blood and AH modulated by a low-molecular components reflection coefficient named σ_s):

$$J_{secr} = L[-\sigma_s \Delta\pi_s]. \tag{3.6}$$

Osmotic pressure and oncotic pressure are two phenomena that occur due to osmosis. Osmosis is the process of the net movement of water through a semi-permeable membrane by diffusion due to the concentration gradient.
The main difference between osmotic pressure and oncotic pressure is that *osmotic pressure* is the pressure needed to stop the net movement

of water across a permeable membrane which separates solvent and solution, whereas *oncotic pressure* is the contribution made to total osmolality by colloids in a solution (hence, it is also known as *colloid osmotic pressure*). Main contributing factors for osmotic pressure are the number of solutes or particles and the degree of ionization, whereas the main contributing factor for oncotic pressure is the number of colloids in a solution (in fact oncotic pressure is a direct function of protein concentration in a compartment).

AH drainage: AH is drained from the eye through two pathways: the *trabecular pathway* (through trabecular meshwork in the anterior chamber, into Schlemm's canal, and subsequently into episcleral veins) and the *uveoscleral pathway* (through ciliary muscle, into supraciliary space, and subsequently into veins in the choroid and sclera), as described in Chapter 1. Both are passive mechanisms.
Therefore, the total flow of AH leaving the eye is given by

$$J_{out} = J_{tm} + J_{uv}. \tag{3.7}$$

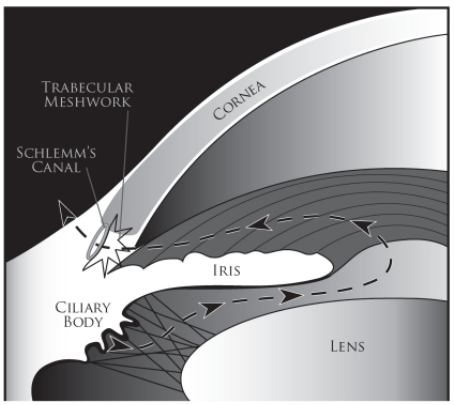

Figure 3.1: *Trabecular pathway [7]*

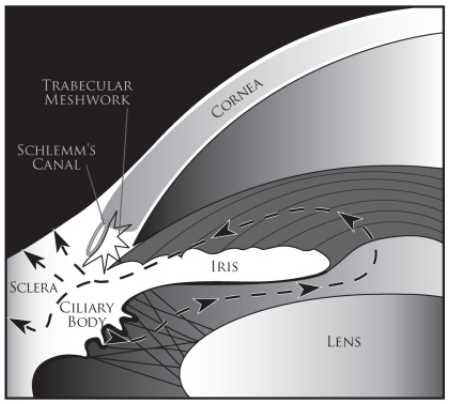

Figure 3.2: *Uveoscleral pathway [7]*

- The *trabecular pathway* is driven by hydrostatic pressures difference $(IOP - EVP)$ between AH and blood and is modulated by the

non-linear hydraulic conductance C_{tm} (Brubaker adjustment):

$$J_{tm} = C_{tm}(IOP - EVP), \text{ with } C_{tm} = \frac{1}{R_0[1 + Q(IOP - EVP)]}, \tag{3.8}$$

where R_0 is the resistance when pressure gradient equals zero and Q is the outflow obstruction coefficient.

- The *uveoscleral pathway* is driven by IOP and is modulated by the non-linear hydraulic conductance C_{uv}:

$$J_{uv} = C_{uv}(IOP - UVP), \text{ with } C_{uv} = \frac{k_1}{k_2 + IOP}, \tag{3.9}$$

where k_1 is the maximum value of uveoscleral flow rate and k_2 is the pressure at which uveoscleral flow rate is at half maximum. The uveoscleral pressure UVP is equal to the atmospheric pressure and therefore $UVP = 0$ in equation (3.9).

From the balance between production and drainage of AH (see eq. (3.3)), it is possible to explicitly compute the steady-state value of IOP as the solution of the following algebraic equation:

$$\begin{aligned} &L[(cBP - IOP) - \sigma_p \Delta\pi_p - \sigma_s \Delta\pi_s] = \\ &= \frac{1}{R_0[1 + Q(IOP - EVP)]}(IOP - EVP) + \frac{k_1}{k2 + IOP} IOP, \end{aligned} \tag{3.10}$$

which is a scalar third-order polynomial equation in the sole unknown IOP. The value obtained solving equation (3.10) in Matlab, using published data for the parameters (representing typical conditions of an healthy eye, see Table 3.1), is: $IOP = 14.9527\, mmHg$.

Parameter	Value and Unit	Meaning
L	$0.3\ \mu l/\min/mmHg$	*hydraulic conductance (total inflow facility)*
cBP	$27.5\ mmHg$	*ciliary blood pressure*
$\Delta\pi_p$	$25\ mmHg$	*oncotic pressure difference*
σ_p	$1\ [-]$	*protein reflection coefficient*
$\Delta\pi_s$	$-450\ mmHg$	*osmotic pressure difference*
σ_s	$0.0515\ [-]$	*low-molecular component reflection coefficient*
EVP	$8\ mmHg$	*episcleral venous pressure*
R_0	$2.2\ mmHg\min/\mu l$	*trabecular outflow resistance when pressure gradient equals zero*
Q	$0.012\ mmHg^{-1}$	*trabecular outflow obstruction coefficient*
k_1	$0.4\ \mu l/\min$	*maximum uveoscleral flow rate*
k_2	$5\ mmHg$	*pressure corresponding to half maximum uveoscleral flow rate*

Table 3.1: *Control state values for the parameters, taken from Szopos' work citeJMO*

3.3.2 Implementation with the software OpenModelica

We implemented the analogue electrical circuit (see Figure 3.3) into the open source software OpenModelica. OpenModelica is an open-source Modelica-based environment for modeling and simulation of complex dynamical systems. In particular, we used the *analogue electric and electronic components environment* that enables the user to draw an electrical circuit that consists of resistors, capacitors, transformers, diodes, transistors, transmission lines, switches, grounds, sources and sensors. It allows one to specify analytical expressions for non-linear components, which turned out to be very useful in the context of the present work to describe non-linear resistances and capacitances. The circuit is then automatically solved by the software that provides the user with all of

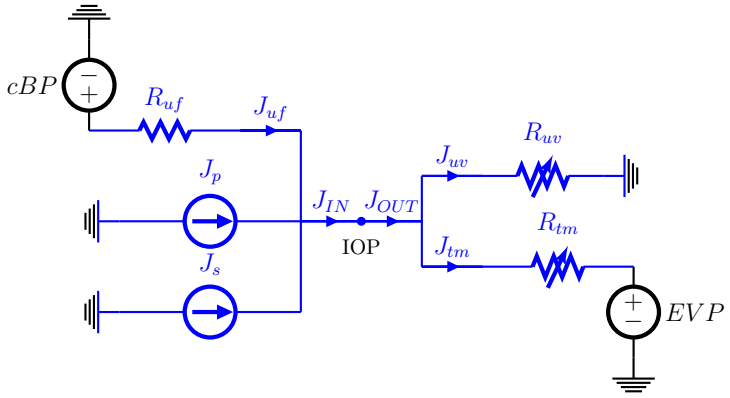

Figure 3.3: *Electrical circuit for the static component of IOP.*
AH production: $R_{uf} = 1/L$ is the resistance of the ultrafiltration branch; the modeling of ultrafiltration driven by oncotic pressure difference and ionic secretion is made by means of two current generators (J_p and J_s respectively).
AH drainage: $R_{tm} = 1/C_{tm}$ is the resistance of the trabecular branch and depends on both IOP and EVP; $R_{uv} = 1/C_{uv}$ is the resistance of the uveoscleral branch and depends on IOP.

the output values of the circuit parameters.

The static model we implemented in OpenModelica is composed of the following sub-models (see Figure 3.4):

- two *sources for constant voltage* that model ciliary blood pressure and episcleral venous pressure;
- an *ultrafiltration resistor* that models the inverse of inflow hydraulic conductance;
- two *sources for constant current* that model the remaining part of ultrafiltration inflow and the ionic secretion inflow;
- a *non-linear trabecular resistor*, that models the inverse of trabecular hydraulic conductance;
- a *non-linear uveoscleral resistor*, that models the inverse of uveoscleral hydraulic conductance.

With the simulation we could verified the steady-state value of IOP: the potential sensor inserted in the circuit to measure IOP (named IOPsen-

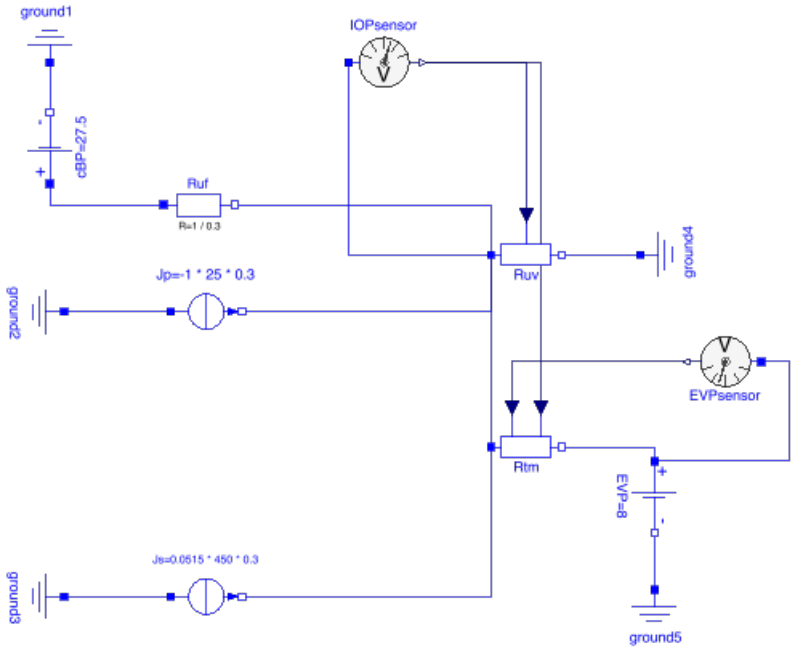

Figure 3.4: *OpenModelica electrical circuit for the static component of IOP*

sor in the circuit) measures a value of 14.9527 mmHg, as shown in Figure 3.5.

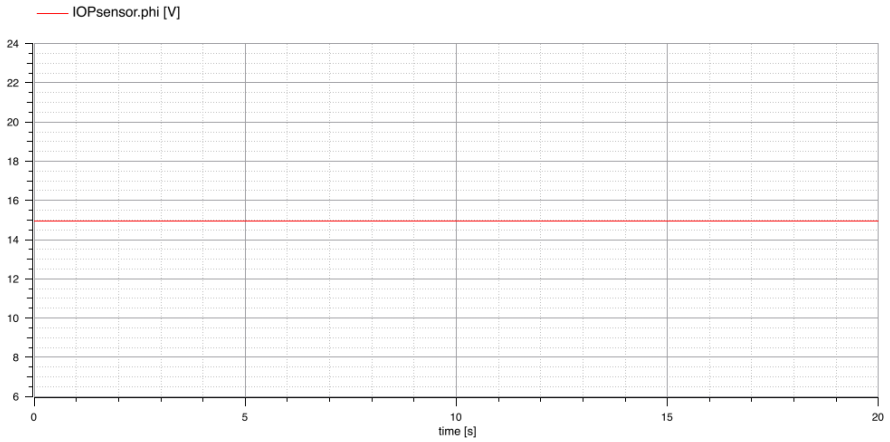

Figure 3.5: *Simulation output in OpenModelica: IOPsensor measures the steady-state IOP*

3.4 Dynamic Models

3.4.1 Ocular hemodynamics

Our first attempt to introduce a non-stationary component in the model stems from the work by Kiel et al [53]. We start from the model in [53] and we simplify it by accounting for the major contributors to AH flow, neglecting the contribution of oxygen delivered by ciliary blood flow and water filtered by capillaries on AH production.
The main assumptions behind the non-stationary model are:

1. pressure is assumed to be spatially uniform inside the eye (and named IOP). It varies as a function of V_{tot} following a curve found in experimental studies:

$$IOP = \overline{IOP} f(V_{tot}), \text{ with} \tag{3.11}$$

$$f(V_{tot}) = 10^{\gamma(V_{tot} - \overline{V_{tot}})}, \tag{3.12}$$

$$\gamma = 0.0215 \quad \mu l^{-1}, \tag{3.13}$$

   where IOP is measured in millimiters of mercury and V_{tot} is measured in microliters. The bar over the variables indicates the respective reference value found in literature ($\overline{IOP} \simeq 15\, mmHg$ and $\overline{V_{tot}} \simeq 7\, ml$ [60]);

2. V_{struct} is a given constant: $V_{struct} = 5.6\, ml$; and

3. V_{ch} and its first derivative are given functions of time: $V_{ch} = V_{ch}(t)$ and $\frac{dV_{ch}}{dt} = G_{ch}(t)$. Their estimates are based on the work of Krakau et al [41] and will be discussed below.

First assumption is based on Friedenwald's formulation for the relationship between variations in pressure and volume inside the eye, denoted by dP and dV respectively [22]. Relative changes in IOP, namely $\frac{dP}{P}$,

are proportional to relative changes in V_{tot}, namely $\frac{dV}{V}$, where the proportionality factor is a constant denoted by k:

$$\frac{dP}{P} = k\frac{dV}{V}. \tag{3.14}$$

Due to the fact that the change in pressure inside the eye is a significant fraction of the eye pressure while the total change in volume is a small fraction of the total volume of the eye, Friedenwald assumed V to be constant and equal to eye volume before distention. Thus k/V can be treated as a constant, accounting for the resistance that the eye exerts to distending forces and determined by the elastic proprieties of cornea, sclera and other boundary structures of the eye. For this reason k/V is named *rigidity* since the value of this constant increases with the rigidity of the eye [23].
Solving the differential equation, and setting $k/V := \gamma_e$ (3.15), we obtain

$$\ln(IOP) - \ln(\overline{IOP}) = \gamma_e(V_{tot} - \overline{V_{tot}}), \tag{3.16}$$

where the subscript e in γ_e indicates that (3.16) is expressed in natural logarithm.
With a simple passage to logarithm to base 10, it follows that

$$\log(IOP) - \log(\overline{IOP}) = \gamma(V_{tot} - \overline{V_{tot}}), \tag{3.17}$$

with $\gamma = \gamma_e/\ln 10$. It is easy to check that expression (3.17) is equivalent to those in (3.11)-(3.12)-(3.13). Friedenwald's estimate of γ was done experimentally by injecting small volume increments into the anterior chamber and measuring the resulting pressure changes for several initial pressures. The estimate resulted in $\gamma = 0.0215\,\mu l^{-1}$, as reported in (3.13).

It is worth remarking that this relationship between IOP and ocular volume came from studies performed on human cadaver eyes, thus not

perfused eye subjected to inevitable postmortem changes. For this reason a relationship based on living human eyes would be more suitable. A new relation that represents the volume response of the eye to changes in IOP, as a function of the initial volume of the eye, was presented in a work of Silver et al [23]. This equation is derived from all the available ocular rigidity data on living human eye and takes the form

$$\Delta V_{tot} = V_{tot}(C + C_0 \ln IOP + C_1 IOP), \text{ with coefficients} \tag{3.18}$$

$$C = -8.03 \cdot 10^{-3}, \tag{3.19}$$

$$C_0 = 4.87 \cdot 10^{-3}, \text{ and} \tag{3.20}$$

$$C_1 = 3.9 \cdot 10^{-5} mmHg^{-1}. \tag{3.21}$$

It gives a larger volume increment for a given increment of pressure than Friedenwald's equation. However, we choose to use Friedenwal's relationship in this thesis, because we saw that the resultant value for ocular rigidity would not change significantly for the purpose of this work.

From the volume balance in (3.1), differentiating with respect to time, accounting for the relation (3.2) in non-stationary conditions, and utilizing (3.11), we obtain the following system of equations describing the new model:

$$\begin{cases} \dfrac{dV_{tot}}{dt} = J_{in} - J_{out} + G_{ch} \\ IOP = \overline{IOP}\, 10^{\gamma(V_{tot} - \overline{V_{tot}})}. \end{cases} \tag{3.22}$$

3.4.2 Implementation with the software OpenModelica

We implement this model in OpenModelica adding to the stationary circuit in Figure 3.4 the contribution of:

- changes in choroidal volume due to blood flow variations (G_{ch}) and

- changes in eye total volume due to structure deformability ($\frac{dV_{tot}}{dt}$).

The former is modeled as a *sinusoidal current source* J_{ch}. This is motivated by the analogy between electrical and hydraulic models (see Chapter 3.2): G_{ch} is the derivative of volume over time, so it is a *flow*, and the analogue of flow is *current*, namely J_{ch}.
The latter is modeled as a *capacitor* C that include the contribution of whole eye deformability.

3.4.3 Ocular deformability

The modeling of changes in eye total volume with an electrical capacitor is motivated by the analogy between *volume* and *charge*, so that the derivative of volume over time is analogue to the derivative of charge over time, namely $\frac{d}{dt}(Cv)$, v being the potential difference across the capacitor. We start inserting a constant capacitance and then tune the modeling with a capacitance that varies non-linearly with IOP. The resultant circuit is presented in Figure 3.6.

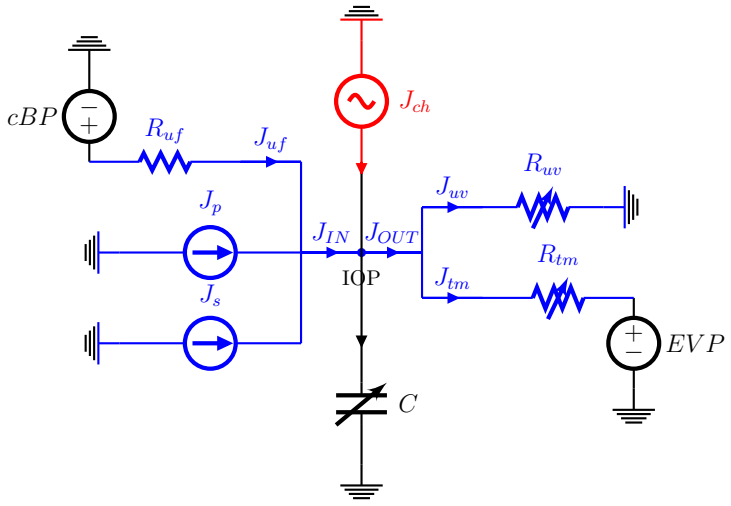

Figure 3.6: *Electrical circuit for the dynamic component of IOP. Elements added are: f_{ch} for pulsatile ocular blood flow and C for deformability of the cornea, sclera and other boundary structure of the eye. Here is depicted the variable capacitance.*

The application of Kirchoff's law to the circuit results in the following

differential equation:

$$L[(cBP - IOP) - \sigma_p \Delta\pi_p - \sigma_s \Delta\pi_s] + J_{ch} = \\ = C\frac{d}{dt}IOP + \frac{1}{R_0[1 + Q(IOP - EVP)]}(IOP - EVP) + \frac{k_1}{k2 + IOP}IOP. \tag{3.23}$$

Note that capacitance C can take two different forms —the first being IOP-independent and the second IOP-dependent— depending on the constant capacitor case or the variable capacitor case respectively, as will be discussed in the following two sections.

3.4.3.1 Constant capacitance

The calibration is done by determining an *amplitude* I for the current generator J_{ch} that guarantees a shape of the output IOP as the one found in literature, that is: baseline IOP around $15\,mmHg$, with oscillations of ± 1 up to $\pm 2\,mmHg$ due to cardiac cycle pulses ([57], based on measurements of IOP by means of the Langham pneumatic tonometer). These oscillations in IOP indeed reflect changes in eye volume due to changes in intraocular blood volume induced by the arterial blood pulse (see Figures 3.7 and 3.8). For this reason the *frequency* f of the sinusoidal current generator is set equal to the frequency of the IOP wave, that is dependent only on the cardiac cycle.
The chosen values for I and f are $619\,\mu l/min = 10.3166\,\mu l/s$ and $1.1\overline{3}\,s^{-1}\,[Hz]$ respectively (based on the work of Krakau [41], that will be briefly illustrated below).
To simulate the circuit, a constant value for the capacitance is estimated. We start from the relationship between IOP and V proposed by Friedenwald (see equation (3.14)) and we approximate it with a linear relation. This approximation is motivated by the fact that we are focusing on IOP variations over a cardiac cycle, which are small ($\leq 2\,mmHg$) with

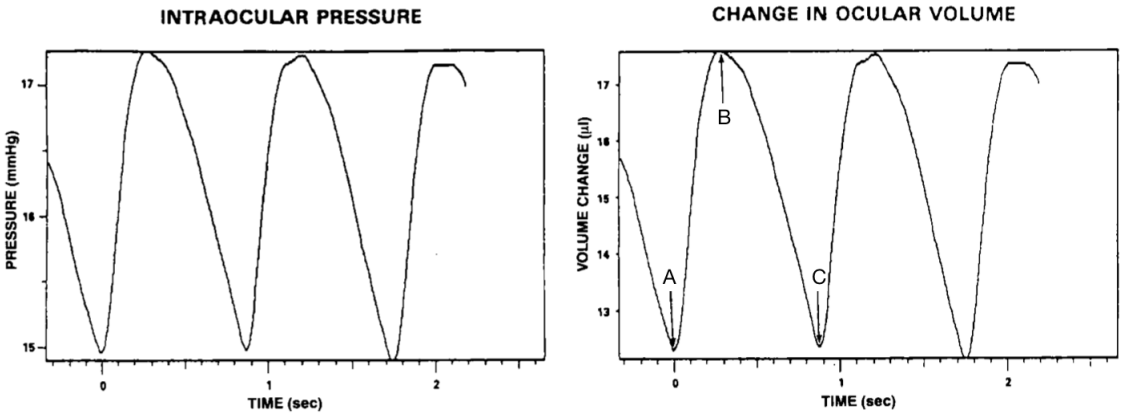

Figure 3.7: *Relationship between ocular volume and IOP [57]. left plot: instantaneous IOP measurements on a healthy human subject taken at 10 ms intervals during a period of suppressed respiratory activity. right plot: change in ocular volume relative to a reference ocular volume at 10 mmHg. The data correspond to the IOP measurement of left plot. The region from A to B represents expansion of the eye; the region from B to C represents contraction.*

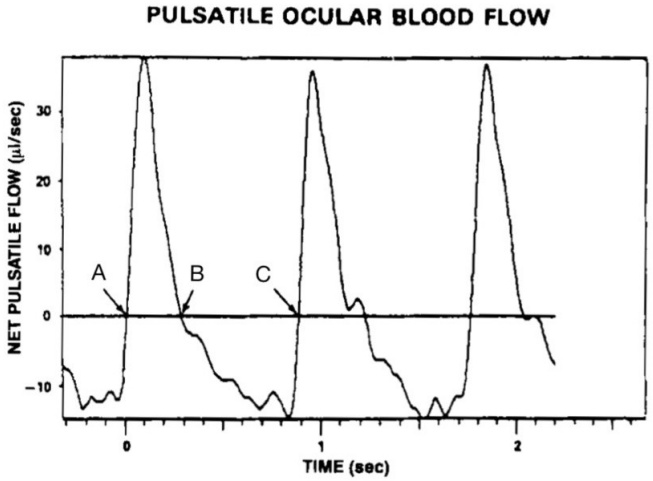

Figure 3.8: *Net pulsatile blood flow corresponding to Figure 3.7 [57]. The region from A to B represents net inflow of blood; the region from B to C represents net outflow; and the points A, B and C are synchronous respectively with points A, B and C in Figure 3.7, right plot.*

respect to the value of IOP ($\overline{IOP} \simeq 15\, mmHg$). Thus, for the sake of this estimation, we assume that IOP is constant and equal to $\overline{IOP}$:

$$\frac{dP}{\overline{IOP}} = \gamma_e dV. \tag{3.24}$$

Integrating the expression (3.24), it follows that

$$\int_{\overline{IOP}}^{IOP} dP = \overline{IOP}\,\gamma_e \int_{\overline{V_{tot}}}^{V_{tot}} dV \tag{3.25}$$

$$IOP - \overline{IOP} = \overline{IOP}\,\gamma_e\,(V_{tot} - \overline{V_{tot}}), \tag{3.26}$$

that can be written as

$$\Delta P = \gamma_e\,\overline{IOP}\,\Delta V \tag{3.27}$$

in order to simplify the notation.
In this way we obtain the following estimation for the capacitance:

$$C = \frac{\Delta V}{\Delta P} = \frac{1}{\gamma_e \overline{IOP}} = 1.35 \quad \mu l/mmHg. \tag{3.28}$$

Thus C depends on Friedenwald's ocular rigidity γ_e, a constant factor that accounts for the elastic proprieties of the cornea, sclera and other boundary structure of the eye, and on IOP steady-state value. The estimation reflects the value of C reported in Krakau's work, and is consistent with IOP being in the range 15-25 mmHg.

The resultant circuit modeled in OpenModelica is shown in Figure 3.9. The IOP measured by the sensor is a sinusoidal wave with average value of $14.9535\, mmHg$ and range of variability $\pm 1.0641\, mmHg$ (see Figure 3.10). Note that the IOP wave goes up to speed with a delay with respect to blood flow: this behavior is explained by the presence of the capacitor.

It is worth considering how the pulsatile ocular blood flow $J_{ch} =$

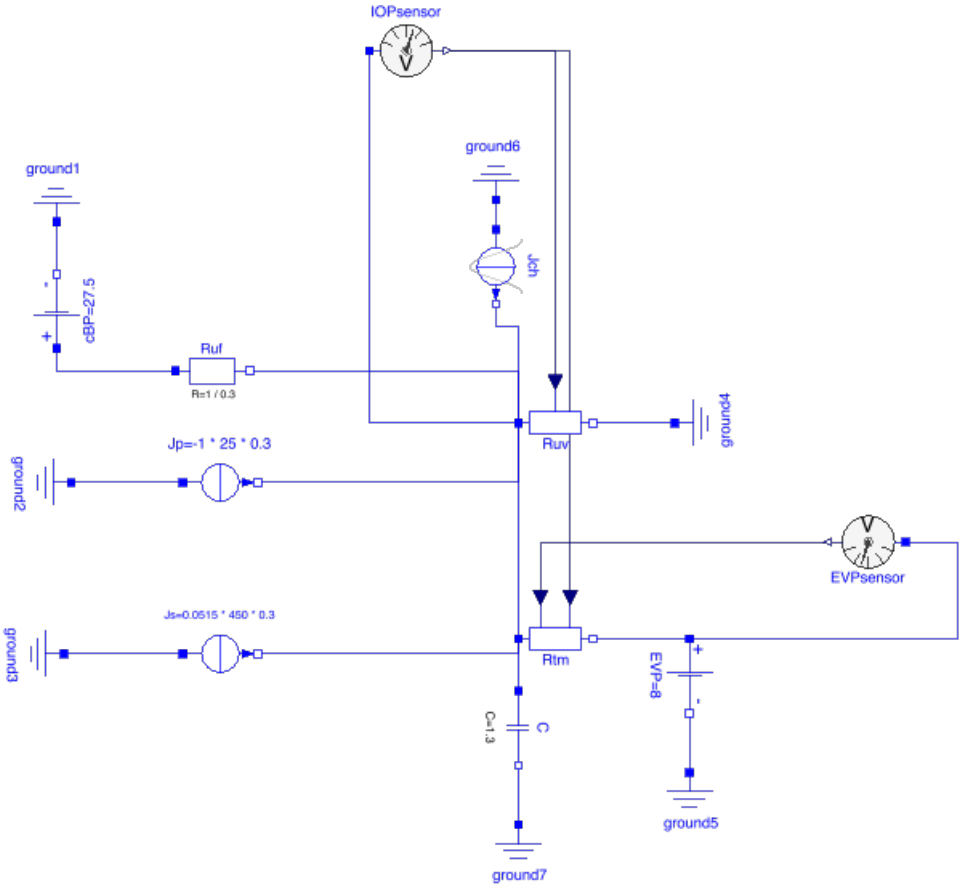

Figure 3.9: *OpenModelica electrical circuit for the dynamic component of IOP, constant capacitance*

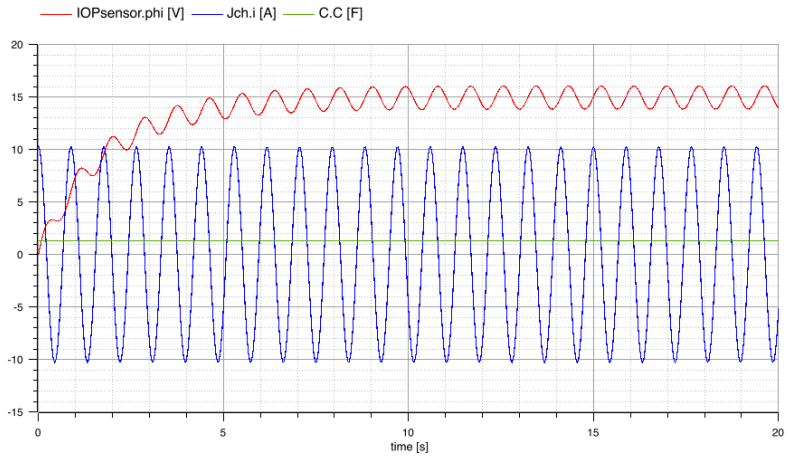

Figure 3.10: *Simulation output in OpenModelica: IOPsensor (red curve) and J_{ch} (blue curve) sinusoidal curves*

$619\,\mu l/min$ is estimated. This global measure called ocular blood flow (OBF) is based on continuous IOP measurements using a pneumotonometer described by Langham [70]. As highlighted in Krakau's work, the deduction of blood flow from the ocular pulse wave, namely the IOP variation in time, can be done basing on certain assumptions:

1. over a pulse stroke period T, ocular blood flow inflow f_i and outflow f_o are equal:
$$\int_0^T f_i(t)dt = \int_0^T f_o(t)dt. \tag{3.29}$$
This hypothesis disregards the effects of transitory manipulations on the eye.

2. because variations in IOP over a pulse cycle are of the order of a few mmHg, linear approximation of Friedenwald's relation can be applied both to volume and pressure, as done previously to assess constant capacitance. It leads to equation 3.27, that can be rewritten as
$$\Delta V = a\Delta P, \tag{3.30}$$
where $a = \frac{\overline{V_{tot}}}{\overline{IOP}\,k} = \frac{1}{\gamma_e \overline{IOP}}$ (see ocular rigidity definition in 3.15) is a constant that depends on ocular rigidity and baseline IOP. The record of the ocular pulse wave represents the difference between inflow and outflow at any time t:
$$V_{tot}(t) - V_{tot}(0) = a\,(IOP(t) - IOP(0)) = \int_0^t (f_i(\tau) - f_o(\tau))\,d\tau. \tag{3.31}$$

3. no reflux should occur ($\nexists f_i(t) : f_i(t) < 0$), and the pulsatile part of blood flow is zero during some moment t_m of the pulsation, that is:
$$f_i(t) \geq 0; \qquad f_i(t_m) = 0. \tag{3.32}$$

4. the outflow is non-pulsatile, meaning that it is steady:

$$f_o(t) = f_o. \tag{3.33}$$

Based on these assumptions, blood flow is estimated as the steepest part of slope of $V_{tot}(t)$, namely the minimum of dV_{tot}/dt.

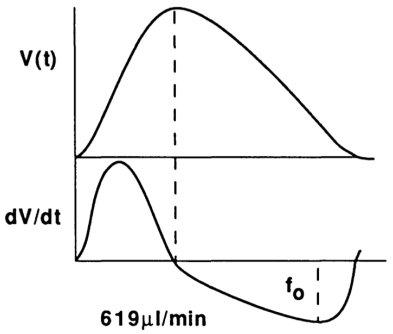

Figure 3.11: *Above: ocular volume $V_{tot}(t)$. Below: dV_{tot}/dt, outflow f_o*

In fact, as highlighted in Krakau's work, it is not the amplitude of the pulse wave —amplitude of $V_{tot}(t)$— that determines the flow, but the steepest part of its slope (f_o in Figure 3.11).

More precisely, starting from a pressure wave the curve is transferred into a volume wave by multiplying it with a constant (see equation 3.30 and Figure 3.7), then the derivative of $V_{tot}(t)$ with respect to time is computed, as shown in Figure 3.8 and Figure 3.11. This is the net flow, and it has its minimum where the inflow is minimum, namely zero. In fact, due to assumption 3., the flow at this point is the outflow (there is no negative inflow), and, because of 4., the volume per minute is found as the minimum of the flow multiplied by 60:

$$J_{ch} = f_o \cdot 60 = 619\,\mu l/min. \tag{3.34}$$

This measure of ocular blood flow includes retinal and choroidal flow. The theoretical basis together with the assumptions behind it are acceptable by researchers [41].

3.4.3.2 Variable capacitance

A more precise non-linear value of the capacitance as a function of IOP can be inferred from equation (3.17):

$$C = \frac{\Delta V_{tot}}{\Delta IOP} = \frac{\frac{1}{\gamma}(\log \frac{IOP}{\overline{IOP}})}{(IOP - \overline{IOP})}. \tag{3.35}$$

We re-simulate the OpenModelica circuit inserting this variable capacitor instead of the constant one that we used before (see Figure 3.12).

Note that equation (3.35) presents the indeterminate form 0/0 when IOP is equal to its baseline value $\overline{IOP}$. To overcome this problem in OpenModelica we use the Taylor series of logarithm

$$\ln(1+x) \simeq x - \frac{x^2}{2} + \frac{x^3}{3} - \ldots, \tag{3.36}$$

defining $1 + x \coloneqq IOP/\overline{IOP}$, so that $IOP - \overline{IOP} = x\overline{IOP}$. In this way we can express the capacitance as:

$$\begin{aligned} C &= \frac{\frac{1}{\gamma}\log(1+x)}{x\,\overline{IOP}} \\ &= \frac{1}{\gamma\, x\, \overline{IOP}} \frac{\ln(1+x)}{\ln 10} \\ &\simeq \frac{1}{\gamma\, \overline{IOP}\, \ln 10}\left[1 - \frac{x}{2} + \frac{x^2}{3} - \ldots\right] \end{aligned} \tag{3.37}$$

Substituting $x = IOP/\overline{IOP} - 1$, we obtain:

$$C = \frac{1}{\gamma\, \overline{IOP}\, \ln 10}\left[1 - \frac{1}{2}\left(\frac{IOP}{\overline{IOP}} - 1\right) + \frac{1}{3}\left(\frac{IOP}{\overline{IOP}} - 1\right)^2 - ...\right]. \tag{3.38}$$

The output of the simulation shows an increased range of variation in IOP wave, namely $\pm 2.12\, mmHg$, with an increased baseline value of $15.0179\, mmHg$ (see Figure 3.13).

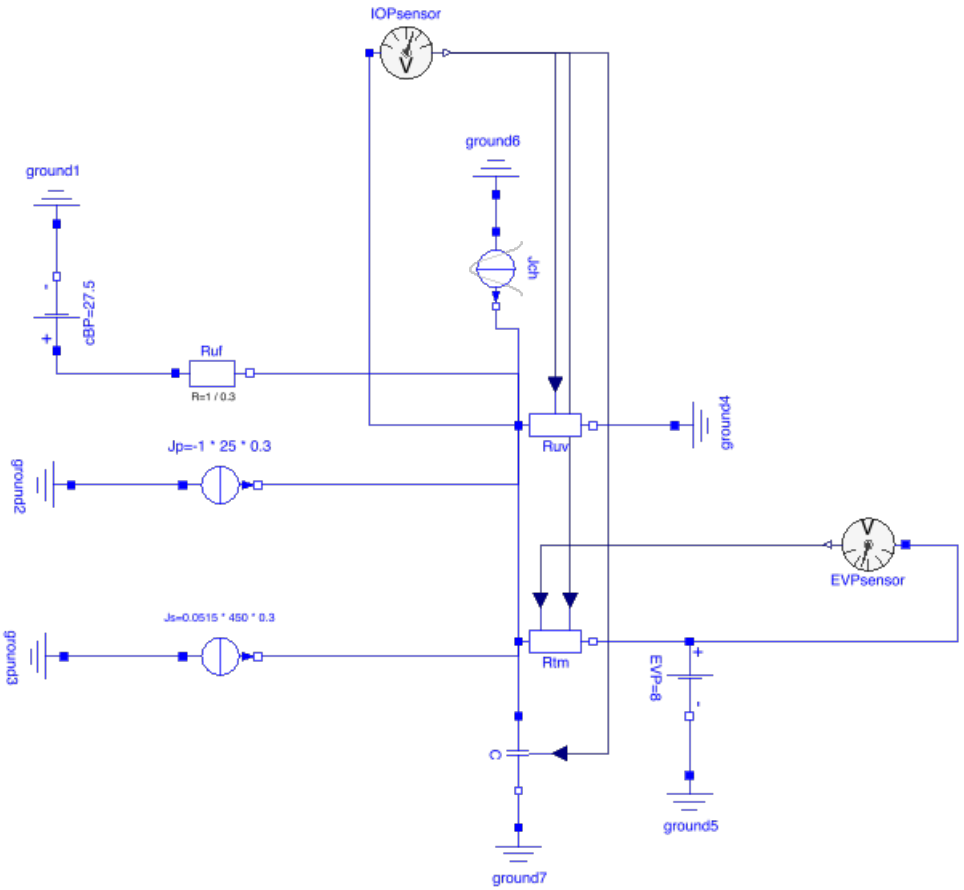

Figure 3.12: *OpenModelica electrical circuit for the dynamic component of IOP, variable capacitance*

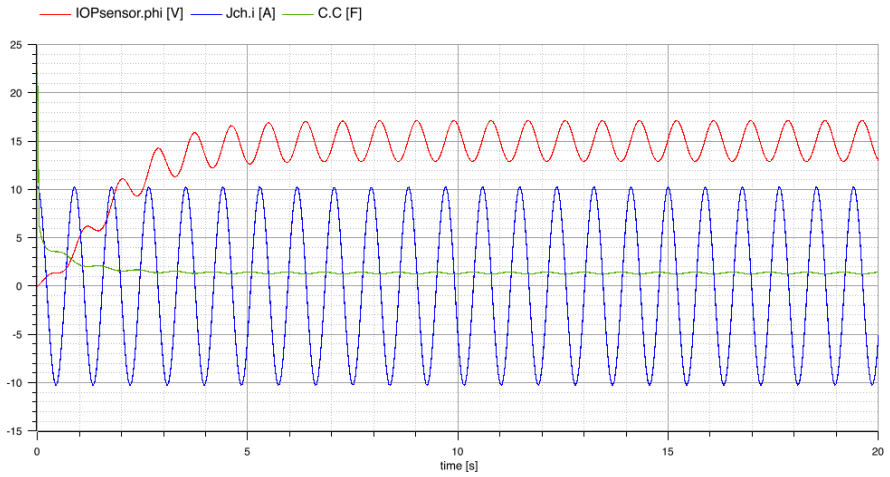

Figure 3.13: *Simulation output in OpenModelica: IOPsensor (red curve), J_{ch} (blue curve) and C (green curve) sinusoidal curves*

Chapter 4

Results of the models

To quantify the influence of parameters' variations on IOP we performed sensitivity analysis on the models.

As a first step, we carried out a ***deterministic sensitivity analysis*** on each model, where we varied the parameters one at a time. We let the parameters take discrete values in the range ±15% of their baseline value. We remark that variations in ciliary blood pressure were obtained from variations in mean arterial pressure.

To perform deterministic sensitivity analysis, we wrote a Python script (named "*driver_deterministic*") that:

(i) defines the set of input parameters,

(ii) "surrounds" the OpenModelica software simulating the circuit for each set of parameters (calling another function named "*wrapper*" in a for-loop that executes the model with the specific set of input parameters selected by the current iteration among those defined in (i)),

(iii) extracts the output (or outputs if we are solving the dynamic model) of the circuit,

(iv) plots the results, that are variations in IOP (or variations in mean IOP and amplitude of IOP oscillations if we are solving the dynamic

model) induced by variations in each parameter while keeping the others constant.

A framework of how these scripts work is depicted in Figure 4.1.

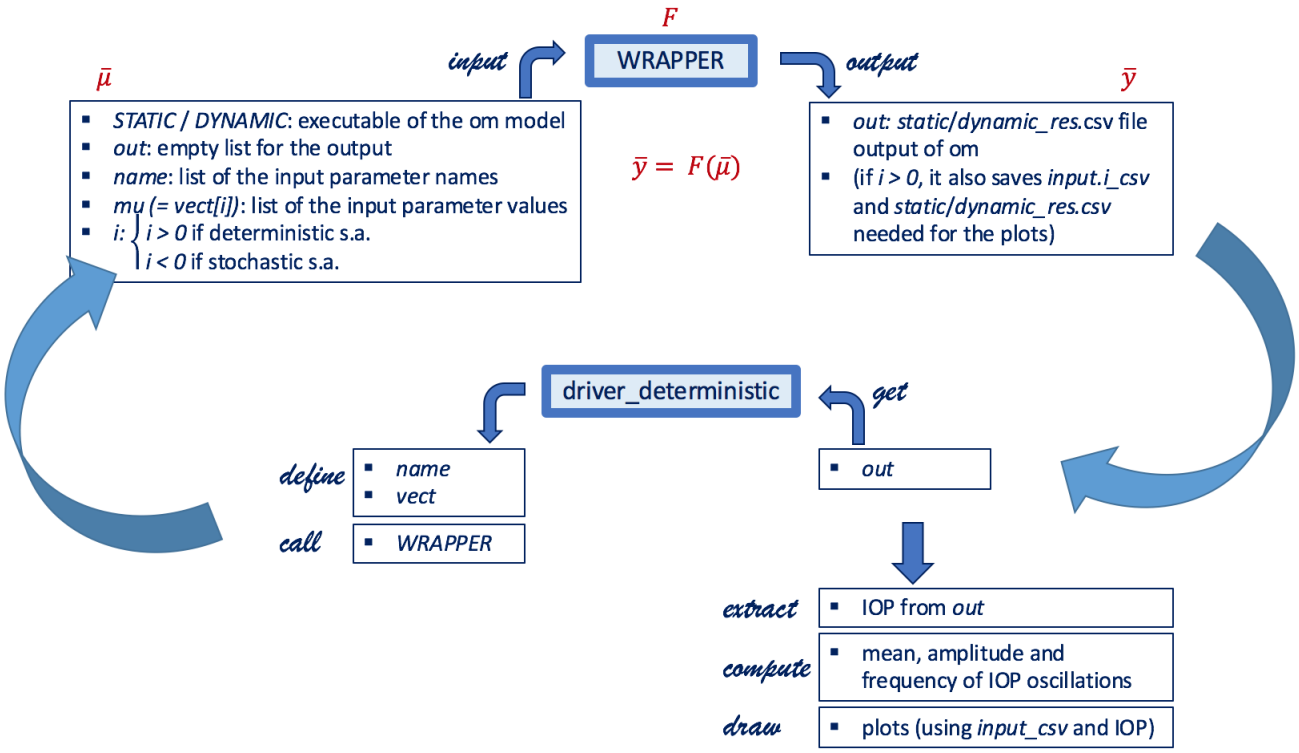

Figure 4.1: *Outline of how we computed deterministic sensitivity analysis on the models. driver_deterministic (i) defines the set of input parameters, (ii) calls the wrapper, (iii) extracts output, and (iv) plot the results. (om: OpenModelica)*

After the deterministic sensitivity analysis, we performed a global ***stochastic sensitivity analysis*** to the models. In this way we could obtain the probability density function of IOP that describes the relative frequency of a given IOP value. Keeping memory of all the outputs of the runs, the code also computes Sobol indices, that are variance-based sensitivity indices. For each parameter, its direct influence on IOP is quantified in terms of *first-order Sobol indices*, and the influence through interactions with other parameters is identified by means of the *total Sobol indices*.

The values of first-order and total indices can be estimated via Monte

Carlo simulations [62] or via a reduced order model using *polynomial chaos expansion* (PCE) [67]. The former method is very costly from the computational viewpoint as it requires many evaluations to ensure convergence, whereas the latter requires considerably less evaluations. We choose to use the reduced order method.
We considered stochastic variations in the parameters following uniform distributions within physiological ranges. For ciliary blood flow and ocular rigidity we considered stochastic variations following a normal distribution as suggested in the literature [24, 71].

In this case, the Python script rests on OpenTURNS, an open source software for the treatment of uncertainties and statistics. It enabled us to:

(i) define the probabilistic distributions for the parameters, chosen to be uniform or normal depending on the parameter,

(ii) do several runs of the meta-model (a global approximation of the model response),

(iii) plot different graphs showing:

- ◇ the comparison between results given by the PCE and results of the effective model, that serves as an indicator of the success of the reduced order method,
- ◇ the probability distribution of the output (or the ouputs in the dynamic model case),
- ◇ the Sobol indices for the output (or the ouputs in the dynamic model case).

A meta-model (also known as surrogate model) is intended to mimic the behavior of a computational model while being inexpensive to evaluate, in contrast to the original model which may take hours or even days of computer processing time [68]. A simple scheme of what meta-model for

uncertainty propagation computes is depicted in Figure 4.2. In meta-

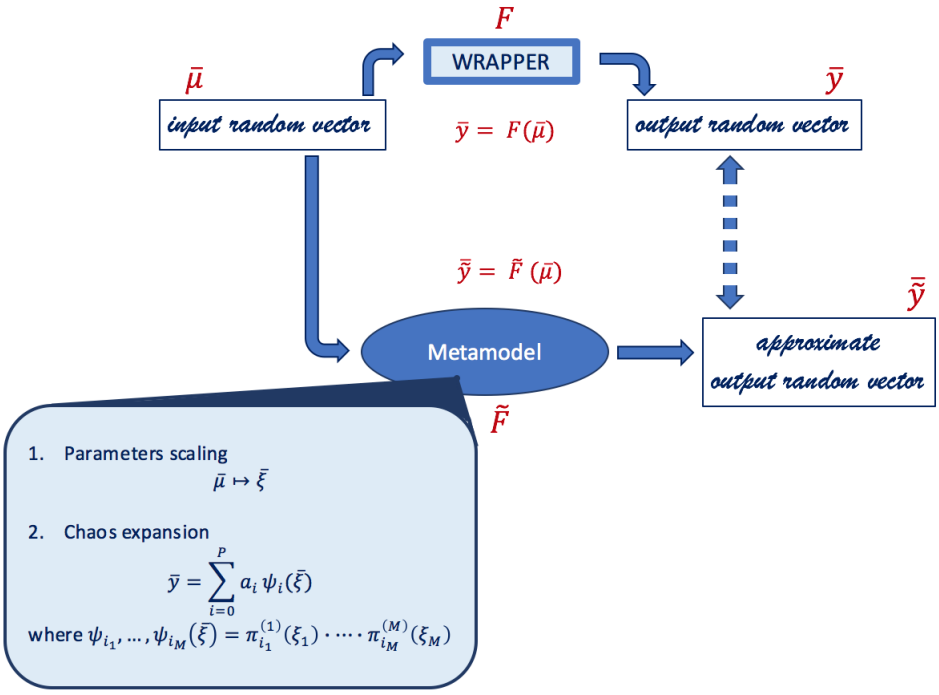

Figure 4.2: *Outline of how meta-model for uncertainty propagation works. $\bar{\xi}$ are the new parameters (with uniform or normal distribution); $(\pi_i)_{i\in\mathbb{N}}$ is a family of orthonormal polynomials (Hermite or Legendre, respectively).*

modeling based on chaos expansions a parameters scaling is performed. New parameters have to satisfy three assumptions:

- continuous probability density functions,
- finite means, and
- being independent one from the others.

Moreover, output random vector of the real model must have finite variance. If these assumptions are satisfied, there exists a family of orthonormal polynomials such that the output random vector can be written as a composition of these polynomials function of the new parameters. Type of polynomial depends on the probability density function of the parameter:

- normally distributed parameters are assigned to Hermite polynomials, and

- uniformly distributed parameters are assigned to Legendre polynomials.

We remark that, in the dynamic case, the IOP waveform computed by the model reaches a periodic state after some seconds of simulation. Thus, variations in mean, amplitude and frequency of IOP oscillations due to parameter changes can be computed as averages over the last five periods —with the simulation stop time set to 20 seconds in OpenModelica. By doing so, we avoid to consider the IOP outputs as a full stochastic process. In future developments of this project, a fully stochastic approach could be adopted that would also allow to examine IOP fluctuations due to the circadian rhythm, namely day/night changes, as we illustrated in Chapter 2.

4.1 Results for the Static Model

4.1.1 Deterministic sensitivity analysis on the static model

The deterministic sensitivity analysis was performed to identify the parameters that most influence the stationary IOP. We simulated the OpenModelica circuit varying the parameters L, R_0, k_1, k_2, EVP, $\Delta\pi_s$ and $\Delta\pi_p$ one at a time, within five samples in the range $\pm 15\%$ of the control state value. Variations in cBP are deduced from variations in mean arterial pressure (MAP), assuming that $cBP = \alpha MAP$, with $\alpha = 0.296$, so that $cBP = 27.5\, mmHg$ when $MAP = 93\, mmHg$ (baseline values). We then considered five samples of MAP varying in the interval $93 \pm 7.6\, mmHg$ [24]. Baseline and discrete values considered for the parameters are listed in Table 4.1.

Variations in IOP due to different values of the parameters are shown

Parameter	Baseline	Discrete values
cBP	$27.5\ mmHg$	$[25.278, 26.389, 27.5, 28.639, 29.778]$
L	$0.3\ \mu l/\min/mmHg$	$[0.255, 0.2775, 0.3, 0.3225, 0.345]$
R_0	$2.2\ mmHg \min/\mu l$	$[1.87, 2.035, 2.2, 2.365, 2.53]$
$\Delta\pi_s$	$-450\ mmHg$	$[-382.5, -416.25, -450.0, -483.75, -517.5]$
$\Delta\pi_p$	$25\ mmHg$	$[21.25, 23.125, 25.0, 26.875, 28.75]$
EVP	$8\ mmHg$	$[6.8, 7.4, 8.0, 8.6, 9.2]$
k_1	$0.4\ \mu l/\min$	$[0.34, 0.37, 0.4, 0.43, 0.46]$
k_2	$5\ mmHg$	$[4.25, 4.625, 5.0, 5.375, 5.75]$

Table 4.1: *Baseline and discrete values taken by the parameters of the static model*

in Figure 4.3. It can be easily seen that the major contributors to the steady-state IOP are, sorted by relevance, $\Delta\pi_p$, $\Delta\pi_s$, cBP, L, C_0, and EVP since they determine a variation range in IOP of 1.63, 1.51, 0.98, 0.81, 0.67 and $0.61\, mmHg$ respectively. Conversely, it seems that k_1 and k_2 do not play a relevant role in determining IOP.

It is interesting to notice that the results presented here differ from

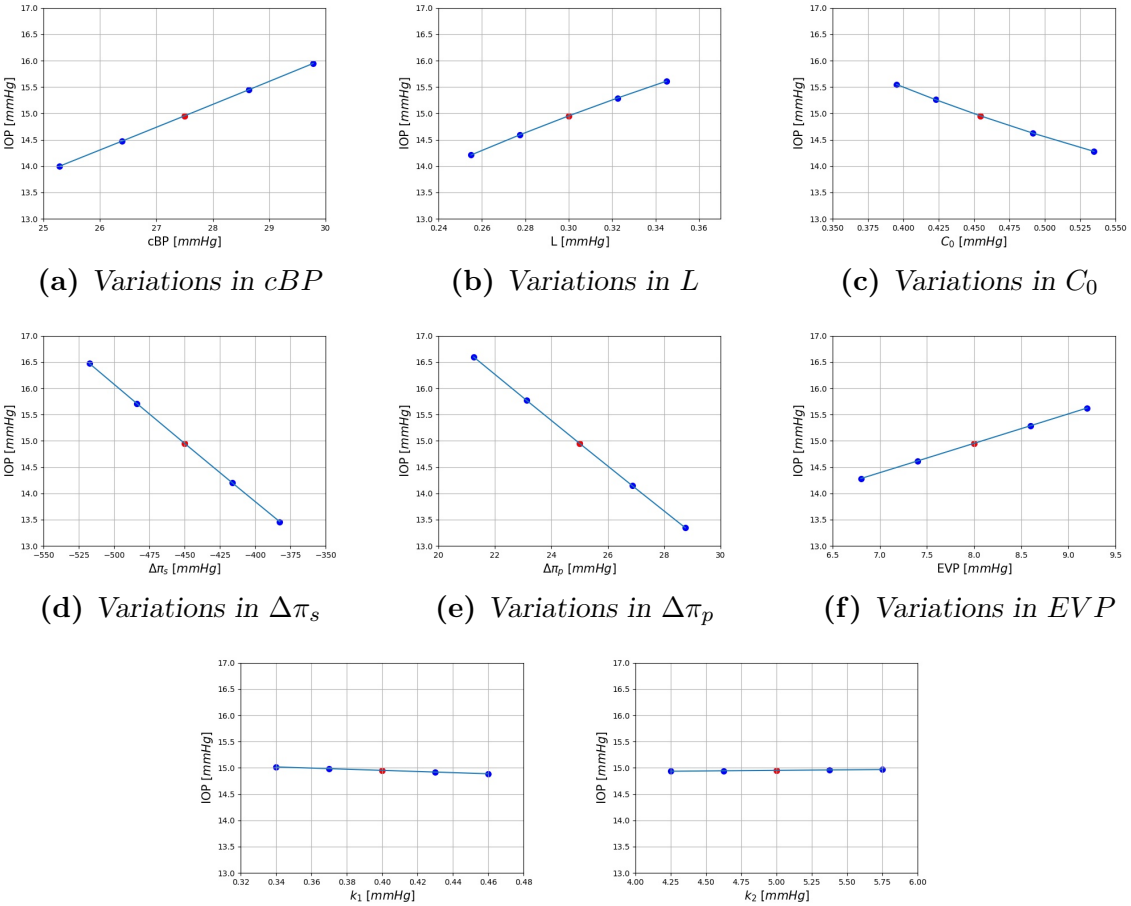

(a) *Variations in cBP* **(b)** *Variations in L* **(c)** *Variations in* C_0

(d) *Variations in* $\Delta\pi_s$ **(e)** *Variations in* $\Delta\pi_p$ **(f)** *Variations in EVP*

(g) *Variations in* k_1 **(h)** *Variations in* k_2

Figure 4.3: *Deterministic sensitivity analysis on the static model: influence of the different factors on* ***IOP****.*
Red dots indicate control state values for the variables and IOP, blue dots indicate sample values used for the analysis.

those reported in [31] in terms of the influence of cBP on IOP. Specifically, the authors in [31] found that cBP was the factor influencing IOP the most, thereby apparently conflicting our results. Actually, this apparent discrepancy is due to the fact that the range for cBP considered in this thesis is narrower than than considered in [31]. In fact, in [31] a normal distribution with mean $\mu = 27.528$ and standard deviation $\sigma = 2.2496$ is assigned to cBP, whereas in our work we just considered the interval $[\mu \pm \sigma] = [27.528 \pm 2.2496]$ (see Figure 4.4, red range), leading to a difference of 32% in cBP variations. These considerations

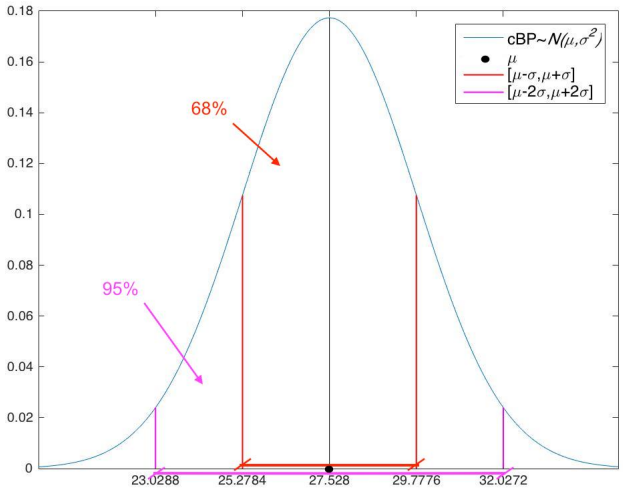

Figure 4.4: *Normal distribution for stochastic variations in cBP*

justify the apparent discrepancy between the results reported in [31], where cBP was found to have the largest influence on IOP, and those reported in this thesis, where cBP was ranked third among the various factors. Actually, Figure 4.5(b) shows what we would have obtained if we had let cBP change in the range $[\mu \pm 2\sigma] = [27.528 \pm 4.4992]$. In that case, the variation range in IOP would have been of almost 2 mmHg, thus inducing the largest effect on IOP. These observations emphasize the importance of selecting an appropriate range of variation for the parameters considered in the sensitivity analysis.

To further validate this analysis we also compared the result of one of

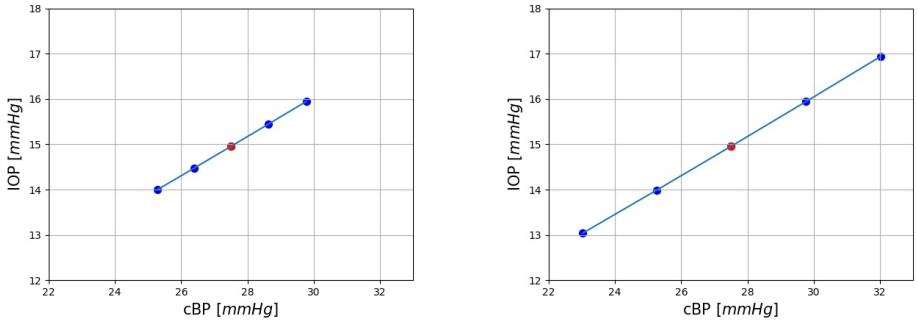

(a) $cBP \in [\mu \pm \sigma]$ **(b)** $cBP \in [\mu \pm 2\sigma]$

Figure 4.5: *Comparison of IOP variations when varying cBP in the range of our assumption (a) and in a range closer to that used in [31] (b).*

the output with the result found in a following work [32] of the authors. In particular, they report that a $25\%\Delta\pi_s$ reduction would induce an average IOP reduction of 2.6 mmHg. For the same reduction in osmotic pressure difference, our model predicts a reduction of 2.4694 mmHg in IOP (see Figure 4.6), thus comparable with what reported by the authors in [31].

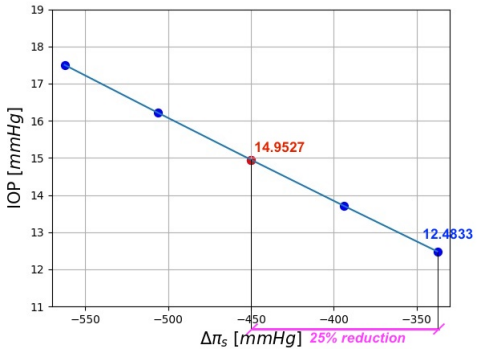

Figure 4.6: *Effect of a 25% reduction in* $\Delta\pi_s$

A more detailed analysis of the deterministic sensitivity analysis outputs depicted in Figure 4.3 shows that:

(a) an increase in blood pressure in the capillaries of the ciliary body cBP causes a significant increase in IOP. This is easily understandable due to the fact that an increase in the upstream pressure nec-

essarily produces an increase in the downstream pressure;

(b) an increase in total inflow facility L leads to an increases in AH inflow, thereby leading to an overall increase in IOP;

(c) an increase in resistance R_0 (corresponding to a decrease in trabecular outflow facility $C_0 = 1/R_0$) causes an obstruction of AH outflow in the trabecular pathway and a consequent increase in IOP. Indeed the obstruction of AH outflow at the level of trabecular meshwork has been recognized as one of the major hypothesis of cause of glaucoma.

Note that our model predictions are in good agreement with those reported by Kiel et al in [39], as depicted in Figure 4.7. The relationship between IOP and facility C_0 predicted by our model fits well the results by Kiel et al when C_0 is in the range 0.2-0.5$\mu l/min/mmHg$, which includes the range of discrete values used in our model for C_0 (thick red curve in figure).

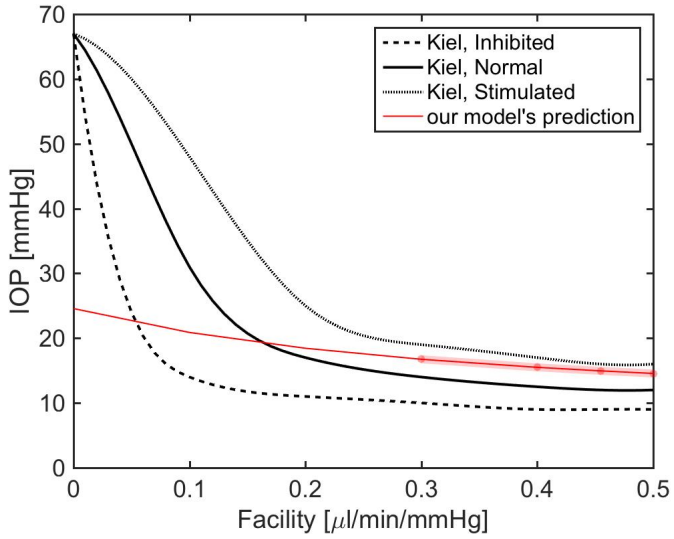

Figure 4.7: *Effect of outflow facility C_0 on IOP, our model's outcome (red curve) compared with those by Kiel et al (black curves). The three curves in black correspond to three different levels of ciliary secretory activity. Thick red curve indicate the range in which we let vary C_0 in the model.*

(d) an increase in osmotic pressure difference causes a decrease in IOP. $\Delta\pi_s$ is defined as the difference between osmotic pressure in the capillaries and osmotic pressure in the posterior chamber. These compartments are separated by the ciliary process, where ions are actively produced and emitted in the posterior chamber. Due to the fact that these ions are actively sent toward the posterior chamber and so $\pi_s^{post.chamb} > \pi_s^{cap}$, osmotic pressure difference results in a negative value so that the resultant flow of AH is directed toward the posterior chamber. An increase in this pressure difference leads to a reduced flow of AH, flowing toward the posterior chamber due to ionic secretion, and so to a decrease in IOP;

(e) an increase in oncotic pressure difference causes a decrease in IOP. $\Delta\pi_p$ is defined as the difference between oncotic pressure in the capillaries and oncotic pressure in the posterior chamber. Due to the fact that $\pi_p^{cap} > \pi_p^{post.chamb}$, the resultant flow of AH occurs from the posterior chamber toward the capillaries. An increase in this pressure difference determines an increase in the flow of AH directed to capillaries and so a decrease in posterior chamber pressure with a consequent decrease in IOP;

(f) an increase in the downstream episcleral venous pressure EVP obviously causes upstream pressure IOP to increase;

(g),(h) variations in k_1 and k_2 almost do not influence IOP, even if an increase in k_1 augments the hydraulic conductance C_{uv} and so the oveoscleral outflow, causing a little decrease in the upstream pressure IOP, and, similarly, an increase in k_2 causes a small increase in IOP;

With these observations in mind, we than quantified the influence of the major determinants on the steady-state IOP in a more complete way using stochastic sensitivity analysis.

4.1.2 Stochastic sensitivity analysis on the static model

To reproduce the same analysis done in [31], we defined uniform distributions with variations in the range ±15% for L, $\Delta\pi_s$, C_0, EVP, k_1 and a normal distribution with mean 27.5 mmHg and standard deviation 2.2496 mmHg for cBP. Parameters $\Delta\pi_p$ and k_2 are kept constant.
The choice to let $\Delta\pi_s$ vary and keep $\Delta\pi_p$ constant has a clinical reason. The oncotic pressure difference $\Delta\pi_p$ is due to the amount of proteins in blood plasma, whereas the osmotic pressure difference $\Delta\pi_s$ is due to the amount of ions expelled in the posterior chamber by the active mechanisms in the non-pigmented epithelial cells. Many of the drugs prescribed to glaucoma patients to lower IOP act on reducing the activity of some ion pumps thereby reducing the osmotic pressure difference. This is why the authors wanted to see what influence $\Delta\pi_s$ has on IOP. Since these drugs cannot act on $\Delta\pi_p$, we did not vary it while investigating the efficacy of hypotensive ocular medications (see the analysis described in Chapter 5).

Distributions for the parameters of the static model are listed in Table 4.2. Here we put also the characterizations for $\Delta\pi_p$ and k_2 that will be used in a subsequent analysis. Figure 4.8 shows that the meta-model

Parameter	Distribution	Properties of the distribution
cBP	Normal	$mean = 27.5$; $standard\,deviation = 2.2496$
L	Uniform	$min = 0.3(1 - 15\%)$; $max = 0.3(1 + 15\%)$
R_0	Uniform	$min = 2.2(1 - 20\%)$; $max = 2.2(1 + 20\%)$
$\Delta\pi_s$	Uniform	$min = -450(1 + 15\%)$; $max = -450(1 - 15\%)$
$\Delta\pi_p$	Uniform	$min = 25(1 - 15\%)$; $max = 25(1 + 15\%)$
EVP	Uniform	$min = 8(1 - 15\%)$; $max = 8(1 + 15\%)$
k_1	Uniform	$min = 0.4(1 - 15\%)$; $max = 0.4(1 + 15\%)$
k_2	Uniform	$min = 5(1 - 15\%)$; $max = 5(1 + 15\%)$

Table 4.2: *Distributions for the parameters of the static model*

matches the OpenModelica model: all the blue points, namely output

values, stay on the identity line. It means that results given by the re-

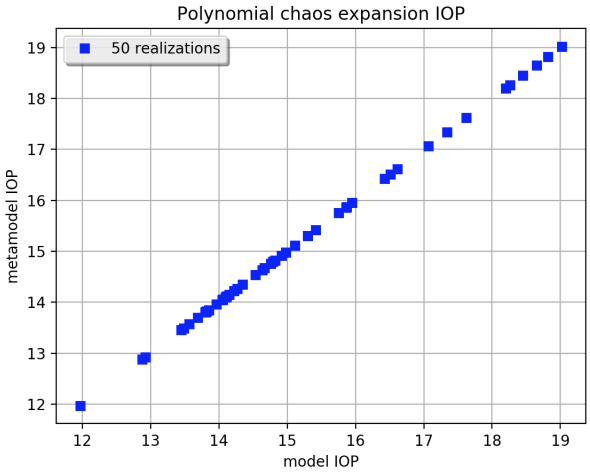

Figure 4.8: *Results of the polynomial chaos expansion method on the static model*

duced order method can be considered reliable.

The IOP probability density function and first and total Sobol indices are reported in Figure 4.9. The simulation outcome is a probability den-

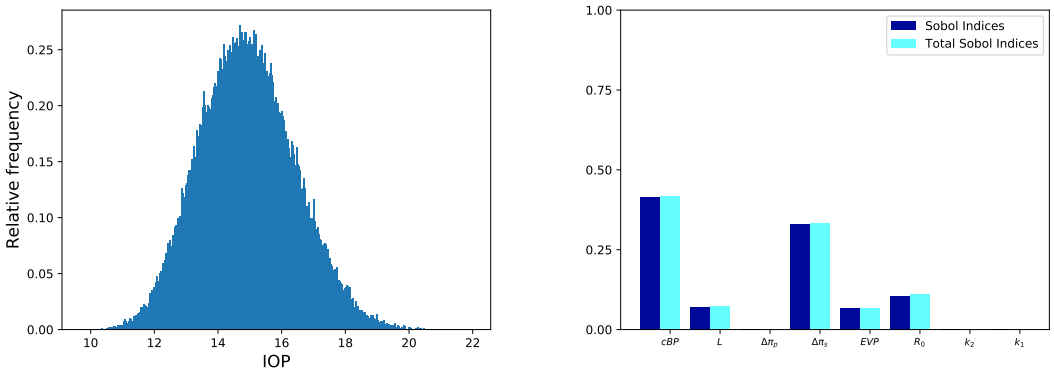

(a) *Probability density function of IOP* **(b)** *First order and total Sobol indices*

Figure 4.9: *Simulation outcome of the static model in normotensive subjects*

sity function that fits a right-skewed Gaussian curve with a frequency peak of 27% at 14.7 mmHg, mean value 14.9272 mmHg and variance 1.5033 mmHg. Values of first order Sobol indices and total Sobol indices are reported in Table 4.3. The results for the Sobol indices (see Figure 4.9(b)) suggest that IOP is strongly influenced by cBP and $\Delta\pi_s$

	First order Sobol indices	Total Sobol indices
cBP	0.415937	0.419351
L	0.071571	0.073956
R_0	0.105556	0.109642
$\Delta\pi_s$	0.331173	0.333904
EVP	0.066953	0.067279
k_1	0.000615	0.000621

Table 4.3: *First order and total Sobol indices of the static model in normotensive subjects*

(Sobol indices 0.42 and 0.33 respectively), and mildly influenced by the levels of L, R_0 and EVP. The influence of k_1 on IOP appears to be minimal. These results are in complete agreement with this reported in [31].

We then let vary all the parameters cBP, $\Delta\pi_s$, C_0, EVP, k_1, $\Delta\pi_p$ and k_2. The first five assume the same distributions as before, and also $\Delta\pi_p$ and k_2 are given uniform distributions with variation in the range $\pm 15\%$. Simulation outcomes show a probability density function that fits a Gaussian curve (see Figure 4.10(a)) with frequency peak of 24% at 14.8 mmHg. Mean value and variance result in 14.9325 mmHg and 1.77 mmHg respectively.
The IOP probability density function and first and total Sobol indices are reported in Figure 4.10. Table 4.4 reports the detailed Sobol indices resulted from the analysis. Note that ultrafiltration, which is driven by oncotic pressure difference $\Delta\pi_p$, influences IOP more than ionic secretion, which is driven by osmotic pressure difference $\Delta\pi_s$. Ciliary blood pressure remains the first determinant for IOP, with a Sobol index of 0.3, followed by oncotic pressure difference, with Sobol index 0.28, and osmotic pressure difference, with Sobol index 0.24.

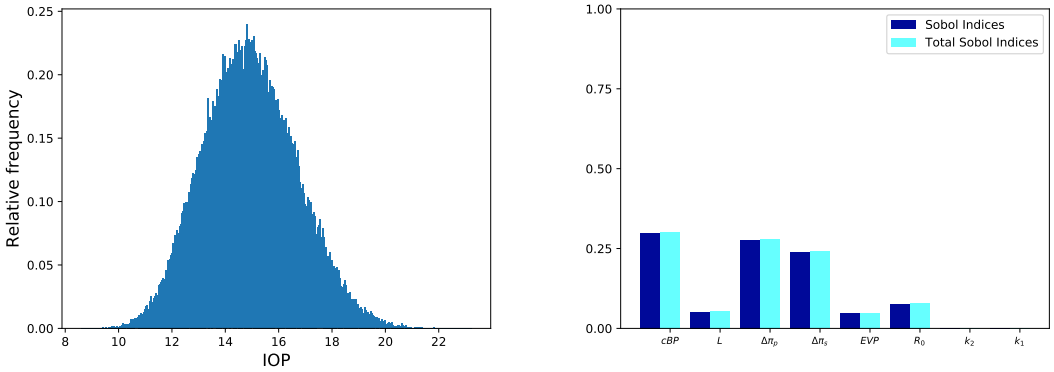

(a) *Probability density function of IOP* **(b)** *First order and total Sobol indices*

Figure 4.10: *Simulation outcome for the static model letting all the parameters vary*

	First order Sobol indices	Total Sobol indices
cBP	0.299788	0.302292
L	0.051671	0.054223
R_0	0.076221	0.080563
$\Delta\pi_s$	0.238795	0.240800
$\Delta\pi_p$	0.277798	0.280125
EVP	0.048273	0.048511
k_1	0.000440	0.000443
k_2	$2.904262e-05$	$2.914157e-05$

Table 4.4: *First order and total Sobol indices for the static model letting all the parameters vary*

4.2 Results for the Dynamic Model with constant capacitance

We performed deterministic sensitivity analysis on the basic dynamic model with constant capacitance described in Section 3.4.3.1. Stochastic sensitivity analysis will be presented for the more complete model with variable non-linear capacitor.

Dynamic IOP is characterized by its mean, the amplitude of oscillations, and the frequency of oscillations. Thus, in this section we quantified the influence of parameters' variations on these three outputs of the dynamic model.

We simulated the OpenModelica circuit varying the parameters, one at a time, within the five samples in the same spirit as previously done for the static model. Here we have one more parameter, namely the value of the constant capacitance C, whose influence on mean, amplitude and frequency has to be taken into account. Baseline and discrete values for the parameters are listed in Table 4.5.

Variations in mean IOP and amplitude of IOP due to different values of the parameters are shown in Figure 4.11 and 4.12, respectively. The model simulations show that the frequency of IOP oscillation is not

Parameter	Baseline	Discrete values
cBP	27.5 $mmHg$	$[25.278, 26.389, 27.5, 28.639, 29.778]$
L	0.3 $\mu l/\min/mmHg$	$[0.255, 0.2775, 0.3, 0.3225, 0.345]$
R_0	2.2 $mmHg \min/\mu l$	$[1.87, 2.035, 2.2, 2.365, 2.53]$
$\Delta\pi_s$	-450 $mmHg$	$[-382.5, -416.25, -450.0, -483.75, -517.5]$
$\Delta\pi_p$	25 $mmHg$	$[21.25, 23.125, 25.0, 26.875, 28.75]$
EVP	8 $mmHg$	$[6.8, 7.4, 8.0, 8.6, 9.2]$
k_1	0.4 $\mu l/\min$	$[0.34, 0.37, 0.4, 0.43, 0.46]$
k_2	5 $mmHg$	$[4.25, 4.625, 5.0, 5.375, 5.75]$
C	1.35 $\mu l/mmHg$	$[1.148, 1.249, 1.35, 1.451, 1.553]$

Table 4.5: *Baseline and discrete values for the parameters of the dynamic model with constant capacitor*

affected by parameter changes. This follows from the fact that the frequency of IOP waveform is imposed by choroidal blood flow waveform which, in our model, is considered given and equal to G_{ch} (see third assumption in Section 3.4.1).

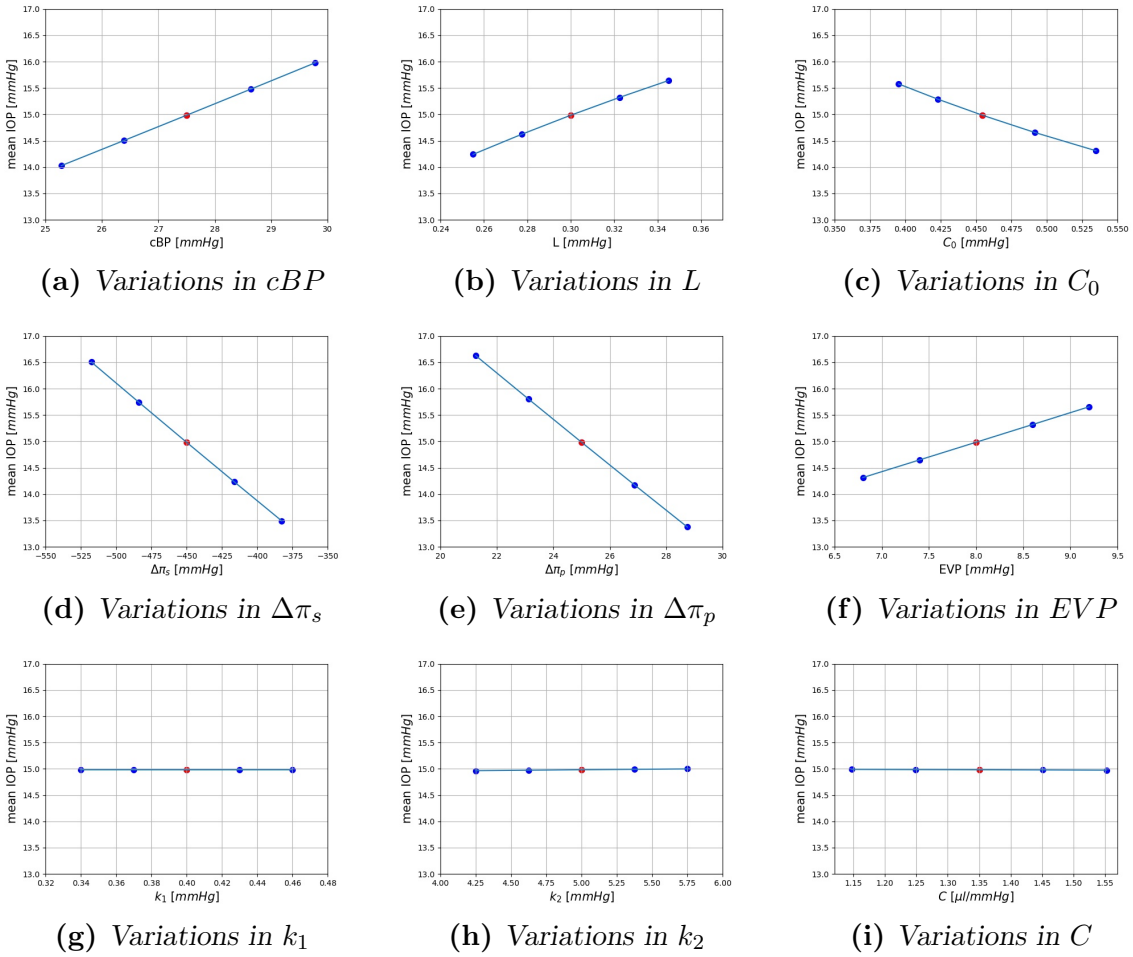

(a) *Variations in cBP* **(b)** *Variations in L* **(c)** *Variations in* C_0

(d) *Variations in* $\Delta\pi_s$ **(e)** *Variations in* $\Delta\pi_p$ **(f)** *Variations in EVP*

(g) *Variations in* k_1 **(h)** *Variations in* k_2 **(i)** *Variations in C*

Figure 4.11: *Deterministic sensitivity analysis on the dynamic model: influence of the different factors on* ***mean IOP****.*
Red dots indicate control state values for the variables and IOP, blue dots indicate sample values used in the anaysis.

In particular, analyzing the influence of the parameters on the mean IOP (see Figure 4.11), we can see that

(a)-(h) simulation results are in perfect agreement with plots in Figure 4.3, obtained for the static model;

(i) the introduction of the capacitor C modeling tissue deformability

does not have an influence on the mean value of IOP, which is determined just by the balance between AH inflow and outflow. However, C is the only parameter that influences the dynamics of IOP, as shown in Figure 4.12.

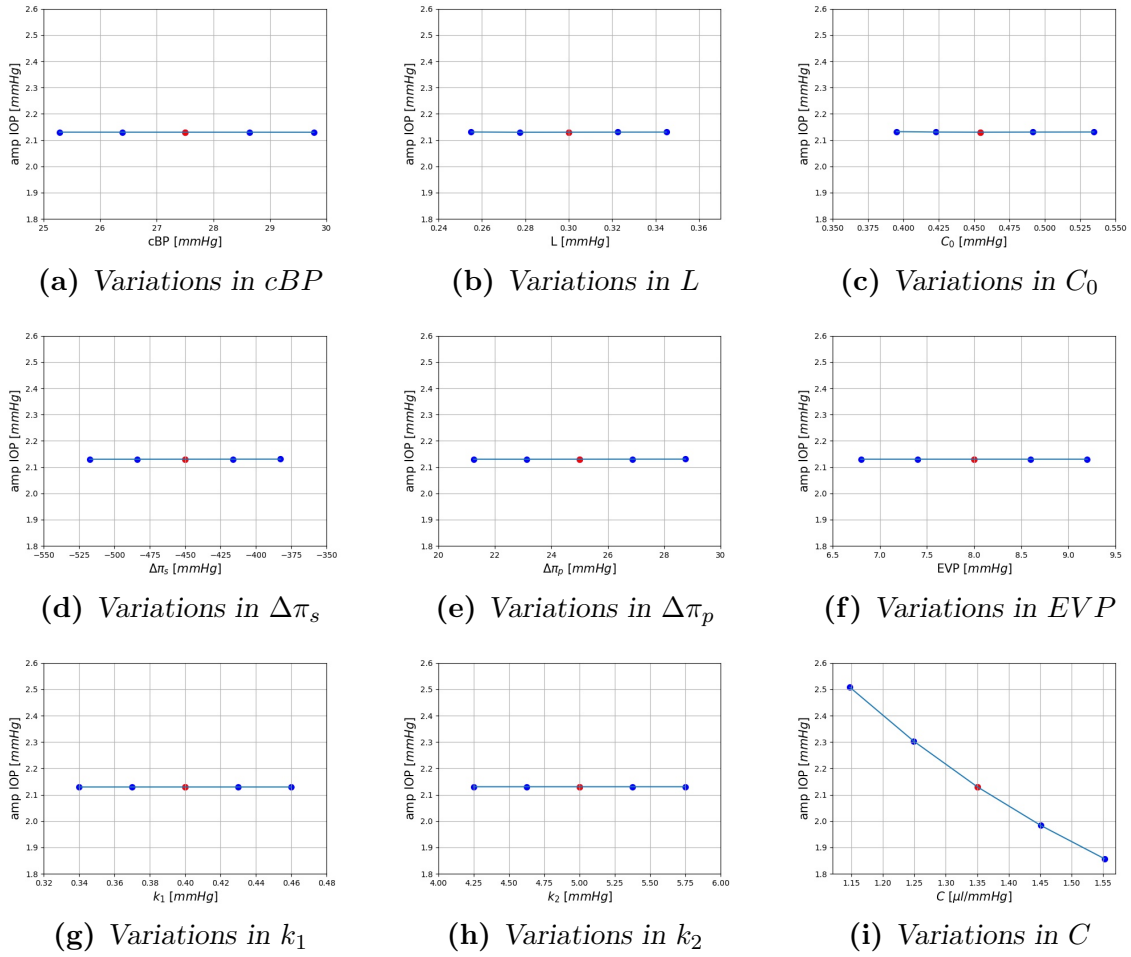

(a) *Variations in cBP* **(b)** *Variations in L* **(c)** *Variations in C_0*

(d) *Variations in $\Delta\pi_s$* **(e)** *Variations in $\Delta\pi_p$* **(f)** *Variations in EVP*

(g) *Variations in k_1* **(h)** *Variations in k_2* **(i)** *Variations in C*

Figure 4.12: *Deterministic sensitivity analysis on the dynamic model: influence of the different factors on the* ***amplitude of IOP*** *oscillations.*
Red dots indicate control state values for the variables and IOP, blue dots indicate sample values used in the analysis.

In fact, increasing the capacitance, tissue deformability is increased so that the internal stress released during the deformation increases. This leads to a reduction in the amplitude of IOP oscillations as can be seen in Figure 4.12(i).

Inversely, a decrease in C, meaning a stiffening of the tissues, implies an

increase in the amplitude of IOP oscillations, being G_{ch} unchanged. Oscillations can be pathological, possibly contributing to glaucoma pathophysiology.
In Figures 4.12(a) - 4.12(h) one can notice that these factors affect the mean value of IOP but do not have any influence on its dynamic part.

4.3 Results for the Dynamic Model with variable capacitance

4.3.1 Deterministic sensitivity analysis on the dynamic model

In this section we present the same analysis as that in the previous section but applied to the dynamic model with non-linear capacitor. Here, the extra parameter is the value of ocular rigidity γ, whose influence on mean, amplitude and frequency has to be taken into account. Coefficient of rigidity in normal eyes in inversely proportional to the volume of the eyeball, as defined in section 3.4.1, and is proportionally affected by axial refraction and radius of corneal curvature. Ocular rigidity has been observed to increase with age and in cases of extreme myopia [add reference]. Similarly, this occurs in intraocular inflammatory disease and often gives rise to the erroneous diagnosis of secondary glaucoma [22]. In one of its work [22], Friedenwald studied the effect of certain drugs on ocular rigidity. He found that ocular rigidity tends to decrease with vasodilators and increase with vasoconstrictors. For these reasons, it is interesting to quantify the influence of ocular rigidity variations on IOP dynamics.
Baseline and discrete values for the parameters are listed in Table 4.6.

Variations in mean IOP and amplitude of IOP due to different values of the parameters are shown in Figure 4.13 and 4.14, respectively.

Parameter	Baseline	Discrete values
cBP	$27.5\ mmHg$	$[25.278, 26.389, 27.5, 28.639, 29.778]$
L	$0.3\ \mu l/\min/mmHg$	$[0.255, 0.2775, 0.3, 0.3225, 0.345]$
R_0	$2.2\ mmHg \min/\mu l$	$[1.87, 2.035, 2.2, 2.365, 2.53]$
$\Delta\pi_s$	$-450\ mmHg$	$[-382.5, -416.25, -450.0, -483.75, -517.5]$
$\Delta\pi_p$	$25\ mmHg$	$[21.25, 23.125, 25.0, 26.875, 28.75]$
EVP	$8\ mmHg$	$[6.8, 7.4, 8.0, 8.6, 9.2]$
k_1	$0.4\ \mu l/\min$	$[0.34, 0.37, 0.4, 0.43, 0.46]$
k_2	$5\ mmHg$	$[4.25, 4.625, 5.0, 5.375, 5.75]$
γ	$0.0215\ \mu l^{-1}$	$[0.0183, 0.0199, 0.0215, 0.0231, 0.0247]$

Table 4.6: *Baseline and discrete values taken by the parameters of the dynamic model with nonlinear capacitor*

Figure 4.13 shows the same results of Figure 4.11: factors cBP, L, C_0, $\Delta\pi_s$, $\Delta\pi_p$, and EVP are determinants for the mean value of IOP, whereas k_1, k_2, and also γ, that is inversely proportional to the capacitance C as specified in equation (3.35), do not play any role in influencing mean IOP.

Figures 4.14(a) - 4.14(f) interestingly show that in the case of a capacitance depending non-linearly on IOP, these factors influence also the amplitude of IOP oscillations. This is a consequence of the fact that these factors influence the value of IOP, and in this case this value enters in the formula for the capacitance. We know from Figure 4.12(i) that the capacitance has an impact on the dynamics of IOP, so it follows that, as a major consequence of the non-linearity, all the parameters contribute to determine the dynamics of IOP. Indeed, in the previous case when C was constant, 4.12(a) - 4.12(f) didn't have any effect on the amplitude of the oscillations.

Figure 4.14(c) is particularly interesting, showing that an increase in the trabecular outflow resistance R_0 (equal to a decrease in C_0) causes the amplitude to increase. A high trabecular outflow resistance has been frequently associated with glaucoma; thus, this phenomenon reveals the importance played by the increase in amplitude of IOP oscillations, not only by its steady-state value, in potentially influencing glaucoma patho-

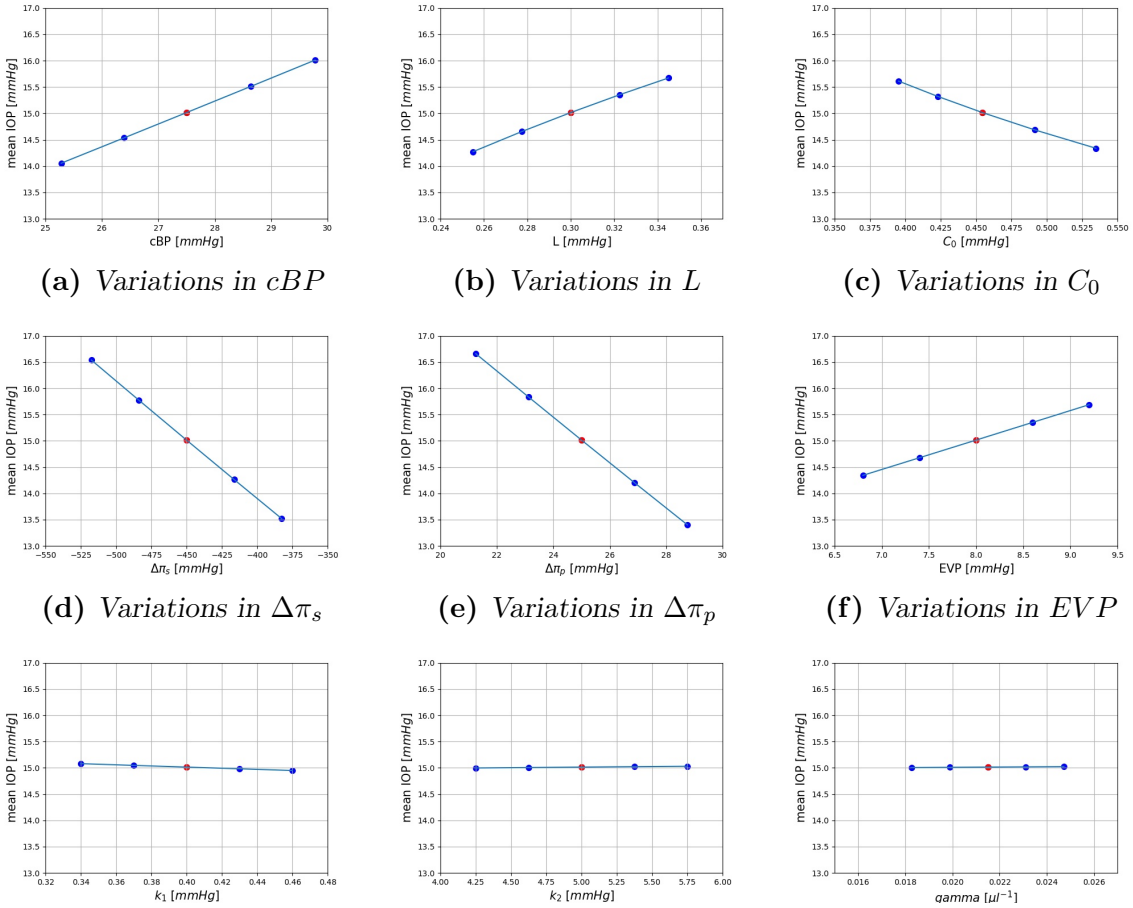

(a) *Variations in cBP* **(b)** *Variations in L* **(c)** *Variations in* C_0

(d) *Variations in* $\Delta\pi_s$ **(e)** *Variations in* $\Delta\pi_p$ **(f)** *Variations in EVP*

(g) *Variations in* k_1 **(h)** *Variations in* k_2 **(i)** *Variations in* γ

Figure 4.13: *Deterministic sensitivity analysis on the dynamic model, with a capacitance depending non-linearly on IOP: influence of the different factors on* ***mean IOP****.*
Red dots indicate control state values for the variables and IOP, blue dots indicate samples used in the circuit.

physiology.

Also in this case, parameters k_1 and k_2 do not have any influence on IOP oscillations.

Figure 4.14(i) is in agreement with the corresponding one in the constant-capacitance case, being γ inversely proportional to C.

Note that the range of variability of the amplitude of IOP oscillations increases of the order of $2\,mmHg$ when we let C depend non-linearly on IOP. To understand this phenomenon we plotted, on the same graph, IOP and C normalized waveforms (see Figure 4.15). The plot shows that

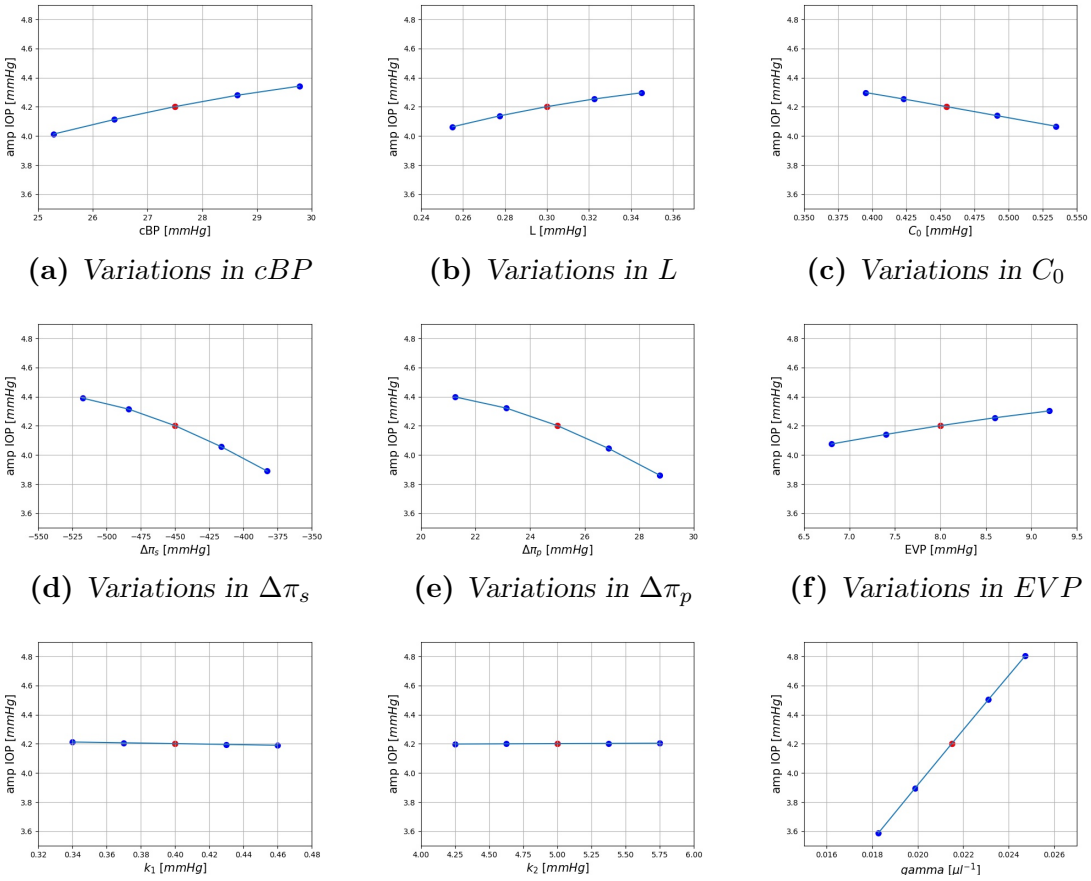

(a) *Variations in cBP* **(b)** *Variations in L* **(c)** *Variations in* C_0

(d) *Variations in* $\Delta\pi_s$ **(e)** *Variations in* $\Delta\pi_p$ **(f)** *Variations in EVP*

(g) *Variations in* k_1 **(h)** *Variations in* k_2 **(i)** *Variations in* γ

Figure 4.14: *Deterministic sensitivity analysis on the dynamic model, with a capacitance depending non-linearly on IOP: influence of the different factors on the* ***amplitude of IOP*** *oscillations. Red dots indicate control state values for the variables and IOP, blue dots indicate sample values used in the analysis.*

when IOP increases C decreases, meaning that tissues become stiffer and less deformable, thereby leading to an increase in the amplitude of IOP oscillations (as we showed in Figure 4.14(i)). Thus the non-linearity amplifies the oscillations.

With these observations in mind, we can quantify in a more complete way the influence of parameter variations on IOP dynamics using stochastic sensitivity analysis.

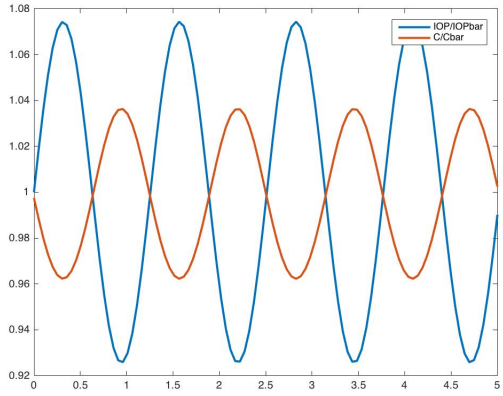

Figure 4.15: *Normalized IOP and normalized nonlinear capacitance*

4.3.2 Stochastic sensitivity analysis on the dynamic model

In this section we report results of the stochastic sensitivity analysis performed on the dynamic model with a non-linear capacitor. We include variability in ocular deformability to quantify the influence of this parameter on the output. We recall that, in this case, the model output is a pressure waveform that reaches a periodic state after about 5 seconds of simulation. Thus, similarly to the deterministic sensitivity analysis, here we have two outputs on which to perform the analysis, namely mean value of IOP and amplitude of its oscillations. As we already remarked, IOP frequency is influenced only by oscillations in choroidal blood flow during the cardiac cycle, so we do not account for it as an output.

All the parameters vary following uniform distributions with variations in the range $\pm 15\%$, except for cBP, whose variations are modeled as before, and ocular rigidity γ. In particular, as reported by Pallikaris et al [71], variations in ocular rigidity follow a normal distribution with mean $0.0125\,\mu l^{-1}$ and standard deviation $0.0049\,\mu l^{-1}$. Due to the fact that assuming this distribution the variable can take negative values, we can not use it in our work. In fact, ocular rigidity gives the sign to the non-linear capacitance (see equation 3.38). We choose to keep

Friedenwald's value of baseline for γ and let it vary as a normal distribution centered on this physiological value and with the standard deviation of [71]. Distribution for the parameters of the dynamic model are listed in Table 4.7.

Parameter	**Distribution**	**Properties of the distribution**
cBP	Normal	$mean = 27.5$; $standard\,deviation = 2.2496$
L	Uniform	$min = 0.3(1 - 15\%)$; $max = 0.3(1 + 15\%)$
R_0	Uniform	$min = 2.2(1 - 20\%)$; $max = 2.2(1 + 20\%)$
$\Delta\pi_s$	Uniform	$min = -450(1 + 15\%)$; $max = -450(1 - 15\%)$
$\Delta\pi_p$	Uniform	$min = 25(1 - 15\%)$; $max = 25(1 + 15\%)$
EVP	Uniform	$min = 8(1 - 15\%)$; $max = 8(1 + 15\%)$
k_1	Uniform	$min = 0.4(1 - 15\%)$; $max = 0.4(1 + 15\%)$
k_2	Uniform	$min = 5(1 - 15\%)$; $max = 5(1 + 15\%)$
γ	Normal	$mean = 0.0215$; $standard\,deviation = 0.0049$

Table 4.7: *Distributions for the parameters of the dynamic model*

Probability density functions (PDF) of mean IOP and amplitude of IOP oscillations and the respective first and total Sobol indices are reported in Figure 4.16. In particular:

- PDF of mean IOP fits a right-skewed Gaussian curve with mean value 15.0112 mmHg and variance 1.7763 mmHg,
- PDF of amplitude of IOP oscillations fits a right-skewed Gaussian curve with mean value 4.1021 mmHg and variance 0.9418 mmHg.

Table 4.8 reports the detailed Sobol indices resulted from the analysis. Note that in both cases, meta-model solutions coincide with solutions of the real model (see Figure 4.17 and 4.18). Simulation outcomes confirm what observed with the deterministic sensitivity analysis. In particular, one can note the existence of a higher order interactions, even if little, among the selected factors in influencing amplitude of IOP oscillations (see Figure 4.16(d), where first order and total Sobol indices present some differences). This is a direct consequence of the non-linearity of

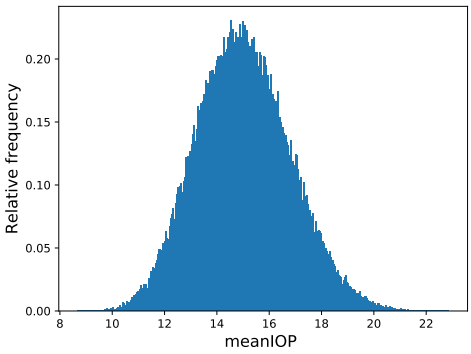

(a) *PDF of mean IOP*

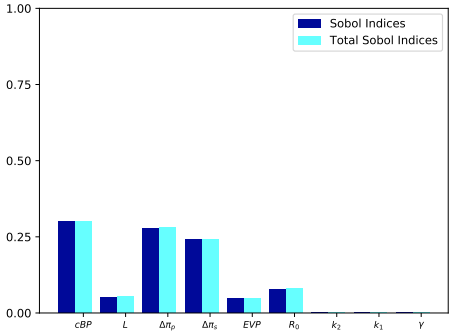

(b) *Sobol indices for mean IOP*

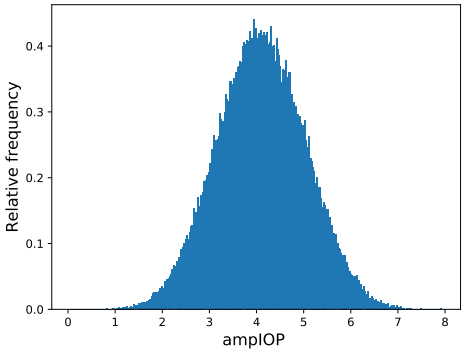

(c) *PDF of amplitude of IOP*

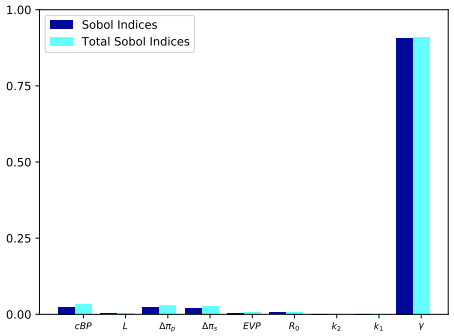

(d) *Sobol indices for amplitude of IOP*

Figure 4.16: *Simulation outcome of the dynamic model letting all the parameters vary*

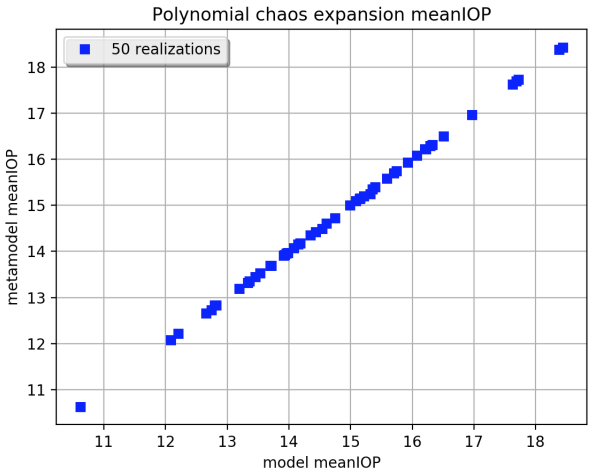

Figure 4.17: *Results of the PCE method on mean IOP*

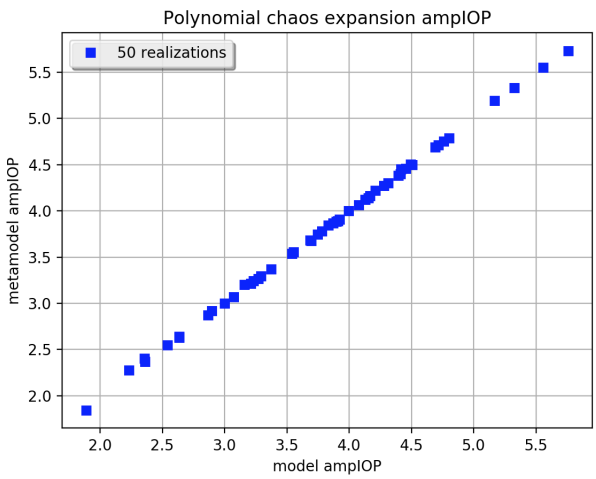

Figure 4.18: *Results of the PCE method on amplitude of IOP*

	First order Sobol indices	Total Sobol indices
mean IOP		
cBP	0.299477	0.301945
L	0.051281	0.053754
R_0	0.076496	0.0807946
$\Delta\pi_s$	0.239955	0.241960
$\Delta\pi_p$	0.276971	0.279259
EVP	0.048239	0.048485
k_1	0.000449	0.000465
k_2	$2.237022e-05$	$4.181879e-05$
γ	0.000197	0.000248
amplitude of IOP		
cBP	0.025009	0.032608
L	0.003025	0.004287
R_0	0.005782	0.007802
$\Delta\pi_s$	0.018739	0.025547
$\Delta\pi_p$	0.022365	0.029526
EVP	0.003972	0.005848
k_1	$2.242507e-05$	$8.477622e-05$
k_2	$7.239656e-06$	$4.062907e-05$
γ	0.915078	0.894257

Table 4.8: *First order and total Sobol indices of the dynamic model letting all the parameters vary*

the model that points out mutual interactions among different parameters. Comparing these results with those in next paragraph (see Figure 4.19(d)), when $\Delta\pi_p$ is kept constant, we can also suggest that interactions among variables are favored by oncotic pressure difference.

To investigate the efficacy of hypotensive ocular medications (see Chapter 5), we performed on the dynamic model the analysis done by the authors in [31]. Here, oncotic pressure difference is kept constant since IOP-lowering medications do not act on it. The simulation outcomes for ocular normotensive subjects show a probability density function for mean IOP that fits a right-skewed Gaussian curve with a frequency peak of 27% at 14.8 mmHg. Mean value and variance of mean IOP PDF are 15.0064 mmHg and 1.5083 mmHg respectively. Regarding amplitude of IOP, the PDF fits a right-skewed Gaussian curve with mean 4.1246 mmHg and variance 0.9333 mmHg. First order and total Sobol indices are listed in Table 4.9

	First order Sobol indices	Total Sobol indices
mean IOP		
cBP	0.414650	0.418088
L	0.070839	0.073232
R_0	0.105785	0.109831
$\Delta\pi_s$	0.332738	0.335441
EVP	0.066942	0.067279
k_1	0.000449	0.000465
γ	0.000270	0.000345
amplitude of IOP		
cBP	0.026757	0.031682
L	0.003530	0.004479
R_0	0.006826	0.008361
$\Delta\pi_s$	0.020424	0.025011
EVP	0.004282	0.005808
k_1	$2.242507e-05$	$8.477622e-05$
γ	0.930086	0.932878

Table 4.9: *First order and total Sobol indices of the dynamic model in normotensive subjects*

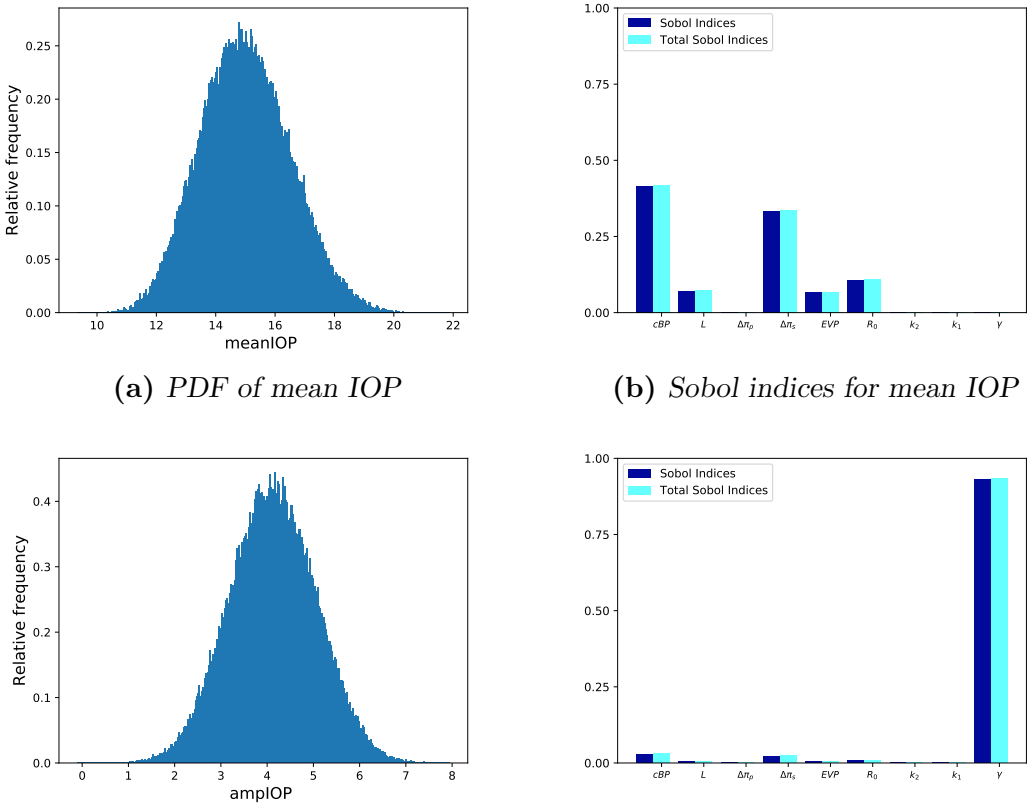

(a) *PDF of mean IOP*

(b) *Sobol indices for mean IOP*

(c) *PDF of amplitude of IOP*

(d) *Sobol indices for amplitude of IOP*

Figure 4.19: *Simulation outcome of the dynamic model in normotensive subjects*

The results for the Sobol indices suggest that mean IOP is strongly influenced by cBP and $\Delta\pi_s$, which show Sobol indices of 0.4 and 0.3 respectively, and mildly influenced by the levels of R_0, L and EVP. The influence of k_1 and γ on mean IOP appear to be minimal. These results are completely in agreement with what found for the static model. Amplitude of IOP oscillations is almost totally influenced by ocular rigidity (Sobol index 0.93) and only minimally by ciliary blood pressure and osmotic pressure difference.

Chapter 5

Clinical applications

Since it is extremely difficult to identify and isolate variations in different biomechanical and hemodynamical properties of the eye in clinical and experimental studies, this mathematical approach may provide very useful insights. In fact, using these models we can predict the outcome of IOP-lowering medications, while accounting for uncertainties and variabilities in the model parameters. Accounting for variability in a systematic manner can help identify some patient-specific factors that influence the efficacy of IOP-lowering medications and aid in the development of novel, effective, and individualized therapeutic approaches in glaucoma management.

We simulate the effect of IOP-lowering medications in different conditions of clinical interest, namely ocular normotensive healthy subjects (ONT) and ocular hypertensive subjects (OHT). Due to the fact that many open angle glaucoma patients continue to experience disease progression despite meeting target IOP levels [13, 14, 52, 42], it can be relevant from a clinical point of view to consider the outcome of IOP-lowering medications also on ONT subjects.

To simulate **ocular hypertensive subjects** we acted on the mean value of the trabecular meshwork outflow facility by decreasing it, as suggested by several clinical observations [4][3]. Thus, we set $C_0 = 0.3\,\overline{C_0}$, letting the mean values of the other parameters at control state

values.

We model the effect of **IOP-lowering medications** by reducing the active ionic secretion by 25%, which sets the mean value of the blood/AH osmotic pressure difference to $\Delta\pi_s = 0.75\,\overline{\Delta\pi_s}$. Mean values of the other parameters remain at control state. This modeling choice is justified by the fact that the sensitivity analyses in both the ONT and OHT cases have identified $\Delta\pi_s$ as an important determinant of IOP levels; in addition, clinical evidence and studies also support this notion [47, 39, 53].

5.1 Results for the Static Model

As a first step, we consider the static model to validate our results with those reported in [31]. Indeed our model can reproduce all the results found by the authors.

5.1.1 Ocular hypertensive subjects

Simulations outcomes show a probability density function that fits a Gaussian curve (see Figure 5.1(a)), but with frequency peak of 17% at 20.07 mmHg and with a more symmetric profile than ONT Gaussian curve that we obtained in Section 4.1.2. Mean value and variance result in 19.8404 mmHg and 2.288 mmHg respectively, which is clinically classifiable as ocular hypertension.

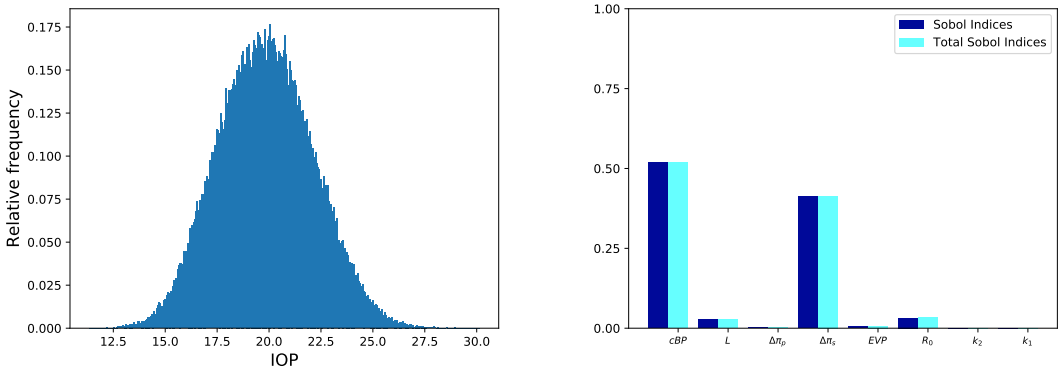

(a) *Probability density function of IOP, OHT case.*

(b) *First order and total Sobol indices, OHT case.*

Figure 5.1: *Simulation outcome of the static model in OHT subjects.*

The Sobol indices values for OHT subjects (Figure 5.1(b) and Table 5.1) show a stronger dependence of IOP on cBP and $\Delta\pi_s$, with Sobol indices 0.52 and 0.41 respectively (versus 0.42 and 0.33 of the normotensive case), and a weaker dependence of IOP on L, C_0 and especially on EVP than for ONT subjects. The influence of k_1 on IOP remains minimal.

	First order Sobol indices	Total Sobol indices
cBP	0.518283	0.519225
L	0.026466	0.027145
R_0	0.031755	0.032849
$\Delta\pi_s$	0.412524	0.413282
EVP	0.006179	0.006269
k_1	0.000876	0.000881

Table 5.1: *First order and total Sobol indices of the static model in the OHT case.*

5.1.2 Ocular normotensive subjects treated with IOP-lowering medications

The IOP probability density function in the ocular normotensive subjects treated with IOP-lowering medications (ONTm) (see Figure 5.2(a)) fits a right-skewed Gaussian curve with a frequency peak of 32% at 12.52 mmHg. Mean value and variance result in 12.4689 mmHg and 1.2718 mmHg, respectively. Thus, our simulations predict a reduction of 2.46

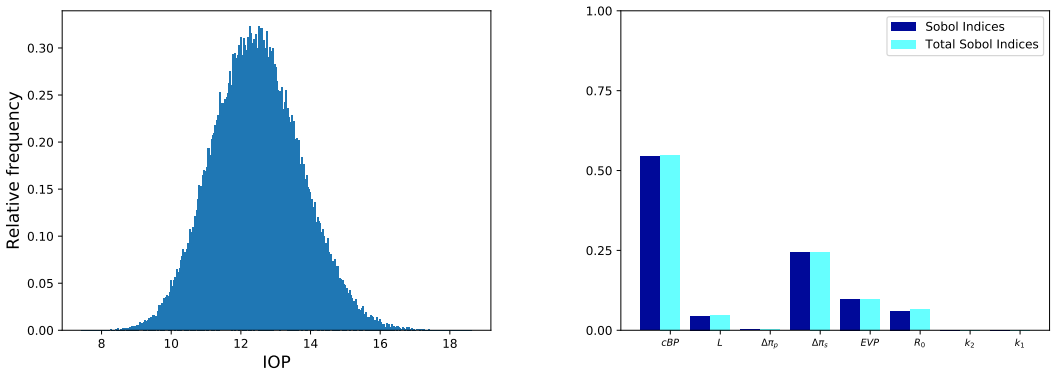

(a) *Probability density function of IOP, ONTm case.*

(b) *First order and total Sobol indices, ONTm case.*

Figure 5.2: *Simulation outcome of the static model in treated ONT subjects.*

mmHg in the mean value of IOP when IOP-lowering medications are administered to ONT subjects.

The results of Sobol indices (Figure 5.2(b), explicit values in Table 5.2) suggest that IOP is mainly influenced by cBP and $\Delta\pi_s$ (Sobol indices

0.54 and 0.24 respectively). On the other hand, L, C_0 and EVP have a limited influence. The influence of the first determinant on IOP is even higher than in the non-treated normotensive case. Also in this case k_1 has a negligible influence.

	First order Sobol indices	Total Sobol indices
cBP	0.543756	0.548145
L	0.044606	0.047110
R_0	0.060677	0.064962
$\Delta\pi_s$	0.243485	0.245468
EVP	0.097704	0.098124
k_1	0.000732	0.000738

Table 5.2: *First order and total Sobol indices of the static model in the ONTm case.*

5.1.3 Ocular hypertensive subjects treated with IOP-lowering medications

We simultaneously account for OHT conditions and IOP-lowering treatment by setting the mean values of C_0 and $\Delta\pi_s$ to $0.3\overline{C_0}$ and $0.75\overline{\Delta\pi_s}$ respectively, letting mean values of the other parameters at control state values.

IOP probability density function in the OHTm case (Figure 5.3(a)) fits a Gaussian curve with frequency peak of 20% at 15.37 mmHg and has a more symmetric profile than the curve in the ONTm case. Mean value and variance result in 15.6516 mmHg and 1.9794 mmHg respectively. Thus, our simulations predict a reduction of 4.19 mmHg in the mean value of IOP when IOP-lowering medications are administered to OHT subjects (versus a reduction of only 2.46 mmHg when patients' initial IOP was already "physiological").

Results of Sobol indices (see Figure 5.3(b) and Table 5.3) are similar to those obtain in the ONTm case, but with an even higher contribution of cBP (Sobol index 0.66) and an even weaker contribution of L, C_0 and

EVP.

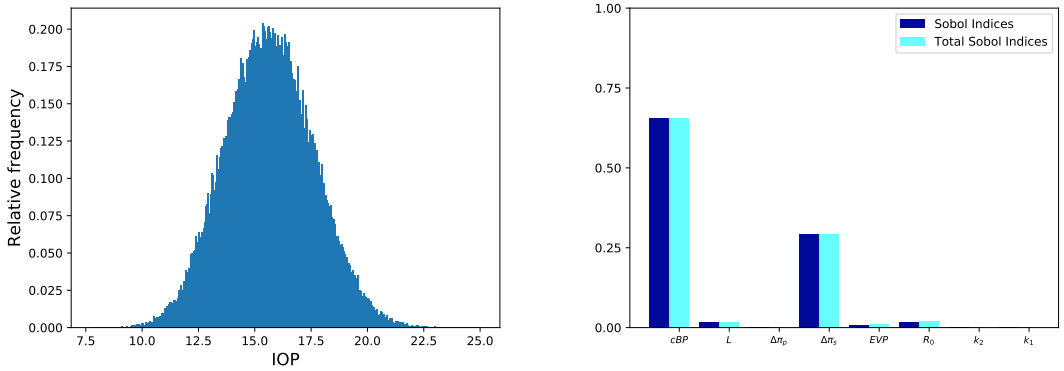

(a) *Probability density function of IOP, OHTm case.*

(b) *First order and total Sobol indices, OHTm case.*

Figure 5.3: *Simulation outcome of the static model in treated OHT subjects.*

	First order Sobol indices	Total Sobol indices
cBP	0.655557	0.656841
L	0.017607	0.018351
R_0	0.018323	0.019524
$\Delta\pi_s$	0.293498	0.294093
EVP	0.009341	0.009462
k_1	0.000997	0.001003

Table 5.3: *First order and total Sobol indices of the static model in the OHTm case.*

The proposed model suggests that the outcomes of IOP-lowering treatments depend on the initial IOP level of the patient and on its individual clinical condition. Specifically, the model predicts mean IOP reductions of 2.46 mmHg and 4.19 mmHg when the pre-treatment IOP mean values are 14.9272 mmHg and 19.8404 mmHg, respectively. These predictions are in good agreement with the work by Rulo et al [34] who reports mean IOP reductions of 2 mmHg and 4.2 mmHg for pre-treatment IOP of 15.3 mmHg and 18.4 mmHg (mean values), respectively.

Moreover, our results demonstrate that first order and total Sobol

indices do not present noticeable differences in any of the four simulated scenarios, suggesting that higher order interactions among the selected factors are minimal.

5.2 Results for the Dynamic Model

We simulate conditions of ocular hypertension and IOP-lowering medications on the complete dynamic model in both normotensive and hypertensive subjects to investigate the influence of ocular rigidity on IOP waveform.

5.2.1 Ocular hypertensive subjects

Simulation outcomes for OHT subjects are presented in Figure 5.4 and Table 5.4.

	First order Sobol indices	Total Sobol indices
mean IOP		
cBP	0.518410	0.519882
L	0.027306	0.028527
R_0	0.031798	0.032948
$\Delta\pi_s$	0.409635	0.410539
EVP	0.005734	0.006063
k_1	0.000989	0.001195
γ	0.001321	0.001853
amplitude of IOP		
cBP	0.066273	0.093631
L	0.004555	0.007688
R_0	0.003914	0.007668
$\Delta\pi_s$	0.048890	0.074327
EVP	0.000431	0.001270
k_1	0.000118	0.000526
γ	0.841835	0.850282

Table 5.4: *First order and total Sobol indices of the dynamic model in the OHT case.*

Mean IOP probability density function in the OHT case (see Fig-

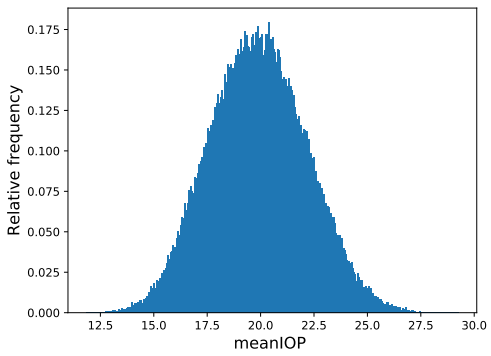

(a) *PDF of mean IOP.*

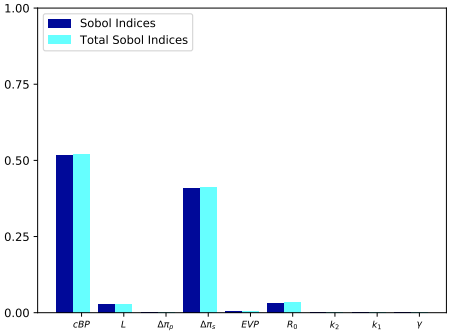

(b) *Sobol indices for mean IOP.*

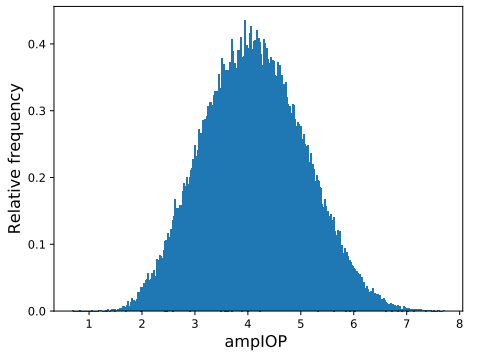

(c) *PDF of amplitude of IOP.*

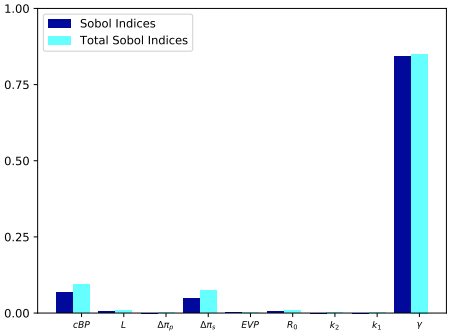

(d) *Sobol indices for amplitude of IOP.*

Figure 5.4: *Simulation outcome of the dynamic model in OHT subjects.*

ure 5.4(a)) fits a Gaussian curve, but with a more symmetric profile than ONT Gaussian curve (see Figure 4.19(a)), mean value of 19.9029 mmHg and variance of 2.2752 mmHg.
Mean IOP Sobol indices values for OHT subjects (see Figure 5.4(b) and upper part of Table 5.4) show a stronger dependence of mean IOP on cBP and $\Delta\pi_s$ than for ONT subjects (Sobol indices 0.52 and 0.41 respectively, versus 0.41 and 0.33 in the ONT case) and a weaker dependence on L, R_0 and EVP. The influence of k_1 on mean IOP remains minimal.

Conversely, amplitude of IOP oscillations appears not to be increased in ocular hypertensive subjects. One can easily expect this outcome looking at the dependence of IOP on R_0, namely the parameter we increased to simulate ocular hypertension, showed in Figure 4.19(d). In fact, its influence on amplitude of IOP oscillations is minimal. Values of mean and variance of amplitude of IOP probability density functions are 4.1113 mmHg and 0.9506 mmHg, respectively.
Amplitude of IOP Sobol indices values for OHT subjects (see Figure 5.4(d) and lower part of Table 5.4) show a weaker dependence of amplitude on γ and a stronger dependence on cBP and $\Delta\pi_s$, even if minimal, than for ONT subjects. Moreover, amplitude of IOP oscillations displays more relevant higher order interactions among the selected factors caused by ciliary blood pressure and osmotic pressure difference.

5.2.2 Ocular normotensive subjects treated with IOP-lowering medications

Simulation outcomes for ONTm subjects are presented in Figure 5.5 and Table 5.5.

The mean IOP probability density function in the ONTm case (see Figure 5.5(a)) fits a right-skewed Gaussian curve with mean 12.5394 mmHg and variance 1.2787 mmHg. Thus, our simulations predict a reduction of 2.47 mmHg in the mean value of IOP when IOP-lowering

medications are administered to ONT subjects.
Results of Sobol indices (see Figure 5.5(b)) suggest that IOP mean value is strongly influenced by cBP and $\Delta\pi_s$ and mildly influenced by the levels of EVP, R_0 and L. In particular, ciliary blood pressure acquires more importance in influencing mean IOP compared to the non-treated case (Sobol index 0.54 versus 0.41 of the ONT case), whereas osmotic pressure difference influence less mean IOP (Sobol index 0.24 versus 0.33 of the ONT case). Interestingly, differently from what founded in the ONT case, here episcleral venous pressure influences mean IOP more that trabecular outflow resistance.

Amplitude of IOP probability density function (see Figure 5.5(c)) fits a right-skewed Gaussian curve with mean 3.6177 mmHg and variance 0.8654 mmHg.
Amplitude of IOP Sobol indices values for treated ONT subjects (see Figure 5.5(d) and lower part of Table 5.5) show a weaker dependence of amplitude of IOP on γ, with Sobol index 0.86 versus 0.93 in the ONT case, and a stronger dependence on cBP and $\Delta\pi_s$ than for non-treated ONT subjects. Higher order interactions among the selected factors are minimal as proved by the equality between first order and total Sobol indices.

5.2.3 Ocular hypertensive subjects treated with IOP-lowering medications

Simulation outcomes for OHTm subjects are presented in Figure 5.6 and Table 5.6.

The mean IOP probability density function (see Figure 5.6(a)) fits a Gaussian curve that has a more symmetric profile than the curve in the ONTm case. Mean value and variance are 15.7158 mmHg and 1.9897 mmHg respectively. Thus, our simulations predict a reduction of 4.19 mmHg in the mean value of IOP when IOP-lowering medications are

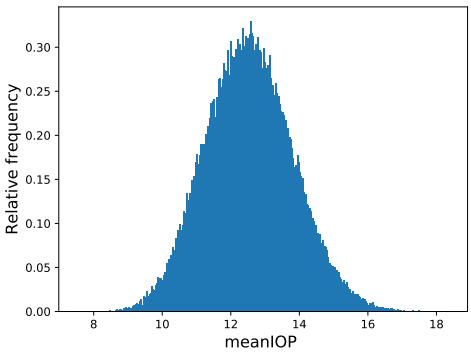

(a) *PDF of mean IOP.*

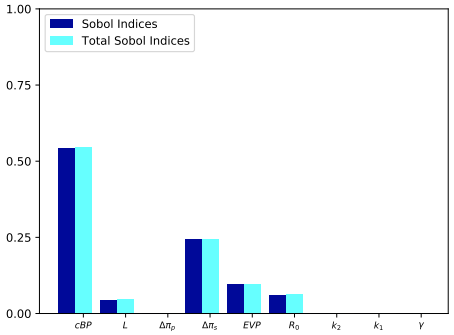

(b) *Sobol indices for mean IOP.*

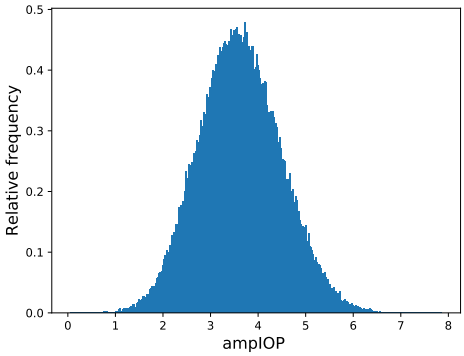

(c) *PDF of amplitude of IOP.*

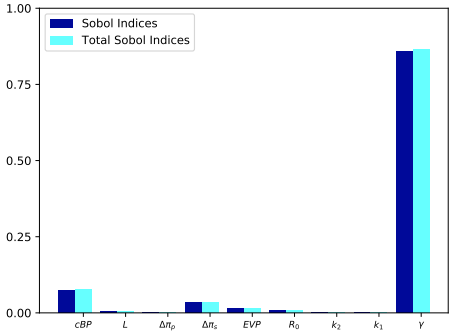

(d) *Sobol indices for amplitude of IOP.*

Figure 5.5: *Simulation outcome of the dynamic model in treated ONT subjects.*

	First order Sobol indices	Total Sobol indices
mean IOP		
cBP	0.543776	0.548188
L	0.044442	0.046933
R_0	0.060691	0.064953
$\Delta\pi_s$	0.242071	0.244158
EVP	0.098181	0.098695
k_1	0.000692	0.000842
γ	0.000508	0.000883
amplitude of IOP		
cBP	0.075069	0.079084
L	0.005329	0.005892
R_0	0.009121	0.010057
$\Delta\pi_s$	0.033665	0.035352
EVP	0.013290	0.014291
k_1	0.000107	0.000192
γ	0.856195	0.862077

Table 5.5: *First order and total Sobol indices of the dynamic model in the ONTm case.*

administered to OHT subjects.
The resultant Sobol indices (see Figure 5.6(b)) show an increased importance of ciliary blood pressure and osmotic pressure difference in influencing mean IOP with respect to the ONTm case (Sobol indices 0.65 and 0.29 respectively, versus 0.54 and 0.24 of the treated normotensive case). Moreover, L, R_0 and EVP show a weaker contribution.

Amplitude of IOP probability density function (see Figure 5.6(c)) fits a Gaussian curve with mean 4.2186 mmHg and variance 0.9388 mmHg. Amplitude of IOP Sobol indices values for treated OHT subjects (see Figure 5.6(d) and lower part of Table 5.6) show a stronger dependence of amplitude of IOP on γ (with Sobol index 0.92) and a weaker dependence on cBP and $\Delta\pi_s$ than for non-treated OHT subjects. Higher order interactions among the selected factors are less important than the OHT case but more important than the ONTm case.

	First order Sobol indices	Total Sobol indices
mean IOP		
cBP	0.653367	0.655015
L	0.018095	0.019120
R_0	0.018385	0.019797
$\Delta\pi_s$	0.292880	0.293688
EVP	0.009254	0.009539
k_1	0.000825	0.000987
γ	0.001620	0.002288
amplitude of IOP		
cBP	0.047305	0.062959
L	0.000310	0.001844
R_0	0.000720	0.002118
$\Delta\pi_s$	0.016615	0.029695
EVP	0.000507	0.001258
k_1	$9.343827e-05$	0.000309
γ	0.916260	0.920722

Table 5.6: *First order and total Sobol indices of the dynamic model in the OHTm case.*

Summarizing, the analysis on the model that takes into account the

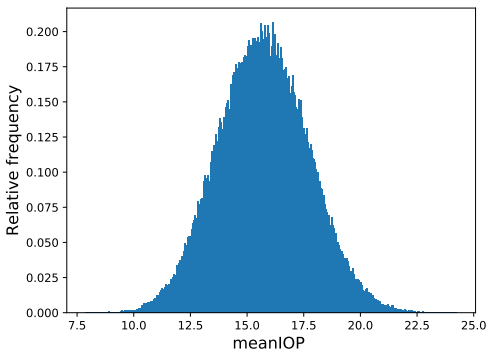

(a) *PDF of mean IOP.*

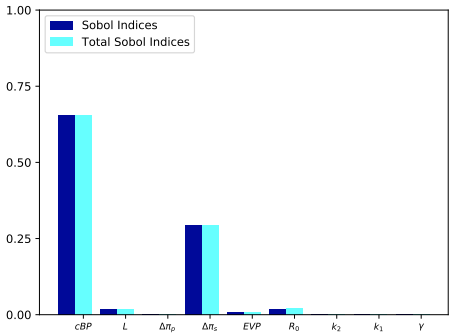

(b) *Sobol indices for mean IOP.*

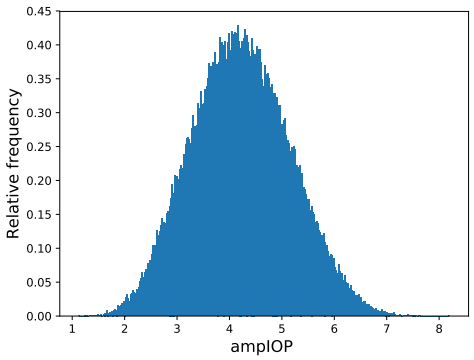

(c) *PDF of amplitude of IOP.*

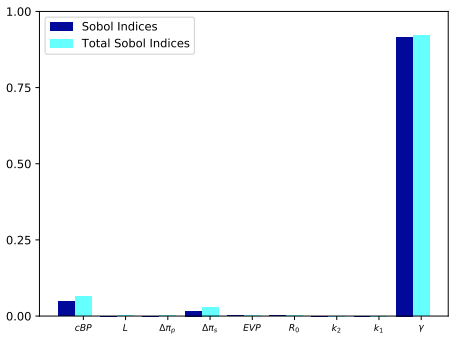

(d) *Sobol indices for amplitude of IOP.*

Figure 5.6: *Simulation outcome of the dynamic model in treated OHT subjects.*

time-dependent evolution of IOP confirms that the outcomes of IOP-lowering treatments depend on the initial IOP level of the patient and on its individual clinical condition. Specifically, the model predicts mean IOP reductions of 2.47 mmHg and 4.19 mmHg when the pre-treatment IOP mean values are 15.0064 mmHg and 19.9029 mmHg, respectively.

As occurs for the static case analysis, these predictions are in good agreement with Rulo et al. However, it is important to remark that they utilize Latanoprost, a prostaglandin analog that increases AH drainage, whereas we model IOP-lowering medications by decreasing AH production. Other studies report IOP reductions ranging from 3 mmHg to 4.4 mmHg in response to brinzolamide [18], from 4.5 mmHg to 6.1 mmHg in response to dorzolamide [54], and from 2.4 mmHg to 4.5 mmHg in response to Latanoprost [63]. The mean IOP reductions reported in these studies are close or slightly higher than those predicted by our model; this might be due to the fact that these studies start from higher pre-treatment IOP levels (ranging from 23.8 mmHg to 28.9 mmHg) than those considered in our simulations.

This analysis also suggests that IOP-lowering effects are more pronounced when AH production is affected rather than AH drainage. In fact, $\Delta\pi_s$, osmotic pressure difference that drives ionic secretion and thus AH production, is more important in influencing mean IOP than R_0 and k_1, that drive AH drainage (trabecular and uveoscleral outflow respectively). The effects of lowering IOP are also more apparent when trabecular outflow is increased instead of the uveoscleral outflow.

Another interesting finding is that a patient's blood pressure (MAP, which determines cBP in our model) strongly influences the outcomes of IOP-lowering treatments. This consideration may explain why the effect of some drugs differ between day-time and night-time and/or among individuals [21, 34, 63, 66].

Chapter 6

Modeling IOP physiology: model extensions

This chapter is a work in progress that aims to extend our model to separately analyze mechanical properties of ocular structures, namely cornea, sclera, vitreous humor, lens and their influence in determining IOP dynamics. Model calibration is ongoing, but the model already provides an insight for future developments of this study.

The next step into the modeling of intraocular pressure dynamics consists in **distinguishing the contribution of different structures inside the eye, namely cornea, sclera, lens and vitreous humor, to the total ocular deformability**.
The main assumptions are:

1. V_{tot} is defined as the sum of eye volumes subtended by cornea ($V_{below,c}$) and sclera ($V_{below,s}$):

$$V_{tot} = V_{below,c} + V_{below,s}. \tag{6.1}$$

   Eye volume subtended by cornea accounts for the anterior chamber volume (that depends on aqueous humor flow); eye volume subtended by sclera accounts for vitreous humor, lens and choroid volumes:

$$V_{below,c} = V_{ant} \tag{6.2}$$
$$V_{below,s} = V_{vitr} + V_{lens} + V_{ch}. \tag{6.3}$$

2. V_{lens} is assumed to be constant over time due to the fact that lens is less deformable than the other structures;

3. V_{vitr} varies subjected to aqueous humor pressure (P_{AH}) and pressure given by pulsatile ocular blood flow (P_{ch});

4. V_{cornea} and V_{sclera} are modeled accounting for the membrane approximation for ***thin-walled structures***. It works by assuming a minimal thickness with respect to the radius of the structure ($h << r$). Implications are that:

   - we consider deformations of the "middle surface" and
   - all stresses and strains do not vary across the thickness of the structure.

Following the anatomical structure of the eye (see Figure 6.1), we designed the circuit shown in Figure 6.2 modeling the contributions of different materials with capacitors having different properties.

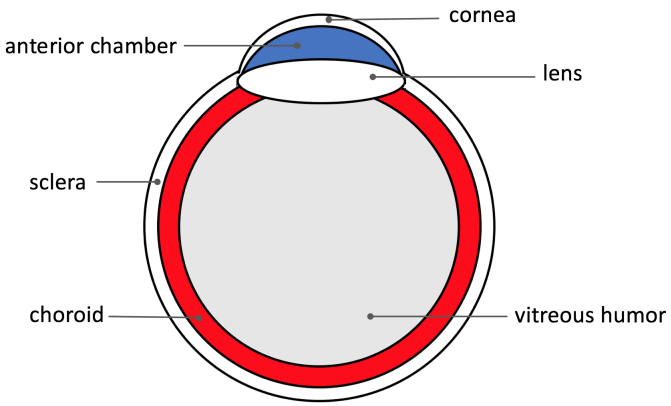

Figure 6.1: *Eye structure.*

There are two compartments in which different fluids (aqueous humor and blood) flow. The presence of the capacitor between the compartments ensures that no mixing of fluids can take place between the two parts of the circuit. Note that the extremities of the circuit are modeled by voltage sources (cBP and EVP), so that an expansion of the model including blood flowing into the brain and systemic circulation can be implemented (for example by integrating other models already developed in the group [69]). Driving forces of the system are:

- currents in the upper part of the circuit that models AH flow and
- current source J_{ch} that models choroid blood flow.

The main challenge is the characterization of constitutive laws for capacitances along the main branch. They describe the relationship between the pressure difference across compartments and the deformation of the tissue structure that separates the compartments.
Capacitor simulates the interaction between flow and structure: if the structure is deformable, then part of the energy of the circuit is stored in its deformation. This event is well explained by electrical capacitance:

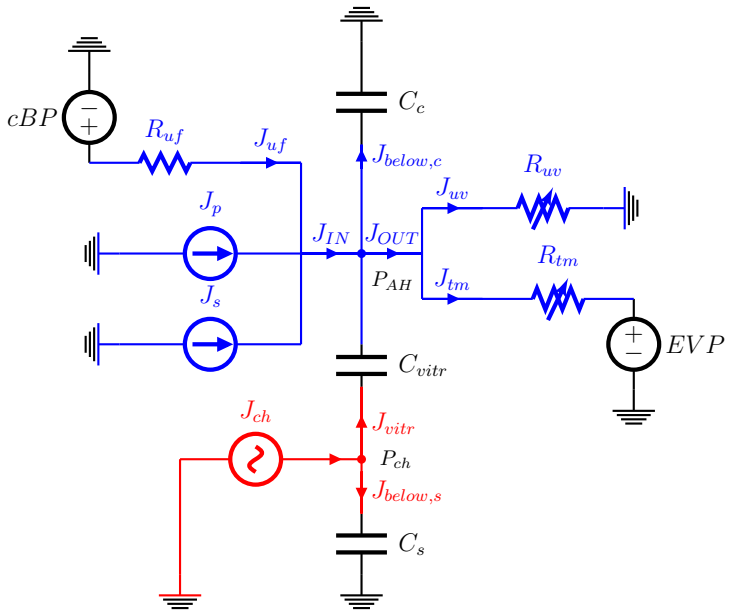

Figure 6.2: *Electrical circuit for the perspective model.*
Flows involved are: aqueous humor flowing across the anterior chamber (AH) that interacts with cornea (c) and vitreous (vitr) and blood flowing through choroid (ch) that interacts with vitreous and sclera (s).

variations in the charge of the capacitor plate (dQ/dt) are analogue to variations in volume of the respective deformable structure (dV/dt). So a capacitor indicates the possibility of the fluid involved in the related part of the circuit to change volume.

The capacitor at the top of the figure models the deformability of the structures placed below the cornea, namely cornea itself and anterior chamber. The capacitor at the very bottom of the figure models the deformability of the structures placed below the sclera, so it includes sclera, vitreous, lens and choroid deformability.

In a complete model there should be also a fourth capacitor for the lens, but we simplified the circuit putting one capacitor that models both vitreous humor and lens deformability. It is justified by the fact that lens is made of a less deformable substance than the others structures we are considering in the eye, so it plays a minor role in the deformation. We can model this property stating that lens volume is constant over time.

To model a structure deformability we need to express the relation between volume of the structure and difference of pressure acting on the structure, as a function of parameters that express its deformability. Cornea and sclera are thin deformable surfaces that act as boundaries for the subtended eye volumes. Thus, to compute the surface deformability, we accounted for changes of volume subtended by the surface and changes of pressure acting on the surface itself. Conversely, vitreous humor is a deformable material that by itself occupies a certain volume, that is exactly the volume we accounted for in the estimate of its capacitance.

6.1 Capacitances for cornea and sclera

To estimate cornea and sclera capacitances, first of all we expressed volume as a function of the deformation through geometrical relations. Then, through elastic theory plus approximation for thin elastic wall, we expressed deformation as a function of pressure difference acting on the structure. This last relation will be expressed as a function of deformability parameters.

- Geometric relations: volume-deformation expressions:

  Due to the fact that we deal with thin structures, we have to consider tangential deformations and not radial deformations. It is because *thin-walled structures don't have bending stiffness*, meaning that they are not capable to offer any resistance in the radial direction, and if stressed in that direction they deform. They just develop a tangential tension as a response to deformations.

  For a sphere, tangential deformation (that is how much tangential length varies) is defined as the change in circumference divided by the

original circumference:

$$\eta_\theta = \frac{2\pi r - 2\pi r_0}{2\pi r_0} = \frac{r - r_0}{r_0} = \frac{\Delta r}{r_0}, \tag{6.4}$$

where r is the new radius of the structure and r_0 is the initial radius of the structure. Thus

$$r = r_0(1 + \eta_\theta). \tag{6.5}$$

We compute the volume of each structure as a function of: initial radius r_0, deformation η (in the following we will omit subscript θ of η_θ for simplicity of notation) and angle α (see Figure 6.3). We suppose that during deformation the parameter that varies less is α because of the presence of the structures that connect cornea with sclera.

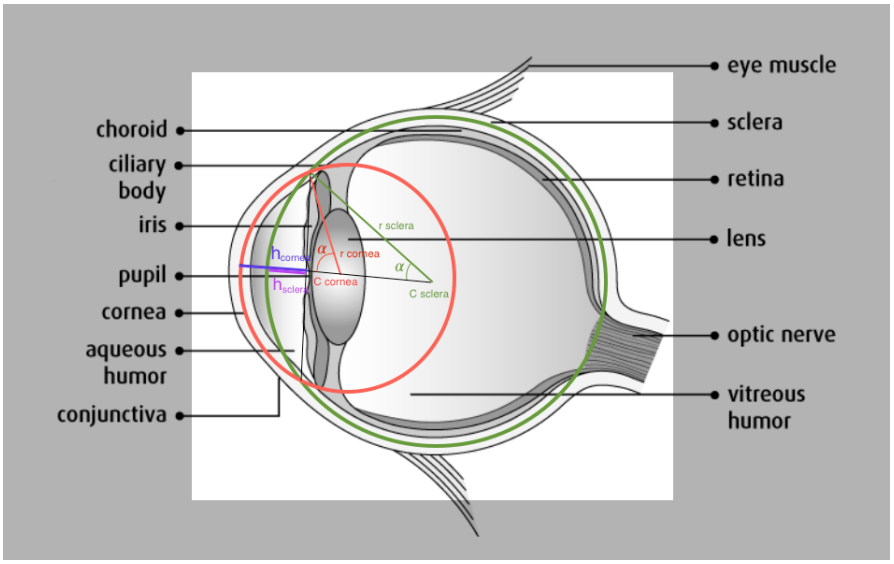

Figure 6.3: *Geometric parameters for cornea and sclera:*
cornea: $r_{0,c} = 7.8\,mm$; $\alpha_c = 48°$;
sclera: $r_{0,s} = 11.5\,mm$; $\alpha_s = 30°$.

– **AH under cornea:**

We compute volume of aqueous humor located below the cornea

as (see Figure 6.3 for geometric parameters values):

$$V_{below,c} = \pi h_c^2 \left(r_c - \frac{h_c}{3} \right), \text{ with} \tag{6.6}$$

$$r_c = r_{0,c}(1 + \eta_c), \tag{6.7}$$

$$h_c = r_c(1 - \cos \alpha_c). \tag{6.8}$$

It results in:

$$V_{below,c} = \frac{\pi}{3} r_{0,c}^3 (1 + \eta_c)^3 \delta c, \text{ with} \tag{6.9}$$

$$\delta c = (1 - \cos \alpha_c)^2 (2 + \cos \alpha_c) = 0.29. \tag{6.10}$$

It is a pure geometric relationship that expresses how volume occupied by aqueous humor changes as a function of the deformation of the cornea η_c.

– **fluids under sclera:**
Eye volume below sclera is computed as:

$$V_{below,s} = \left[\frac{4}{3} \pi r_s^3 - \pi h_s^2 \left(r_s - \frac{h_s}{3} \right) \right], \text{ with} \tag{6.11}$$

$$r_s = r_{0,s}(1 + \eta_s), \tag{6.12}$$

$$h_s = r_s(1 - \cos \alpha_s). \tag{6.13}$$

It results in:

$$V_{below,s} = \frac{\pi}{3} r_{0,s}^3 (1 + \eta_s)^3 \delta_s, \text{ with} \tag{6.14}$$

$$\delta_s = [4 - (1 - \cos \alpha_s)^2 (2 + \cos \alpha_s)] = 3.95 \tag{6.15}$$

and is given by the sum of choroidal volume V_{ch}, vitreous humor volume V_{vitr} and lens volume V_{lens}.

- Mechanical properties: theory of elasticity:
We next found a dependency of cornea and sclera tangential deforma-

tion on the respective transmural pressures.

1. Tension T, that is the force acting on the wall to keep the sphere from distending/exploding, balances the pressure force that acts to push the sphere from the inside to the outside (transmural pressure $\Delta p = p_{in} - p_{ext}$ multiplied by the cross-sectional area of the sphere):

$$T = \Delta p \pi r_0^2. \tag{6.16}$$

   For the thin-walled sphere, one can thinks of the wall area as a long, skinny rectangle of length $2\pi r_0$ and height t (wall thickness). The wall tension is equal to the wall mechanical stress σ_θ multiplied by the area over which it acts:

$$T = \sigma_\theta (2\pi r_0 t). \tag{6.17}$$

   It follows the *Law of Laplace*, that express the dependence of the tangential stress σ_θ on the transmural pressure:

$$\sigma_\theta = \frac{\Delta p \, r_0}{2t}. \tag{6.18}$$

   This equation shows that wall stress increases with pressure and with the shape factor $r_0/(2t)$: it doesn't depend on radius alone, wall thickness always comes into play regardless of how thin the wall may be.

2. To determine the compliance of the thin-walled sphere, we need some information about the biomechanics of the structure of interest, that is how the material behaves in response to stress. The constitutive law can follow a linear elastic, non-linear elastic, or viscoelastic behavior if time is involved in the deformation properties. In this work we assume that the eye is made of ***linear***

elastic materials that behave according to *Hooke's law*:

$$\sigma_\theta = E\eta_\theta. \tag{6.19}$$

E is a property of the material itself called Young's modulus of elasticity. The equation describes a linear relation between mechanical stress and strain. Substituting the expressions of tangential stress (see (6.18)) in this equation, it follows:

$$\eta_\theta = \Delta p \frac{r_0}{2tE}. \tag{6.20}$$

This expression is valid both for cornea and sclera tangential deformation, specifying typical radius, thickness and Young's modulus for the two structures ($t_c = 0.52\,mm$, $E_c = 10.3\,MPa$ [33] and $t_s = 0.67\,mm$ [36] , $E_s = 41.83\,MPa$ [15, 19])

3. To characterize the capacitor as we did in equation (3.28), we have to write an expression for the increment in volume of the structure. It can be done in the same way both for volume under cornea and under sclera, specifying respective values for the parameters r_0, δ and η:

$$\begin{aligned}
\Delta V = V - V_0 &= \frac{\pi}{3} r_0^3 (1+\eta)^3 \delta - \frac{\pi}{3} r_0^3 \delta && (6.21)\\
&= \frac{\pi}{3} r_0^3 \delta [1 + 3\eta^2 + 3\eta + \eta^3 - 1] && (6.22)\\
&= \pi r_0^3 \delta [\eta + \cancel{\eta^2} + \frac{\cancel{\eta^3}}{\cancel{3}}] && (6.23)\\
&\simeq \pi r_0^3 \delta \eta, && (6.24)
\end{aligned}$$

where the approximations in (6.23) are valid for small deformations ($\eta << 1$).

4. Finally, the estimate for the capacitor follows using expression (6.20) of the tangential strain in (6.24):

$$\Delta V = \pi r_0^3 \delta \frac{r_0}{2tE} \Delta p \quad \Longrightarrow \quad C = \frac{\Delta V}{\Delta p} = \frac{\pi}{2} \frac{r_0^4 \delta}{tE}. \tag{6.25}$$

This estimate is valid both for cornea and sclera, with their specific values for the parameters involved in the formula, with the approximations:

(i) linear elastic structures and

(ii) small deformations.

Resulting values of corneal and scleral capacitances are 41.96 $\mu l/mmHg$ and 516.21 $\mu l/mmHg$ respectively. We note that we expected similar or slightly smaller quantities with respect to the value of capacitance found in the constant-capacitor model (see Chapter 3.4.3.2). By now, we still can't propose verified hypotheses to justify these high values of capacitances. However, we point out that the available data on ocular tissues needed to calibrate the model are few and usually difficult to interpret. Inconsistent use of data may be the problem in the aforementioned estimation of corneal and scleral capacitances.
Note that it is extremely relevant to ophthalmology that the thickness t of the structure is an explicit parameter in the formula: in fact, central corneal thickness (CCT) can be measured clinically with corneal pachymetry and a reduction in CCT has been associated with glaucoma.

6.2 Capacitance for vitreous humor

The capacitor at the interface between choroid and aqueous humor, that is vitreous humor capacitor, is more difficult to calibrate. Less is known about vitreous body than other structures and fluids in the eye. Thus, here, for simplicity and in analogy with what we found before, we assumed C_{vitr} to be constant and estimated it by solving a simplified circuit

in which we forced aqueous humor pressure P_{AH} to take the value of intraocular pressure found in (3.38). For this purpose, we inserted the sinusoidal voltage source IOP and excluded from the circuit currents that represent aqueous humor flow. In fact, these currents are the ones that set the mean value of IOP that here is formerly included in the sinusoidal voltage source. Solving the electrical circuit, we have:

$$\begin{cases} J_{vitr} = J_c \\ J_{ch} = J_{vitr} + J_s, \end{cases} \tag{6.26}$$

with

$$\begin{cases} J_c \coloneqq C_c \dfrac{dP_{AH}}{dt} \\ J_{vitr} \coloneqq C_{vitr} \frac{d}{dt}(P_{ch} - P_{AH}) \\ J_s \coloneqq C_S \frac{dP_{ch}}{dt}. \end{cases} \tag{6.27}$$

The solution of the system of non-linear equations (6.26) in the two unknown C_{vitr} and $\frac{dP_{ch}}{dt}$ gives the expression for the capacitance that accounts for vitreous humor:

$$C_{vitr} = C_c \frac{dP_{AH}}{dt} \left[\frac{J_{ch}}{C_s} - \left(\frac{C_c}{C_s} + 1 \right) \frac{dP_{AH}}{dt} \right]^{-1} \tag{6.28}$$

6.3 Implementation with OpenModelica and initial results of the new model

The scarcity of clinical data on ocular tissue parameters makes the use of mathematical models particularly attractive and important. Until here we have modeled IOP physiology following a bottom-up reasoning, that is: (i) assuming and discussing hypotheses, (ii) formulating physical laws, and (iii) characterizing model parameters, especially capacitances,

by means of ocular geometric parameters. Value of the parameters are taken from literature.
However, results of the last model would request some further analysis since they do not permit us to calibrate the model starting from the mathematical expressions we found. In fact, corneal and scleral capacitances turn out to be much more higher than the previously found value of constant capacitances, namely 1.35 $\mu l/mmHg$. More importantly, vitreous capacitance turns out to be dependent on the derivative of anterior chamber pressure (P_{AH}), that necessarily takes negative values also. Clearly, it can't be possible, because capacitances can take only positive values. This last outcome may be explained looking to the values of voltage differences across the three capacitors of the model. In fact, while voltage difference across cornea and sclera, namely P_{AH} and P_{ch} respectively (see Figure 6.2), are quite high as referred to ground, voltage difference across vitreous humor in our model is imposed by $P_{ch} - P_{AH}$, which turns out to be a small value of pressure (analogue of voltage in our electrical analogy, as explained in Section 3.1).

To overcome these model shortcomings, here we start to simulate the circuit following a different method. We set initially all capacitances to the baseline value of ocular rigidity (as discussed in Section 3.4.3.1), namely 1.35 $\mu l/mmHg$, then we vary the parameters to calibrate the model validating it with curves of pressure that can be found in literature.
Simulation outcome of the model with vitreous, corneal, and scleral capacitances set to 1.35 $\mu l/mmHg$ is shown in Figure 6.5. The electrical circuit implemented in OpenModelica is depicted in Figure 6.4. The curve goes up to speed in around 20 seconds, then it reaches a periodic state characterized by (i) mean value of 14.95 mmHg, (ii) amplitude of oscillations around 0.71 mmHg, and (iii) frequency determined by choroidal blood flow oscillations, as remarked for previous models. Note that in

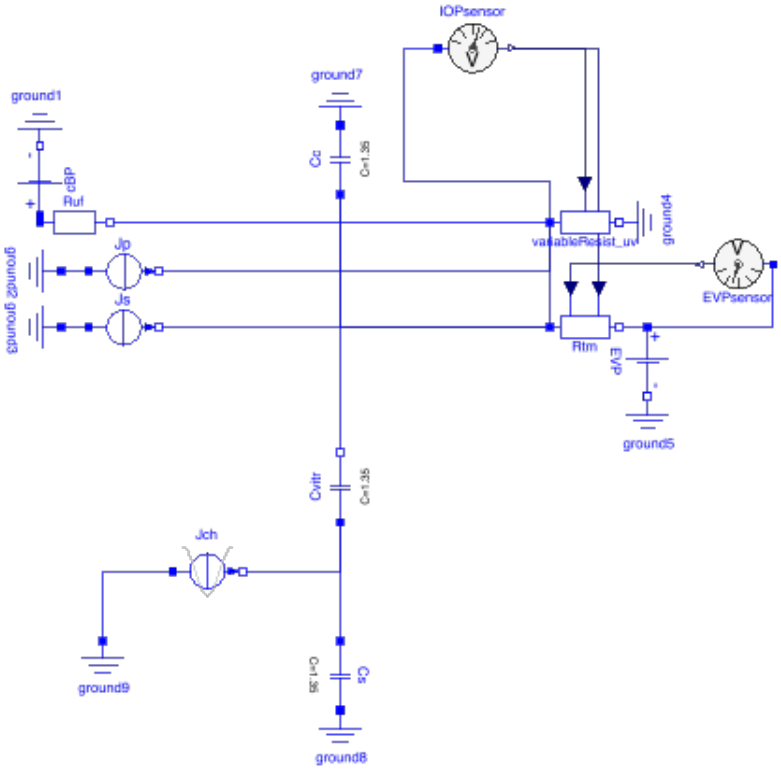

Figure 6.4: *OpenModelica electrical circuit with corneal, scleral, and vitreous capacitances set to* $1.35\,\mu l/mmHg$

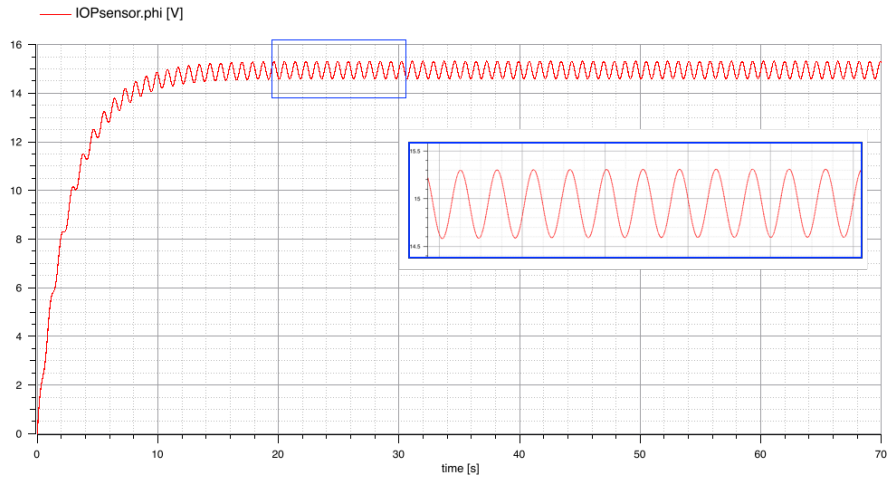

Figure 6.5: *Simulation output in OpenModelica when all capacitances are set to* $1.35\,\mu l/mmHg$

the case of only one capacitor, IOP curve takes 5 seconds to go to speed, while here, with different capacitors for the three structures, it takes four times that period. It is because each capacitor takes times to be charged. The curve reproduces well typical IOP shapes that can be measured in clinics.

To assess the role of the outer tunic of the eye made of connective tissue in determining IOP diurnal fluctuations, we let vary corneal and scleral capacitances.
Firstly, we simulate increased capacitances for cornea and sclera. It means that the external shell of the eye is able to deform more than vitreous humor, and this is more realistically what occurs in a physiological eye. To simulate the model, we set corneal and scleral capacitances to 2.2 $\mu l/mmHg$. Simulation output is depicted in Figure 6.6. Main con-

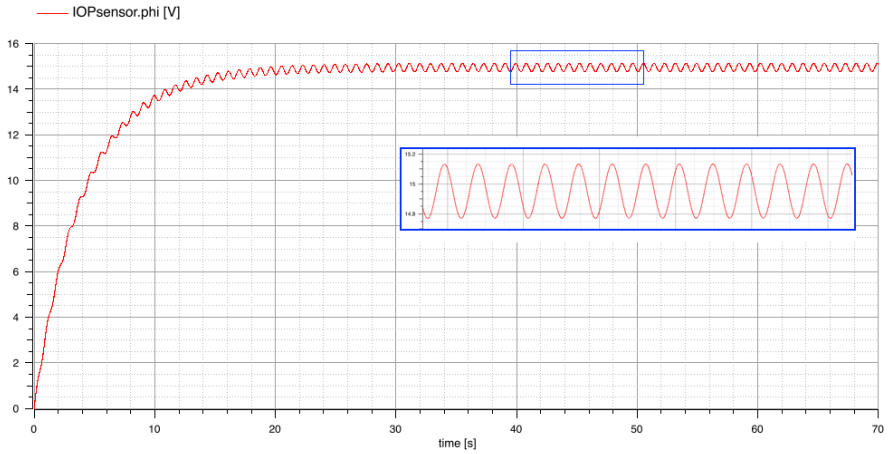

Figure 6.6: *Simulation output in OpenModelica when corneal and scleral capacitances are set to* $2.2\,\mu l/mmHg$*, and vitreous humor capacitance is set to* $1.35\,\mu l/mmHg$

siderations are that the curve goes up to speed more slowly (it takes around 40 seconds to reach a periodic state), and amplitude of IOP oscillations considerably diminishes. In particular, (i) mean value of ocular pressure does not vary from the previous model, (ii) amplitude of oscillations drops to 0.18 mmHg, and (iii) frequency does not vary, being still

determined by cardiac cycle.

Next, we simulate decreased capacitances for cornea and sclera, always keeping the value for vitreous humor constant. The simulation with corneal and scleral capacitances equal to 0.5 $\mu l/mmHg$ gives as output a curve that reaches the periodic state after 10 seconds. (i) Resultant

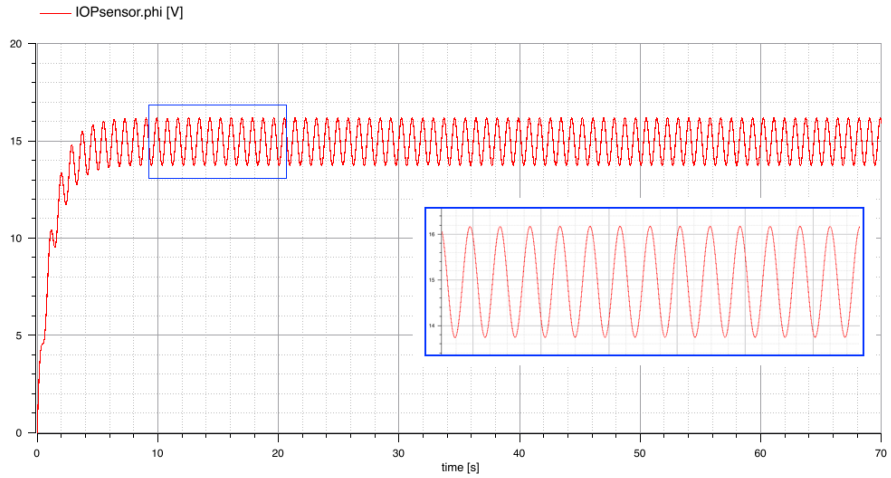

Figure 6.7: *Simulation output in OpenModelica when corneal and scleral capacitances are set to* $0.5\,\mu l/mmHg$*, and vitreous humor capacitance is set to* $1.35\,\mu l/mmHg$

mean IOP is unvaried, (ii) amplitude of oscillations increases to 1.22 mmHg, and (iii) frequency is clearly unvaried.

Two early considerations can be done:

(i) corneal and scleral capacitances are shown to influence the time interval before which the pressure curve reaches a periodic state. In particular, increased values of capacitances produce an high increase in the time needed to reach the periodicity, while decreased values of capacitances produce a decrease in this time interval.

(ii) corneal and scleral capacitances are shown to influence the amplitude of IOP oscillations. In particular, increased values of capacitances produce an high decrease in output amplitude of oscillations, while decreased values of capacitances produce a similar increase in output amplitude.

Second remark is completely in agreement with results given by our two dynamic models (compare with Figures 4.12(i) and 4.14(i) of Chapter 4) and confirms that a decrease in the capacitance of cornea and sclera, namely a stiffening of ocular tissues, implies an increase in the amplitude of IOP oscillations.

To establish which is the major determinant of amplitude of oscillations among the two ocular shells, we vary one by one corneal and scleral capacitances.

The model with corneal and vitreous humor capacitances keep at 1.35 $\mu l/mmHg$ and scleral capacitance raised to 2.2 $\mu l/mmHg$ predicts an amplitude of oscillations of 1.22 mmHg. The curve reaches a periodic state after 30 seconds.

The model with scleral and vitreous humor capacitances keep at 1.35 $\mu l/mmHg$ and corneal capacitance raised to 2.2 $\mu l/mmHg$ predicts the same amplitude of oscillations, but the curve reaches a periodic state after 40 seconds.

The opposite is predicted by simulating the model with scleral and corneal capacitances lowered one by one to 0.5 $\mu l/mmHg$, while keeping other parameters constant. In particular, scleral capacitance does not determine changes in the time needed to reach the periodic state (20 seconds), while corneal capacitance determines a lowering in the period (15 seconds). Both the models predict amplitude of IOP oscillations of the order of 0.62 mmHg.

To assess the role of vitreous humor deformability, we simulate an increase in vitreous capacitance, namely to 2.2 $\mu l/mmHg$. The outcome of the model is a curve with (i) unvaried mean value, (ii) amplitude of oscillations that resembles the one obtained if scleral or corneal capacitance is decreased, namely 0.61 mmHg, and (iii) obviously unvaried frequency. IOP fluctuations curve is depicted in Figure 6.8 Lastly, we simulate a de-

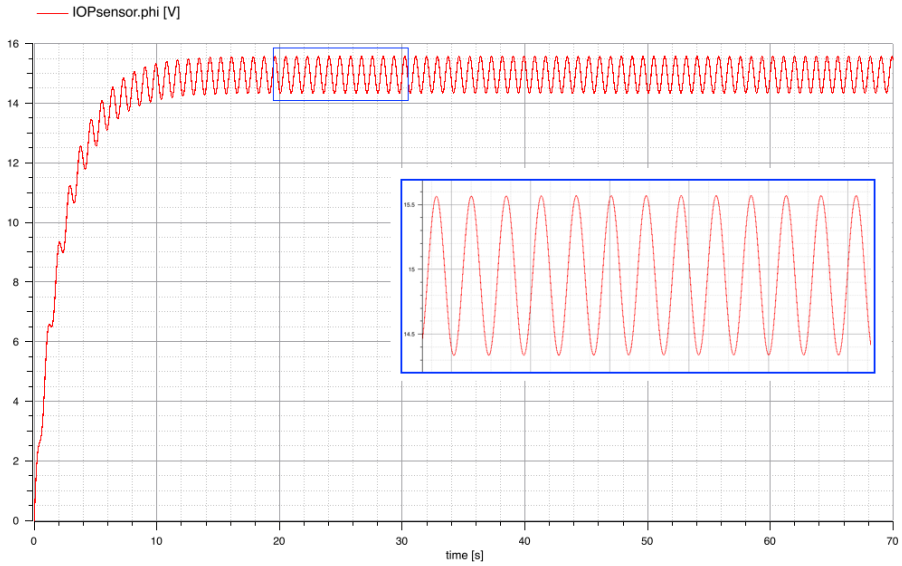

Figure 6.8: *Simulation output in OpenModelica when vitreous humor capacitance is set to* $2.2\,\mu l/mmHg$*, and corneal and scleral capacitances are set to* $1.35\,\mu l/mmHg$

crease in vitreous capacitance, namely to 0.5 $\mu l/mmHg$, that produces a curve with once again no changes in time needed to reach the periodic state (see Figurefig:omv0e5), (i) unvaried baseline, (ii) amplitude of oscillations close to the one obtained by increasing corneal or scleral capacitance, namely 0.23 mmHg, and (iii) still unvaried frequency.

Thus we can conclude that:

- mean value of IOP curve is neither influenced by corneal capacitance, nor by scleral capacitance, nor by vitreous capacitance. Even interactions between these three parameters could not cause a variation in mean IOP. This confirms that *mean value of intraocular pressure is just aqueous humor-dependent.*
- *the main determinant for the length of the time interval is coroidal deformability*, which delays the reaching of the periodic state if increased,
- also sclera contributes to the time needed to reach the periodic

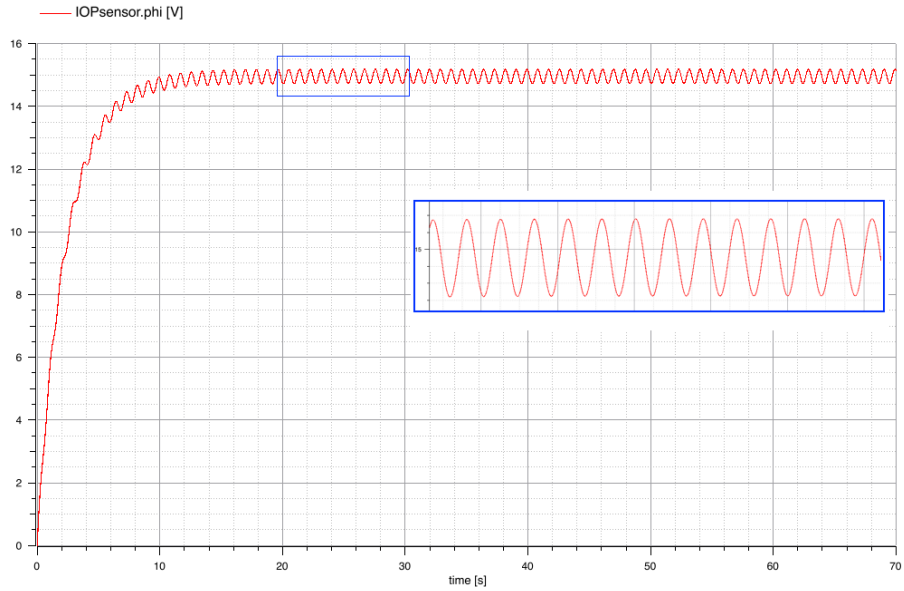

Figure 6.9: *Simulation output in OpenModelica when vitreous humor capacitance is set to* $0.5\,\mu l/mmHg$*, and corneal and scleral capacitances are set to* $1.35\,\mu l/mmHg$

state, but to a lesser extent, while vitreous humor does not have any influence on it,

- *cornea and sclera contribute together to amplitude of IOP oscillations*, determining a decrease if increased, and
- also vitreous humor contributes to the amplitude, but to a lesser extent. Besides, it causes an increase in amplitude of oscillations if raised, and a decrease if lowered.

Chapter 7

Conclusions and future developments

The work in this thesis has been motivated by the need of identifying and ranking patient-specific parameters related to ocular biomechanics and hemodynamics that contribute to intraocular pressure (IOP) dynamics. The characterization of the most influencing parameters can aid improving the current options for glaucoma therapies which, to date, concern IOP-lowering medications only. In particular, it aims to be particularly useful in elucidating and acting on those cases of glaucoma patients that progress to blindness even though IOP is within normal levels and those cases of subjects whose IOP is higher than the "physiological" that never develop glaucoma. Moreover, ocular hypertension, namely elevated IOP, is associated with many other diseases. Thus, it is of great clinical interest to identify the factors influencing its diurnal oscillations.

In this thesis three electrical analogue models for aqueous humor (AH) flow, ocular blood flow and ocular structure deformability, all together contributing to IOP dynamics, are presented. Oscillations in parameters that occur between day and night and during night are not considered here.

The first model takes inspiration from a work by Szopos et al [31]. To successively extend the model, we implemented it in the open source software OpenModelica. This time-independent model is able to simulate and reproduce the mechanism of *AH inflow and outflow* thus simulating

the *steady-state IOP*. It predicts a value of pressure of 14.9527 mmHg, that is perfectly comparable with values of "physiological" IOP that can be found in literature.

The subsequent two models are developments of the static model. They take into account the *time-dependence of choroidal blood flow and changes in eye total volume due to structure deformability*, in addition to AH inflow and outflow, thus simulating *IOP time-fluctuations*. As a first step, ocular deformability, which is expressed as variations in ocular volume on variations in ocular pressure, is simply a constant. With the model we can simulate IOP dinamics, that is characterized by its baseline steady-state value, namely 14.9535 mmHg, amplitude of its oscillations, namely $\pm$1.0641 mmHg, and its frequency, namely 1.13 s^{-1}. The curve predicted by the model reproduces well the typical IOP signal which can be acquired in clinics. Sensitivity analysis performed on this model shows that (i) the steady-state value is determined by AH inflow and outflow parameters, as predicted by the static model too, (ii) the *amplitude of IOP oscillations is determined by the value of the capacitance which models changes in ocular volume*, and (iii) the *frequency of the curve is determined by choroidal blood flow pulsations*, which in turn are determined by the cardiac cycle.

In the second dynamic model, pressure is assumed not to be constant while estimating ocular deformability. Thus the capacitance takes a more complex form resulting in an expression that is IOP-dependent. The curve predicted by this model, even resembling the curve of pressure of the previous model, displays higher amplitude of oscillations. In particular, values of baseline and amplitude of IOP oscillations are 15.0179 mmHg and $\pm$2.12 mmHg respectively. Due to the fact that frequency depends only on the cardiac cycle via choroidal blood pulsations, it remains unvaried. Sensitivity analysis performed on this model shows that (i) consistently with the previous models, the steady-state value is deter-

mined by AH inflow and outflow parameters, (ii) the *amplitude of IOP oscillations here is determined both by the value of the capacitor, which models changes in ocular volume, and by AH parameters*, and (iii) the frequency of the curve is determined by choroidal blood flow pulsations, as previously remarked. Note that result (ii) is a direct consequence of the non-linearity of the model. In fact, AH parameters influence the value of IOP (result (i)), which in this model enters in the formula for the capacitance. We know from result (ii) of the previous model that the capacitance has an impact on the dynamics of IOP, so it follows that, in the non-linear capacitance model, all the parameters contribute to determine the amplitude of IOP oscillations. This is also the reason why this models shows an increased amplitude in IOP oscillations.

More specifically, sensitivity analysis performed on the three models is able to establish and rank parameters whose variations influence IOP steady-state or/and its dynamics. All models have *baseline IOP* determined primarily by *ciliary blood pressure* (cBP), namely the value of voltage that drives AH ultrafiltration. In particular, resultant first order Sobol index (S.I.) for cBP is 0.3 both in the static and in the dynamic model. Secondly, oncotic pressure difference ($\Delta\pi_p$), that drives ultrafiltration, and osmotic pressure difference ($\Delta\pi_s$), that drives ionic secretion, play a relevant role in influencing mean value of IOP. Values of S.I. result in 0.28 and 0.24 respectively, both in the static model and in the dynamic one. Conversely, capacitors of the dynamic models do not influence mean IOP at all. *Oscillations of pressure* in the eye are mainly characterized by *ocular rigidity*, that accounts for the elastic proprieties of the cornea, sclera and other boundary structures of the eye. In particular, the constant-capacitance model shows that the capacitor is the only determinant for amplitude of IOP oscillations, while the variable-capacitance model interestingly reveals a more complex interaction of AH parameters with the parameter of ocular rigidity in determining

amplitude of IOP oscillations. However, ocular rigidity remains the first determinant with S.I. 0.92, followed by cBP (S.I. 0.025), $\Delta\pi_p$ (S.I. 0.022) and $\Delta\pi_s$ (S.I. 0.019).

Another interesting result of our model is the possibility to predict IOP-lowering medications outcomes in various conditions of clinical interest, while accounting for uncertainties and variabilities in the model parameters. Since it is extremely difficult to identify and isolate variations in different biomechanical and hemodynamical properties of the eye in clinical and experimental studies, this mathematical approach may prove to be very useful in simulating in a virtual way the response to medications administered to subjects in various circumstances which could be patient-specific. In particular, we simulate the effect of IOP-lowering medications in ocular normotensive healthy subjects (ONT) and ocular hypertensive subjects (OHT). The latter is simulated by decreasing the mean value of the trabecular meshwork outflow facility, namely setting $C_0 = 0.3\overline{C_0}$. Due to the fact that many open angle glaucoma patients continue to experience disease progression despite meeting target IOP levels, and that subjects that do not show particularly high ocular pressures can develop glaucoma, both cases are interesting from a clinical point of view. We simulate medications intended to lower ocular pressure by reducing the active ionic secretion by 25%, namely setting $\Delta\pi_s = 0.75\overline{\Delta\pi_s}$, as explained in Chapter 5. An example of possible application of our analysis in a real case may be the simulation of an increase in ocular rigidity parameter γ, a recurring phenomenon which can occur with aging, extreme myopia, or when drugs which act as vasoconstrictors are administered (Section 4.3.1). With the models presented in this project, we may be able to investigate the effect and efficacy of IOP-lowering medications also in this particular case in an easy, quick and especially non invasive way. It aims to be useful in a long term perspective in order to develop the research for future clinical applications.

This study suggests that the inclusion of uncertainty in AH flow and ocular viscoelasticity parameters of our model is a promising approach that can aid patient-specific assessment of glaucoma management and help in the development of novel, effective, and individualized therapeutic approaches in glaucoma treatment. Future developments of the model will include:

1. the influence of specific biomechanical factors, such as axial length and scleral and corneal thickness, in addition to ocular rigidity that is yet present in our model, on IOP fluctuations. A step toward this direction has been shown in Chapter 6;

2. uncertainty applied on choroidal blood flow, that will enable to take into account choroidal perfusion abnormalities. They can be due to diseases that cause severely elevated blood pressure (such as malignant hypertension or eclampsia), inflammatory conditions (particularly various types of arteritis), vaso-occlusion by microemboli, iatrogenic causes, or ocular compression related to cataract surgery [8, 38], to name some of the possible causes;

3. the coupling between AH flow and choroidal blood flow with retinal blood flow and ciliary blood flow;

4. cerebrospinal fluid flow, which determines intracranial pressure and would permit to couple the eye with the brain. Moreover, a lowering of this pressure has been identified as a risk factor for glaucoma, as illustrated in Section 1.2.1, thus it may be interesting to have this parameter in the model;

5. the addition of uncertainty on each of the parameter added to the model, to quantify the influence of parameters' variations on IOP dynamics;

6. autoregulation mechanisms, in particular ciliary blood flow autergulation;

7. to enlarge range of oscillations in parameters that occur between day and night and during night to simulate IOP fluctuations due to diurnal and circadian changes;

8. several further effects that have not been considered in the present model but which might play an important role, such as distribution of stress, strain, fluids, oxygen, carbonic dioxide and nutrients within the ocular tissues. Such developments would require the use of more complex two- or three-dimensional approaches, for which the present model could provide boundary conditions.

In a long term perspective, the software developed within this project will be integrated in a larger virtual simulator for ocular biophysics with the aim of providing clinical researchers with new effective tools to improve the current options for patient therapies. In principle, a clinical researcher could input some patient-specific parameters in the model and even define the patient-specific geometry of the eye. Moreover, the effects of some drugs may be assessed simply varying related parameters of the model.

Bibliography

[1] http://www.skatefins.com/.

[2] https://entokey.com/ocular-circulation-2/.

[3] W. Stamer, T. Acott. Current understanding of conventional outflow dysfunction in glaucoma. *Current Opinion in Ophthalmology*, 2012.

[4] Y. Kwon, J. Fingert, M. Kuehn, W. Alward. Primary open-angle glaucoma. *The New England Journal of Medicine*, 2009.

[5] M.A. Kass, S.M. Podos, R.A. Moses, B. Becke. Prostaglandin E_1 and aqueous humor dynamics. *Investigative Ophthalmology & Visual Science*, 1972.

[6] T.J. Bennett. Scanning laser ophthalmoscopy. https://www.opsweb.org/?page=SLO.

[7] M. Goel, R.G. Picciani, R.K. Lee, S.K. Bhattacharya. Aqueous humor dynamics: A review. *The Open Ophthalmology Journal*, 2010.

[8] A. Gaudric, G. Coscas, A.C. Bird. Choroidal ischemia. *American Journal of Ophthalmology*, 1982.

[9] M.O. Gordon, J.A. Beiser, J.D. Brandt. The ocular hypertension treatment study: baseline factors that predict the onset of primary open-angle glaucoma. *Archives of ophthalmology*, 2002.

[10] R. Brubaker. Computer-assisted instruction of current concepts in aqueous humor dynamics. *American Journal of Ophthalmology*, 1976.

[11] R.F. Brubaker. The physiology of aqueous humor formation. In *Applied pharmacology in the medical treatment of glaucoma*. 1984.

[12] G. Guidoboni, A. Harris, J.C. Arciero, B. Siesky, A. Amireskandari, A.L. Gerber, A.H. Huck, N.J. Kim, S. Cassani, L. Carichino. Mathematical modeling approaches in the study of glaucoma disparities among people of African and European descents. *Journal of Coupled Systems and Multiscale Dynamics*, 2013.

[13] J. Caprioli, A. Coleman. Intraocular pressure fluctuation: a risk factor for visual field progression at low intraocular pressures in the advanced glaucoma intervention study. *Ophthalmology*, 2008.

[14] J. Caprioli, A. Coleman. Blood flow in glaucoma discussion; blood pressure, perfusion pressure, and glaucoma. *American Journal of Ophthalmology*, 2010.

[15] R. Grytz, M. Fazio, M. Girard, V. Libertiaux, L. Bruno, S. Gardiner, C. Girkin, J.C. Downs. Material properties of the posterior human sclera. *ELSEVIER*, 2014.

[16] A.M. Bron, C. Creuzot-Garcher, S. Goudeau-Boutillon, P. d'Athis. Falsely elevated intraocular pressure due to increased central corneal thickness. *Graefe's Archive for Clinical and Experimental Ophthalmology*, 1999.

[17] G. Regev, A. Harris, B. Siesky, Y. Shoshani, P. Egan, A. Moss, M. Zalish, D. WuDunn, R. Ehrlich. Goldmann applanation tonometry and dynamic contour tonometry are not correlated with central corneal thickness in primary open angle glaucoma. *Journal of Glaucoma*, 2011.

[18] J. Siggers, C. Ethier. Fluid mechanics of the eye. *Annual Review of Fluid Mechanics*, 2012.

[19] R.E. Norman, J.G. Flanagan, S.M. Rausch, I.A. Sigal, I. Tertinegg, A. Eilaghi, S. Portnoy, J.G. Sled, C.R. Ethier. Dimensions of the human sclera: Thickness measurement and regional changes with axial length. *ELSEVIER*, 2014.

[20] R. Chowdhury, M. Fautsch. Intracranial pressure and its relationship to glaucoma: Current understanding and future directions. *Med Hypothesis Discov Innov Ophthalmol*, 2015.

[21] N. Orzalesi, L. Rossetti, A. Bottoli, P. Fogagnolo. Comparison of the effects of latanoprost, travoprost, and bimatoprost on circadian intraocular pressure in patients with glaucoma or ocular hypertension. *Ophthalmology*, 2006.

[22] J.S. Friedenwald. Contribution to the theory and practice of tonometry. *American Journal of Ophthalmology*, 1973.

[23] D.M. Silver, O. Geyer. Pressure-volume relation for the living human eye. *Current Eye Research*, 2000.

[24] H.D. Sesso, M.J. Stampfer, B. Rosner, C.K. Hennekens, J.M. Graziano, J.E. Manson, R.J. Glynn. Systolic and diastolic blood pressure, pulse pressure, and mean arterial pressure as predictors of cardiovascular disease risk in men. *Hypertension*, 2000.

[25] J.D. Brandt, J.A. Beiser, M.A. Kass, M.O. Gordon. Central corneal thickness in the ocular hypertension treatment study (OHTS). *Ophthalmology*, 2001.

[26] R. Hollows, P. Graham. Intraocular pressure, glaucoma, and glaucoma suspects in a defined population. *British Journal of Ophthalmology*, 1966.

[27] A. Heijl, M.C. Leske, B. Bengtsson, L. Hyman, L.M. Dong, Z. Yang, Early Manifest Glaucoma Trial Group. Predictors of long-term progression in the early manifest glaucoma trial. *Ophthalmology*, 2007.

[28] A. Heijl, M.C. Leske, B. Bengtsson, L. Hyman, M. Hussein, Early Manifest Glaucoma Trial Group. Reduction of intraocular pressure and glaucoma progression: results from the early manifest glaucoma trial. *Archives of ophthalmology*, 2002.

[29] R.M. Siatkowski, B.L. Lam, D.R. Anderson, W.J. Feuer, A.M. Halikman. Automated suprathreshold static perimetry screening for detecting neuro-ophthalmologic disease. *Ophthalmology*, 1996.

[30] N. Ehlers, F.K. Hansen. Central corneal thickness in low-tension glaucoma. *Acta Ophthalmologica*, 1974.

[31] M. Szopos, S. Cassani, G. Guidoboni, C. Prud'homme, R. Sacco, B. Siesky, A. Harris. Mathematical modeling of aqueous humor flow and intraocular pressure under uncertainty: towards individualized glaucoma management. *Journal for Modeling in Ophthalmology*, 2016.

[32] S. Cassani, G. Guidoboni, M. Szopos, C. Prud'homme, R. Sacco, B. Siesky, A. Harris. Mathematical modeling and statistical analysis of aqueous humor flow towards individualized glaucoma treatment. *ARVO*, 2016.

[33] J.ø. Hjortdal. Young's modulus of elasticity for the human cornea. *ELSEVIER*, 1994.

[34] A. Rulo, E. Greve, H. Geijssen, P. Hoyng. Reduction of intraocular pressure with treatment of latanoprost once daily in patients with normal-pressure glaucoma. *Ophthalmology*, 1996.

[35] C.A Johnson. Selective versus nonselective losses in glaucoma. *Journal of Glaucoma*, 1994.

[36] S. Vurgese, S. Panda-Jonas, J.B. Jonas. Scleral thickness in human eyes. *ELSEVIER*, 2012.

[37] Community Eye Health Journal. Understanding and caring for a schiotz tonometer. `https://www.cehjournal.org/article/understanding-and-caring-for-a-schiotz-tonometer/`, 2014.

[38] T. Iida, R.F. Spaide, J. KantorJ. Retinal and choroidal arterial occlusion in wegener's granulomatosis. *American Journal of Ophthalmology*, 2002.

[39] J.W. Kiel. Physiology of the intraocular pressure. In *Pathophysiology of the Eye, 4. Glaucoma*, chapter III. Akademiai Kiado, 1998.

[40] J.W. Kiel. Anatomy. In *The Ocular Circulation*, chapter II. Morgan and Claypool Life Sciences, 2010.

[41] C.E.T. Krakau. Calculation of the pulsatile ocular blood flow. *Investigative Ophthalmology and Visual Science*, 1992.

[42] P. Ehrnrooth, P. Puska, I. Lehto, L. Laatikainen. Progression of visual field defects and visual loss in trabeculectomized eyes. *Graefe's Archive for Clinical and Experimental Ophthalmology*, 2005.

[43] S. Chen, P. Lu, W-F. Zhang, J-H. Lu. High myopia as a risk factor in primary open angle glaucoma. *International Journal of Ophthalmology*, 2012.

[44] Enhanced medical Services. `http://www.emseye.com/store/haag-streit-tonometer-t-900.html`.

[45] R.P. Copt, R. Thomas, A. Mermoud. Corneal thickness in ocular hypertension, primary open-angle glaucoma, and normal-tension glaucoma. *Archives of ophthalmology*, 1999.

[46] R. Moses. Intraocular pressure. In *Adler's Physiology of the Eye*, chapter Clinical Application. 1981.

[47] R. Moses. Intraocular pressure. In *Adler's Physiology of the Eye*, chapter Clinical Application. 1987.

[48] M.W. Ansari, A. Nadeem. The eyeball: Some basic concepts. In *Atlas of ocular anatomy*, chapter II. Springer, 2016.

[49] National Eye Institute (NEI). Ocular hypertension treatment study (OHTS). `https://nei.nih.gov/glaucomaeyedrops/`.

[50] T. Sugiyama, M. Araie, C.E. Riva, L. Schmetterer, S. Orgul. Use of laser speckle flowgraphy in ocular blood flow research. *Acta Ophthalmologica*, 2010.

[51] S. Bill, C.L. Phillips. Uveoscleral drainage of aqueous humour in human eyes. *Eye Research*, 1971.

[52] J. Danias, S. Podos. Comparison of glaucomatous progression between untreated patients with normal-tension glaucoma and patients with therapeutically reduced intraocular pressures. the effectiveness of intraocular pressure reduction in the treatment of normal-tension glaucoma. *American Journal of Ophthalmology*, 1999.

[53] J.W. Kiel, M. Hollingsworth, R. Rao, M. Chen, H.A. Reitsamer. Ciliary blood flow and aqueous humor production. *Progress in Retinal and Eye Research*, 2011.

[54] E. Lippa, L. Carlson, B. Ehinger, L. Eriksson, K. Finnström, C. Holmin, S. Nilsson, K. Nyman, C. Raitta, A. Ringvold. Dose response and duration of action of dorzolamide, a topical carbonic anhydrase inhibitor. *Archives of ophthalmology*, 1992.

[55] R. Funk, J.W. Rohen. Scanning electron microscopic study on the vasculature of the human anterior eye segment, especially with respect to the ciliary processes. *Eye Research*, 1990.

[56] Eye hospital RUTNIN. Glaucoma. `http://www.rutnin.com/en/eye_knowledge/detail.29.1.html`.

[57] D.M. Silver, R.A. Farrel, M.E. Langham, V. O'Brien, P. Schilder. Estimation of pulsatile ocular blood flow from intraocular pressure. *Acta Ophthalmologica*, 1987.

[58] A. London, I. Benhar, M. Schwartz. The retina as a window to the brain-from eye research to CNS disorders. *Nature Reviews Neurology*, 2013.

[59] J.W. Kiel, A.P. Shepherd. Autoregulation of choroidal blood flow in the rabbit. *Investigative Ophthalmology and Visual Science*, 1992.

[60] W.-Q. Feng, Y. Chen, Y.-X. Zhou, M.-G. Shi. Measurement of human eye volume in vivo with MRI and its clinical value. *Zhonghua Shiyan Yanke Zazhi/Chinese Journal of Experimental Ophthalmology*, 2011.

[61] R. Maheshwari, N.S. Choudhari, M.D. Singh. Tonometry and care of tonometers. *Journal of Current Glaucoma Practice*, 2012.

[62] I. Sobol. Sensitivity analysis for nonlinear mathematical models. *Mathematical and Computer Modelling*, 1993.

[63] A. Bayer, J. Henderer, T. Kwak, J. Myers, J. Fontanarosa, G. Spaeth. Clinical predictors of latanoprost treatment effect. *Journal of Glaucoma*, 2005.

[64] L.R. Stamper. Dynamic contour tonometry. *GLAUCOMA TODAY*, 2004.

[65] L.W. Herndon, J.S. Weizer, S.S Stinnett. Central corneal thickness as a risk factor for advanced glaucoma damage. *Archives of ophthalmology*, 2004.

[66] P. Watson, J. Stjernschantz. A six-month, randomized, double-masked study comparing latanoprost with timolol in open-angle glaucoma and ocular hypertension. *Ophthalmology*, 1996.

[67] B. Sudret. Global sensitivity analysis using polynomial chaos expansion. *Reliability Engineering & System Safety*, 2008.

[68] B. Sudret. Meta-models for structural reliability and uncertainty quantification. *Archive ouverte HAL*, 2012.

[69] F. Salerni, R. Repetto, G. Guidoboni, C. Prud'homme, M. Szopos. Design and development of a mathematical model to analyse visual impairment in astronauts.

[70] M. Langham, K. To'mey. A clinical procedure for measuring the ocular pulse. *Experimental Eye Research*, 1987.

[71] I. Pallikaris, G. Kymionis, H. Ginis, G. Kounis, E. Christodoulakis, M. Tsilimbaris. Ocular rigidity in patients with age-related macular degeneration. *ELSEVIER*, 2006.

[72] B.U. Seifertl, W. Vilser. Retinal vessel analyzer (RVA) —design and function. *Biomedizinische Technik. Biomedical Engineering*, 2002.

[73] S. Mosaed, J.H. Liu, R.N. Weinreb. Correlation between office and peak nocturnal intraocular pressures in healthy subjects and glaucoma patients. *American Journal of Ophthalmology*, 2005.

[74] B.J. Fan, J.L. Wiggs. Glaucoma: genes, phenotypes, and new directions for therapy. *The Journal of Clinical Investigation*, 2010.

[75] O. Kosoko-Lasaki, G. Gong, G. Haynatzki, M.R. Wilson. Race, ethnicity and prevalence of primary open-angle glaucoma. *Journal of the National Medical Association*, 2006.

[76] R. Shah, R. Wormald. Glaucoma. *Clinical Evidence*, 2011.

[77] R. David, L.M. Zangwill, Z. Tessler, Y. Yassur. The correlation between intraocular pressure and refractive status. *Archives of ophthalmology*, 1985.

[78] S. Makita, T. Fabritius, Y. Yasuno. Quantitative retinal-blood flow measurement with three-dimensional vessel geometry determination using ultrahigh-resolution doppler optical coherence angiography. *Optics Letters*, 2008.

[79] M.J. Doughty, M.L. Zaman. Human corneal thickness and its impact on intraocular pressure measures: a review and meta-analysis approach. *Survey of Ophthalmology*, 2000.

[80] M. Zhou, W. Wang, W. Huang, X. Zhang. Diabetes mellitus as a risk factor for open-angle glaucoma: A systematic review and meta-analysis. *PLoS ONE*, 2014.